

https://dspace.org/

An investigation into urban heat islands and their impacts on air quality in the Msunduzi municipality, KwaZulu-Natal

Maluleke, Amukelani

2019

https://hdl.handle.net/10539/28870

Downloaded from a DSpace repository. https://dspace.org/

University of the Witwatersrand

An investigation into Urban Heat Islands and their impacts on air quality in the Msunduzi Municipality, KwaZulu-Natal

A thesis submitted in fulfilment of the requirements for a Master of Science degree at the University of the Witwatersrand



UNIVERSITY OF THE
WITWATERSRAND,
JOHANNESBURG

Amukelani Maluleke, 740700

Supervisor: Prof Fethi Ahmed

School of Geography, Archaeology and Environmental Studies

Acknowledgments

My first thanks to the South African National Space Agency (SANSA) for funding my Master of Science degree and making it possible for me to complete my postgraduate studies. Secondly, the Msunduzi Municipality Air Quality department for air quality data provision and thirdly, the South African Weather Service for providing meteorological data at no cost towards this study. I am grateful to Professor Fethi Ahmed's support and dedication towards the completion of my degree.

The presence of my parents will always be a blessing. I thank God for their love, sacrifices and encouragement towards shaping who I am becoming. To my siblings, thank you all for your support. It took me longer than I had expected to complete this study, but I thank God for pulling me through and keeping His promises.

"Let us not become weary in doing good, for at the proper time we will reap a harvest if we do not give up."

Galatians 6:9

Declaration

I Amukelani Maluleke (Student number: 740700), registered for the degree of Master of Science in the year 2018 at the University of the Witwatersrand, Johannesburg. I hereby declare that this dissertation is my own unaided work. It is being submitted in fulfilment of the requirements for the degree of Master of Science. It has not been submitted before for any degree or examination in any other University. I am aware that plagiarism is wrong, and I have followed the required conventions in referencing the thoughts and ideas of others.

Signature  Date 17/05/2019

Amukelani Maluleke (740700)

Abstract

The active changing of the landscape through processes such as urbanisation and land use change continue to modify land and atmosphere interactions. One resulting phenomenon from these modifications is the development of urban heat islands due to increases in land surface temperature. The excessive heat retention at the surface contributes to increases in air temperatures. For polluted cities, this raises several challenges as the formation, transport and dissipation of pollutants is reliant on atmospheric thermal dynamics. The aims of this study are two-fold, firstly it aims to investigate and characterise the urban heat island effect in the Msunduzi Municipality by assessing the relationships between land surface temperature and land cover characteristics. Secondly, the study intends to provide an understanding of the contribution of the presence of the urban heat island to local air pollution in the municipality. Through the use of seasonal Landsat 8 satellite acquisitions from 2013 to 2017 and the MODIS AOD 3K product, the study applied remote sensing analysis techniques in an attempt to reach the following objectives: (i) to investigate and characterise the nature and extent of the surface urban heat island effect in the Msunduzi Municipality, (ii) to determine the relationship between land surface temperature and different land cover classes using remote sensing land cover indices and, (iii) to assess the impact on pollutant concentrations with the development of the atmospheric urban heat island whilst briefly evaluating MODIS Aerosol Optical Depth as a potential proxy for measured air pollutants in the Msunduzi Municipality.

The study finds that SUHIs are clearly visible, especially during autumn and summer in concentrated patches. The generally large SUHI is predominantly located in the CBD and with isolated patches seasonally occurring over artificial surfaces and bare ground. The SUHI effect is marked during autumn (SUHI intensity = 2.65 degrees Celsius) where rural areas are notably cooler than urban areas. Built-up areas are constant sinks of heat throughout all seasons, although the SUHI is well observed during autumn. The contribution of LST to air temperature ($r = 0.70$; $R^2 = 0.49$) is considerable, indicating substantial links between surface characteristics and the lower atmosphere.

Assessing the seasonal NDVI, FVC and NDBI contributions to LST indicate that the presence of vegetation contributes to the cooling of the surface, with the dense location of built-up areas resulting in excessive heat retention. In some instances, especially during autumn and summer,

correlations between LST and NDVI and FVC are observed at -0.839 and summer -0.735, respectively. This indicates that the presence of vegetation likely contributes to reductions in LST in contrast to built-up areas having the opposite effect. The relationships between LST, NDVI, FVC and NDBI are however moderate during other seasons and their magnitude varies between the seasons.

Pollution concentrations in the municipality vary between winter and spring, with generally higher concentrations during the winter. There are marked diurnal patterns of pollutants, where high concentrations are typical during early morning periods. This is attributable to the inversion conditions dominant in the vicinity of the monitoring stations. The development of the UHI notably impacts on the cycles of pollutants, with O_3 concentrations particularly sensitive to sustained increases in air temperature, especially during spring. The spatial distribution of aerosols is predominately above the Pietermaritzburg city, with fewer instances where the surrounding areas experience high AOD observations. The application of AOD as a potential proxy for air pollutants is circumstantial in this study, however it does provide better spatial assessments for aerosols and pollutants. The study concludes on the importance of understanding land and atmosphere interactions towards mitigating for climate change and creating sustainable and resilient cities.

Keywords

Urban heat island; Land surface temperature; Land cover indices; Air pollution; Remote Sensing; Msunduzi Municipality, Pietermaritzburg

Contents

Acknowledgments i
Declaration ii
Abstract iii
List of Figures vii
List of Tables ix
List of Abbreviations and Acronyms x
Chapter 1: Introduction 1
1.1 Background 1
1.2 Research problem 4
1.3 Research Question 4
1.4 Aims and Objectives 4
1.4.1 Overall aim of the study 4
1.4.2 Specific research objectives 5
1.4.3 Significance of research 5
1.4.4 Structure of Thesis 6
Chapter 2: Literature Review 8
2.1 The Urban Heat Island 8
2.2 Factors influencing SUHI 11
2.3 UHI impacts 13
2.4 Relationship between LST and land cover indices 14
2.5 Impact of inversions and urban heat islands on local atmospheric pollution 16
2.6 The detection and studying of urban heat islands 17
2.7 Satellite remotely sensed data 19
2.7.1 Remotely-sensed thermal data 19
2.7.2 Remotely-sensed air quality data 19
2.8 Literature Summary 21
Chapter 3: Materials and Methods 23
3.1 Study area 23
3.2 Materials 25
3.2.1 Data and data sources 25
3.2.2 Landsat 8 OLI/TIRS data 26
3.2.3 Meteorological data 26
3.2.4 Air quality data 27
3.3 Pre-processing 27
3.3.1 Data Calibration 28
3.3.2 Atmospheric Correction 28
3.4 Land Cover Indices 29
3.4.1 NDVI 29
3.4.2 Fractional vegetation cover 29
3.4.3 NDBI 30
3.5 Land Cover Classification 30

3.6 Land Surface Temperature 31
3.6.1 LST processing methods 31
3.6.2 Brightness Temperature 33
3.6.3 Top of Atmospheric Spectral Radiance 34
3.6.4 Land Surface Emissivity 34
3.7 MODIS Aerosol Optical Depth 37
3.7.1 MODIS AOD product 37
3.8 Statistical Analyses 37
3.8.1 Existence of SUHI in the Msunduzi Municipality 37
3.8.2 Relationship between LST and land cover indices 38
3.8.3 Assessment of impact of SUHIs on urban pollution and MODIS AOD as proxy for measured pollutants 39
Chapter 4: Results and Discussion 40
4.1 Results 40
4.1.1 Land Cover/Land Use patterns 40
4.1.2 Urban Heat Islands 43
4.1.3 Mean LST class distribution 51
4.1.4 Land surface temperature and ambient air temperature 53
4.1.5 Land surface temperature and land cover indices 60
4.1.6 LULC influences on land surface temperature 63
4.1.7 Correlation analysis 68
4.1.8 UHIs and Air Quality 71
4.1.9 MODIS Aerosol Optical Depth as proxy for pollutants 90
4.2 Discussion 97
Chapter 5: Conclusion and Recommendations 102
5.1 Conclusion 102
5.2 Recommendations 103
References 105

List of Figures

Figure 1. Variation of surface and atmospheric temperatures over different land uses (Voogt, 2002 in Wong et al., 2011).....8
Figure 2. Isotherms illustrating a city layout pattern within a UHI (2a) with a concurrent cross section of air temperature measured within the urban canopy layer and surface temperatures measured under optimum UHI conditions (2b) (after Voogt, 2004).....10
Figure 3. The Msunduzi Municipality with the highlighted city of Pietermaritzburg and the location of the monitoring stations. 23
Figure 4. A scheme for land surface temperature computation using the raster calculator tool on ArcMap software. 36
Figure 5. Land use/Land Cover classified maps of the Msunduzi Municipality (2013-2017)40
Figure 6. Land Surface Temperature Autumn Maps for the Msunduzi Municipality (2013-2017). 44
Figure 7. Land Surface Temperature Winter Maps for the Msunduzi Municipality (2013-2017). 45
Figure 8. Land Surface Temperature Spring Maps for the Msunduzi Municipality (2013-2017). 47
Figure 9. Land Surface Temperature Summer Maps for the Msunduzi Municipality (2014-2017). 49
Figure 10. Seasonal Mean Land Surface Temperature Maps for the Msunduzi Municipality (2013-2017).....50
Figure 11. Seasonal Mean Land Surface Temperature Class Distribution (2013-2017). 51
Figure 12. A graphical analysis showing mean LST extracted from 1000m buffers against ambient air temperature observations between central Pietermaritzburg and Pietermaritzburg Airport (2013-2017).....53
Figure 13. A scatterplot showing the relationship between satellite retrieved LST and measured ambient air temperature at the locality of monitoring stations. 54
Figure 14. Location of buffer zones between areas classified urban and rural in the Msunduzi Municipality. 55
Figure 15. A graph showing comparison of LST between 1800m buffers between rural and urban areas in the Msunduzi Municipality.....56
Figure 16. A graph showing the mean differences of LST between SUHI buffers located in rural and urban areas in the Msunduzi Municipality. 57
Figure 17. A schematic representation of value distribution on spatial autocorrelation (ESRI, 2017). 58
Figure 18. Seasonal Mean NDVI Maps for the Msunduzi Municipality (2013-2017). 60
Figure 19. Seasonal Mean FVC Maps for the Msunduzi Municipality (2013-2017). 61
Figure 20. Seasonal Mean NDBI Maps for the Msunduzi Municipality (2013-2017). 62
Figure 21. Location of the North-to-South and West-to-East sampling transects. 64
Figure 22. North-to-South sectional comparison between mean LST, NDVI, NDBI and FVC for summer and winter. 65
Figure 23. West-to-East sectional comparison between mean LST, NDVI, NDBI and FVC for summer and winter. 66

Figure 24. Mean Land Surface Temperature per Land Cover Class between summer and winter (2013-2017). 67
Figure 25. Time plot showing hourly pollutant concentrations (ppb) versus wind speed and ambient air temperature, PMB Central Station (Jul-Aug 2017). 74
Figure 26. Windrose indicating wind speed frequency counts by percentage wind direction, PMB Central Station (Jul-Aug 2017). 74
Figure 27. Time plot showing hourly pollutant concentrations (ppb) versus wind speed and ambient air temperature, PMB Airport Station (Jul-Aug 2017). 75
Figure 28. Windrose indicating wind speed frequency counts by percentage wind direction, PMB Central Station (Jul-Aug 2017). 75
Figure 29. Time variation illustrating pollutant mean diurnal, weekly and monthly cycles for NOx, NO, NO2 and SO2 (ppb), PMB Central Station (Jul-Aug 2017). 77
Figure 30. Time variation illustrating pollutant mean diurnal, weekly and monthly cycles for NO_x, NO, NO_2 and SO_2 (ppb), PMB Airport Station (Jul-Aug 2017). 77
Figure 31. Time variation illustrating pollutant mean diurnal, weekly and monthly cycles for PM_{10}, $PM_{2.5}$ and O_3 (ppb), PMB Airport Station (Jul-Aug 2017). 78
Figure 32. Time plot showing hourly pollutant concentrations (ppb) versus wind speed and ambient air temperature, PMB Central Station (Sept-Oct 2017). 80
Figure 33. Windrose indicating wind speed frequency counts by percentage wind direction, PMB Central Station (Aug-Sept 2017). 80
Figure 34. Time plot showing hourly pollutant concentrations (ppb) versus wind speed and ambient air temperature, PMB Airport Station (Sept-Oct 2017). 81
Figure 35. Windrose indicating wind speed frequency counts by percentage wind direction, PMB Airport Station (Aug-Sept 2017). 81
Figure 36. Time variation illustrating pollutant mean diurnal, weekly and monthly cycles for NO_x, NO, NO_2 and SO_2 (ppb), PMB Central Station (Aug-Sept 2017). 82
Figure 37. Time variation illustrating pollutant mean diurnal, weekly and monthly cycles for PM_{10}, $PM_{2.5}$ and O_3 (ppb), PMB Airport Station (Aug-Sept 2017). 83
Figure 38. Time variation illustrating pollutant mean diurnal, weekly and monthly cycles NO_x, NO, NO_2 and SO_2 (ppb), PMB Airport Station (Aug-Sept 2017). 83
Figure 39. Mean hourly pollutant concentration versus mean hourly ambient air temperature during winter (PMB Central Station). 85
Figure 40. Mean hourly pollutant concentration versus mean hourly ambient air temperature during winter (PMB Airport Station). 85
Figure 41. Mean hourly pollutant concentration versus mean hourly ambient air temperature during spring (PMB Central Station). 86
Figure 42. Mean hourly pollutant concentration versus mean hourly ambient air temperature during spring (PMB Airport Station). 87
Figure 43. MODIS Aerosol Optical Depth spatial variations between July 10th, 2017 to September 10th, 2017 during the morning period, 07h00 to 09h00, in the Msunduzi Municipality. 92
Figure 44. Extracted MODIS AOD in relation to monitored selected pollutants in the Pietermaritzburg CBD (10 July 2017 – 10 Sept 2017) 94
Figure 45. Extracted MODIS AOD in relation to monitored selected pollutants at the Pietermaritzburg airport (10 July 2017 – 10 Sept 2017) 95

List of Tables

Table 1. Band arrangement and specifics of Landsat 8 OLI/TIRS (after USGS, 2016). 26
Table 2. Split-Window Coefficient Values (Sobrino *et al*., 1996 in Skokovic *et al*., 2014). .33
Table 3. Classified maps accuracy assessment showing: Producer, User Accuracies; Overall Accuracy and Kappa coefficients (2013-2017). 42
Table 4. Seasonal SUHI intensity 56
Table 5. output results from spatial autocorrelation analysis 59
Table 6. Summary statistics for correlation analysis between LST, NDVI, NDBI and FVC for N-S and W-E transects 68
Table 7. Monitored pollutants per station located in the Msunduzi Municipality 72
Table 8. Table showing the summary statistics for monitored pollutants and selected meterological variables (July-August 2017) at the PMB Central and Airport stations. 73
Table 9. Table showing the summary statistics for monitored pollutants and selected meterological variables (September-October 2017) at the PMB Central and Airport Stations. 79
Table 10. Pearson correlation coefficients between selected air pollutants and ambient air temperature observations. 88
Table 11. Tables showing the returns of correlation coefficients between AOD and measured air pollutants (a) central Pietermaritzburg, (b) Pietermaritzburg Airport 95

List of Abbreviations and Acronyms

AOD – Aerosol Optical Depth
CBD – Central Business District
FVC – Fractional Vegetation Cover
GIS – Geographical Information System
LSE – Land Surface Emissivity
LST – Land surface temperature
LULC – Land use/Land cover
MISR – Multiangle Imaging Spectro Radiometer
MODIS – Moderate Resolution Imaging Spectroradiometer
NDBI – Normalised Difference Built-up Index
NDVI – Normalised Difference Vegetation Index
NO – Nitrous oxide
NO_2 – Nitrogen dioxide
NO_x – Nitrogen oxides and their derivatives
O_3 – Surface ozone
OLI – Operational Land Imager (Landsat)
PM_{10} – Particulate Matter (10 µm)
$PM_{2.5}$ – Particulate Matter (2.5 µm)
RS – Remote Sensing
SO_2 – Sulphur dioxide
SUHI – Surface urban heat island
TIR – Thermal Infrared Region
TIRS – Thermal Infrared Sensor
TOA – Top of Atmosphere UHI – Urban heat island
UHI – Urban heat island
USGS – United States Geological Survey

Chapter 1: Introduction

1.1 Background

It is widely accepted and documented that the alteration of vegetated surfaces to impervious surfaces as well as the alteration of vegetated and wetlands into agricultural or bare waste land has significant impact on land surface characteristics (Pal and Akoma, 2009). One of these characteristics comes in the form of land surface thermal dynamics which include the extent of absorption of solar radiation, evaporation rates, surface temperature, albedo, transmission of heat to the soil, heat storage, and wind turbulence. The culmination of the changes of these surface properties can then have considerable impacts on local weather, air quality and the climate (Streutker, 2002) especially over cities through modifying energy and water balance processes, thus affecting certain environmental processes (Weng *et al*., 2004).

One of the most recognisable of these impacts is the urban heat island (UHI) which describes the effect of temperatures of the central urban area being notably several degrees higher than observations in the surrounding rural areas of similar elevation (Streutker, 2002). A warmer surface temperature exists in the urban area due to changes in land cover and population density, referred to as the urban heat island (UHI). Traditionally, UHI is linked with temperature differences between urban and rural areas through the use of *in situ* climatological data. The term surface UHI (SUHI) is however used to explicitly distinguish UHIs measured using land surface temperature (LST). Therefore, SUHI has been widely recognised as a surrogate index indirectly addressing the heat island effect (Shastri and Ghosh, 2019). Urban temperature rise is influenced by the processes of urbanisation which drastically sees changes in the patterns of land use/land cover such as changes in vegetation composition, water and increases in built-up areas. The concentration of increased temperature in urban areas is further guided by the spatial configuration and composition of an urban area especially through horizontal and vertical urban expansion, building spacing and building materials (Pal and Ziaul, 2017).

The types of spatial patterns that have characterised urbanisation are now recently being observed to have adverse impacts on the urban environment. The notion of cities as facility hubs is exacerbated by urbanisation which is the main driving process of land cover changes

and consequently the increase in land surface temperature (Voogt and Oke, 2003). Given how many cities in the world are already major sources of pollution, the increasing replacement of vegetated surfaces by impervious surfaces and the subsequent increases in surface temperature in urban areas, triggers the possibility of city environments being unhealthy and unsustainable for city dwellers.

Developing countries are experiencing increasing urbanisation and continue to put the health of the environment and public human health at risk. It is projected that land surface temperature along with various sorts of pollutants are expected to rise rapidly and are predicted to expose about 69 percent of the world's population to this vulnerability by the year 2050 (United Nations, 2010). It becomes therefore important to understand the relationships between surface temperature and air pollution in terms of concentrations and spatial variability in an urban environment. However, to understand and appreciate these interactions between urban micrometeorology and air pollution requires the committed gathering of data, observation and assessing of these urban phenomena.

The observation and studying of urban heat islands were initially carried out using high maintenance and expensive *in situ* measurements of meteorological variables which often produced biased data due to a low spatial resolution (Voogt and Oke, 2003). Through the advent of remote sensing thermal data, the first surface urban heat island (SUHI) observations were reported by Rao (1972). This has since seen numerous employments of sensor-platform combinations to capture remote observations of urban heat islands and surface temperatures that influence the urban heat island effect over a wide range of scales (Voogt and Oke, 2003).

Remotely sensed thermal data allow for the analysis of land surface temperature (LST) which is heavily influenced by the structure of urban areas and their LULC types (Xiao *et al*., 2007). Through the analysis of remotely sensed data, the modification of land cover and the spatial structure of cities is seen to cause both local air and surface temperatures to increase compared to those observed in surrounding rural areas (Streukter, 2002). Therefore, LST plays a substantial role in the energy balance of the surface by particularly modulating the air temperature of the lowest layers of the atmosphere (Xiao *et al*., 2007).

Thermal imagery allows for the estimation of LST through various algorithms depending on the configuration of the thermal bands. Landsat 8 TIRS data allow for the use of split-window

algorithms for LST estimation (Rozenstein *et al*., 2014). However, single channel retrieval methods can also be employed on the data (Wang *et al*., 2015). The application of remote sensing can then provide the necessary tools to study the relationships between the surface and the atmosphere. The land cover/land use of an urban area is also noted as an important parameter in the analysis of urban heat islands (Feizizadeh and Blaschke, 2013). Thus, the formation of UHIs through the heating of urban areas depends highly on the type of surfaces that make up the urban fabric and their respective thermal properties. From this, UHIs can be considered as a response to urban land transformation (Feizizadeh and Blaschke, 2013) and an integral part of city climates as they represent the modification of the local climate by the urban fabric initiated by anthropogenic activities (Preston-Whyte, 1970).

The urban heat island effect has been subject to multiple studies in different cities around the world and various reasons for the urban/rural temperature variance have been submitted: Houston, Texas (Streutker, 2002), Pakistan (Shah and Ghauri, 2015), Shanghai (Li *et al*., 2011) and Egypt (Abutaleb *et al*., 2014). The notable reasons for the urban/rural temperature variance and consequently the urban heat island effect according to Oke (1978) in Tyson and Preston-Whyte (2000) are: excessive counter radiation from absorption of outgoing long-wave radiation and re-emission by a polluted urban atmosphere; reduced net long-wave radiation loss from urban canyons as buildings result in the reduction in the sky view factor; substantial daytime heat storage by artificial urban materials leading to night release; anthropogenic heat from building sides; reduced evaporation from deforestation and the surface waterproofing of the city and the decreased loss of sensible heat due to the reduction of wind speed in the urban canopy. This is not an exhaustive list, but it covers the major factors leading to the formation of urban heat islands.

Air pollution as noted in the above list is also a problem for most South African cities (Zunckel *et al*., 2004). It presents an important factor in the studying of urban heat islands as the increase in urban albedo and the re-radiation of longwave radiation is considerably due to high levels of pollution (Streutker, 2002). The understanding of the combined consequences of urban heat and air pollution island effects is an important aspect as it prioritises the understanding of the strong interactions between urban micrometeorology and air pollution (Sarrat *et al*., 2006). This bases the core concept of the study where remote sensing provides the necessary tools to understand the relationships between city fabric (land use/land cover) and its interaction with

incoming solar radiation and air quality in creating a unique thermal environment due to the varying properties that make up urban areas.

1.2 Research problem

The impacts of urban heat islands on air quality in South African cities have been under studied. In addition, a deficit of remotely sensed medium-to-high resolution UHI studies of cities in South Africa is a concern. This limits the understanding of the impacts UHIs have in the context of South African cities in terms of their spatial patterns and UHI distribution, air pollution and potential threats to environmental and human health. It is therefore important to recognise that in order to promote sustainable urban land planning in our city landscapes, the understanding of the relationships between the urban fabric, the atmosphere and air quality will provide a base to inform policies and the development of mitigation strategies to ideally reduce the impact of UHIs and air pollution in priority areas.

The Msunduzi Municipality provides a unique environment especially with the city of Pietermaritzburg lying in a deep basin where it experiences regular down-valley advection of cold air and a sustained inversion layer capping the city (Tyson and Preston-Whyte, 2000). These factors carry serious implications for the residents of Pietermaritzburg as they are potentially exposed to sustained periods of pollution especially with the proximity of fixed pollution sources. An investigation into the presence and extent of urban heat islands could potentially reveal the spatial patterns between surface urban heat islands (SUHIs) and pollution over the city and its surrounding areas. Furthermore, assessing the relationships between LST and parameters of land cover (land cover indices) in a unique terrain of the municipality would bring light to the links between the thermal characteristics of the urban fabric and their impact in the distribution of surface temperature in the city landscape.

1.3 Research Question

How does the presence of urban heat islands influence the spatial and temporal variation of measured air pollutants in the Msunduzi Municipality?

1.4 Aims and Objectives

1.4.1 Overall aim of the study

The study aims to understand the relationships between land cover and land surface temperature in the Msunduzi Municipality and how these parameters influence the resulting air temperature. In addition, due to temperature and other meteorological parameters playing a significant role in the distribution of certain pollutants (Lourens *et al*., 2011), the study aims to add onto the understanding of the spatiotemporal distribution of measured air pollutants. The study then further aims to give an account of the thermodynamic nature of the city fabric to aid the understanding of the interactions between the distribution of surface temperature and air pollution using remote sensing techniques over a period of five (5) years (2013-2017). This ultimately provides the characterisation of the links between temperature, land cover/land use and air pollutants in the Msunduzi Municipality.

1.4.2 Specific research objectives

- To investigate and characterise the nature and extent of the surface urban heat island effect in the Msunduzi Municipality

- To determine the relationship between land surface temperature and different land cover classes using remote sensing land cover indices

- To assess the impact on pollutant concentrations with the development of the atmospheric urban heat island whilst briefly evaluating MODIS Aerosol Optical Depth as a potential proxy for measured air pollutants in the Msunduzi Municipality

1.4.3 Significance of research

The studying of urban heat islands presents an opportunity to understand the extent to which the local climate of cities has been transformed by human activity through urbanisation and land transformation (Feizizadeh and Blaschke, 2013). It is important to note that about 60% of South Africans live in urban areas and this may result in about more than 50% (Stats SA, 2009) of the population being negatively impacted by the adverse effects of UHIs. Urbanisation in South Africa is propelled by the distinctive urban spatial patterns guided by Apartheid legislature where places of residency for the majority were situated far from the city (Berrisford, 2011). This has seen the recent surge into urban spaces (Stats SA, 2009) and thus leaving a greater portion of the population under threat of the increased heat in urban spaces

and its consequent effects – particularly due to the increased air pollution in most cities across South Africa (Lourens *et al*., 2011).

The use of GIS and Remote Sensing techniques offer the possibility of identifying, analysing and mapping UHIs and their impacts on the environment. In the case of the analysis of the relationship between UHIs and air quality, the study would ultimately provide information that would assist in the adaption of better air quality and land planning policies (Stone Jr, 2005). In addition, with appreciating the substantial role cities have on local and regional scale meteorology, decision makers may promote resilience in urban environments by incorporating research driven decisions to address both current and future risks related to climate change (Lee and Hughes, 2016).

It has come to attention that despite the various climate hazards faced by cities, it is only a few that have developed adaptation agendas on a global scale. Even more so, these existing adaptation agendas vary widely thus making comparison and evaluation difficult (Lee and Hughes, 2016). This has been attributed to a lack of technical resources, low institutional capacity and in most cases, constrained financial and human resources. This therefore creates a situation whereby cities fail to recognise the interaction between certain climatic hazards and the guiding processes behind them (Lee and Hughes, 2016). This study, therefore, gives provision to some of the necessary knowledge in creating a possible network of information for better adaptation strategies for South African cities concerning air quality, land use planning and urban micrometeorology.

1.4.4 Structure of Thesis

Chapter 1 is the introduction to the study which includes the background to the phenomena of surface urban heat islands and their influence on air pollution as well the associated impacts. In addition, this chapter delivers the research problem as well as the research question with further details on the aims and the specific objectives of the study. To end chapter 1, the significance of the research is offered to highlight the urgency to address the state of the cities and their potential threat to climate change and how GIS and Remote Sensing are necessary tools to aid in assessing the environment.

Chapter 2 provides a detailed review of literature on the study of surface urban heat islands with the use of GIS and Remote Sensing. This chapter discusses the phenomena of UHIs/SUHIs with regards to their formation and impacts. In addition, the interlinked associations of heat islands, air pollution and temperature inversions are dealt with amongst the data required for the analysis thereof.

Chapter 3 describes the study area and its significance to the study of SUHIs, particularly with air pollution associations. This chapter also serves to make available the data and data analysis techniques used for the study and the relevant structures and treatment of the datasets as well as their limitations.

Chapter 4 is the results and discussion section where the attempts to reach the objectives outlined in chapter 1 are provided and discussed at length. This chapter provides the results for each objective.

Chapter 5 concludes on the study with the conclusions and recommendations section. Here, a detailed conclusion to each objective and the extent to which it was achieved is discussed. This section also rounds up on the study to provide a holistic summary to the aims the study intended to address. Finally, recommendations are provided in the interest of further SUHI and air pollution research as well as suggestions that the Msunduzi Municipality can explore in mainly reducing heightened levels of pollution and mitigating for the impacts of SUHIs.

Chapter 2: Literature Review

2.1 The Urban Heat Island

The presence of heat islands in different layers of the lower urban atmosphere can be distinctly classed into two categories, namely: the atmospheric urban heat island and the surface urban heat island (Yuan and Bauer, 2007). Atmospheric urban heat islands (AUHIs) include the canopy layer (the region closest to the surface) heat island and the boundary layer (region above the canopy layer) island which indicate the heating of the urban atmosphere, while the surface urban heat island (SUHIs) describes the relative heating up of urban surfaces in contrast to the surrounding rural areas and is normally recorded as land surface temperature through airborne or satellite thermal infrared remote sensing (Yuan and Bauer, 2007). Surface temperatures have a secondary, but a notable influence on air temperatures especially in the canopy layer (Figure 1). SUHIs are present during both day and night; however, they are most intense during the day and during summer (Voogt and Oke, 2003). This differs for AUHIs, wherein they can be minor or absent during the day on some occasions. These are most intense at night and during winter.

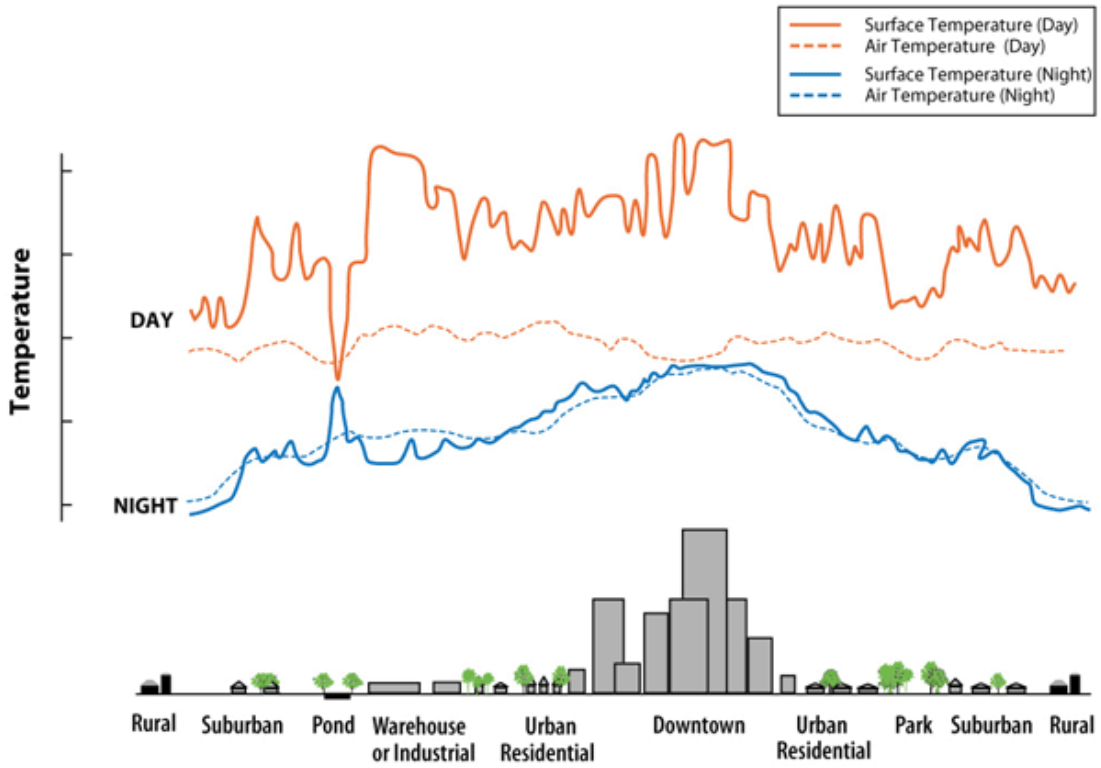

FIGURE 1. VARIATION OF SURFACE AND ATMOSPHERIC TEMPERATURES OVER DIFFERENT LAND USES (VOOGT, 2002 IN WONG ET AL., 2011).

The secondary influence of land surface temperatures can be seen for example, vegetated areas like parks usually have cooler surface temperatures which consequently contribute to cooler air temperatures (Wong and Yu, 2005). Conversely, concentrated built-up areas lead to warmer air temperatures. As air mixes within the atmosphere, it is important to note that the relationship between surface and air temperature is not always constant (Voogt and Oke, 2003). The heating of urban areas and the formation of urban heat islands (UHIs) is a response to urban land transformation and has become of great interest in numerous science disciplines (Feizizadeh and Blaschke, 2013). It is an integral part of the city climate as it represents the modification of local climate by the urban fabric (Preston-Whyte, 1970).

The basic understanding of urban heat islands stems from the energy budget equation that explains the balance of incoming and outgoing energy flows or fluxes (Tyson and Preston-Whyte, 2000). What results in the urban heat island effect is broadly determined by the relative difference in energy flux and storage terms noted between the urban canopy layer and surrounding rural areas (Tyson and Preston-Whyte, 2000). The typical comparison of the surface energy budgets between cities and their surrounding rural areas often reveals notable contrasts. This is due to LULC contrasts and most notably anthropogenic activity. Due to these contrasts, the retention and transfer of heat is affected and can then lead to varied surface and air temperatures between urban and rural areas (Voogt and Oke 2003).

The studying of urban climatology recognises that UHIs are a signal that reveals a range of important land surface changes that affect human health, ecosystem function, local weather and possibly the climate (Voogt and Oke, 2003). The result of these changes in the land surface is mainly due to an increasing population leading to intensified pressure on natural resources particularly in developing countries (Feizizadeh and Blaschke, 2013). In addition, this rapid population increase occurs in combination with urbanisation and expansion. These lead to invasion into agricultural and green areas, therefore destructing vegetation coverage (Feizizadeh and Blaschke, 2013). The obvious LULC changes, especially the conversion of vegetated surfaces to impervious surfaces in cities, in aggregation with population growths have adverse environmental impacts such as increased surface heat retention (Feizizadeh and Blaschke, 2013). These issues represent a phenomenon that characterises the relationship between land use/land cover and the climate of an urban area, with regard to temperature dynamics.

The UHI phenomenon has been considered as a very well researched example of anthropogenic climate modification in urban climate studies (Arnfield, 2003). When urban heat islands are observed it is seen that isotherms (lines of equal temperature) form a pattern that is similar to the layout of the city or an urbanised region that is surrounded by cooler areas. The structure of the urban heat island is characterised by a sharp rise in the canopy layer air temperature boundary situated between rural and suburban areas (Voogt, 2004). This rise is followed by a gradual and often variable increase near the downtown core of an urban area – where the warmest temperatures are observed (Figure 2).

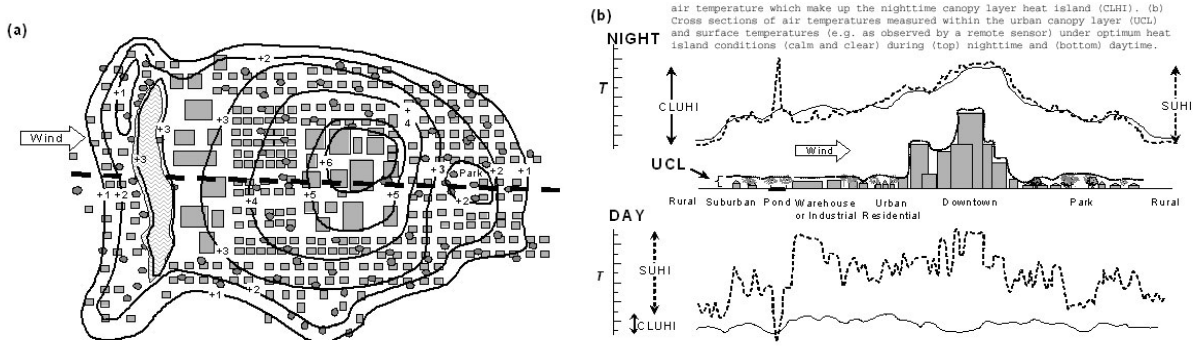

FIGURE 2. ISOTHERMS ILLUSTRATING A CITY LAYOUT PATTERN WITHIN A UHI (2A) WITH A CONCURRENT CROSS SECTION OF AIR TEMPERATURE MEASURED WITHIN THE URBAN CANOPY LAYER AND SURFACE TEMPERATURES MEASURED UNDER OPTIMUM UHI CONDITIONS (2B) (AFTER VOOGT, 2004).

In the boundary layer, the urban heat island indicates much reduced variability than other heat island types. A cross section through the UHI shows a dome-like shape followed by the transportation of warmer air downwind of the city (Voogt, 2004). Increasing studies analyse urban climates with a focus on ambient temperature contrasts between cities and their surrounding rural – a method that describes the UHI effect (Feizizadeh and Blaschke, 2013). Although UHIs had been considered as the contrast between urban and rural areas, recent developments in cities have reduced the once distinct borderline between 'urban' and 'rural' areas due to urban growth and urbanisation (Ngie *et al*., 2014). As a result, UHIs can be considered in terms of the difference between the central parts of the city and its surrounding areas and these are influenced by various factors at the Earth's surface (Ngie *et al*., 2014).

2.2 Factors influencing SUHI

Most environmental issues stem from anthropogenic activities and the urban heat island phenomenon displays the effects which result from the extent to which the environment has been altered by humans. The notable causative factors of the UHI phenomenon include urbanisation and various anthropogenic activities (Ngie *et al*., 2014). These factors alter the physical characteristics of the surface such as albedo, thermal capacity, heat conductivity and moisture. Notable factors that contribute to the formation of UHIs are the increased use of pavements, building structures, the use of concrete, asphalt and metal in urban spaces which leads to the heat retention by the Earth's surface (Wang *et al*., 2007). In addition, the replacement of soil and vegetation which particularly helps to reduce air temperature through evaporation also influences the increase of surface temperatures and consequently ambient air temperature (Ngie *et al*., 2014).

The properties of urban materials especially with regards to solar reflectance, thermal emissivity and heat capacity influence the development of urban heat as they control how incoming solar radiation is reflected, emitted and absorbed (Ngie *et al*., 2014). Furthermore, urban geometry also influences UHI development where the configurations of buildings within a city are found to impact on the wind flow, energy absorption and the ability of a surface to emit longwave radiation back into the atmosphere (Ngie *et al*., 2014). This is through the presence of narrow streets and tall buildings creating what is called urban canyons where air movement is intercepted (Voogt and Oke, 2003).

The geographic location of a city factors in the climate and topography of the area which have an influence on UHI formation. Oke (1973) notes that nearness to large water bodies and mountainous terrain can influence local wind patterns and impact of the formation of urban heat islands. An example can be seen with how mountain ranges serve to block wind from reaching a city or on other occasions form flows of winds that pass through a city – impacting on the heat distribution within city and thus the development of UHIs (Oke, 1973). It has also been outlined that in general, episodes of calm winds and clear skies encourage the formation of UHIs as these conditions capitalise on the amount of solar energy reaching the urban surface while maintaining less amount of heat that can be convected away. This process can also work

conversely where strong winds and cloud cover would work to suppress UHIs through the convection or reflection of warm air away (Ngie *et al*., 2014).

The relationship between LULC patterns or changes and urbanization has a crucial impact on the intensity and spatial pattern of the urban heat island effect (Chen *et al*., 2006). Different land uses influence UHI in different ways, attributable to the varying surface properties. An important factor in assessing UHIs and LULC patterns is land surface temperature (LST) (Feizizadeh and Blaschke, 2013). The alteration of surface soil, water content and vegetation has shown through LST research that it can influence the balance of land surface energy (Feizizadeh and Blaschke, 2013). Therefore, incoming and outgoing radiation of urban surfaces is closely related to the distribution of LULC characteristics (Feizizadeh and Blaschke, 2013). Chen *et al*. (2006) studied LULC patterns within urban areas where it was found that a high concentration of impervious surfaces, high population density and frequent anthropogenic activities add to the intensity of urban heat islands.

Another factor that contributes to the formation and presence of urban heat island is heat produced from anthropogenic activities and the functions of a city such transportation, industrial processes and the totalling of all energy use for heating and cooling. This largely depends on the functions of the city (Voogt, 2004). In most cases, urban heat islands are usually easily identified in cities located in valleys which are characterised by enhanced nocturnal cooling that occurs through katabatic drainage of cold air (Tyson and Preston-Whyte, 2000). This situation allows for the immediate discerning of the city warming effect in such cities than those located on ridges which in any case tend to be warmer by night than adjacent valleys. The factors contributing to the formation and proliferation of urban heat islands are also responsible for numerous socio-economic, public human and environmental health impacts (Tyson and Preston-Whyte, 2000).

2.3 UHI impacts

The elevation of temperatures from urban heat islands, especially during summer, can affect the environment of a community and their quality of life. In some instances, some heat island impacts can be considered positive such as in the prolonging of the growing season (Baker *et al*., 2002). However, most SUHI and UHI impacts are noted to have implications on the health of the environment and the public. These include:

(i) Effects on localised precipitation where induced uplift due to increasing temperature sees rising parcels of air eventually cooling and forming rain-producing clouds which can bring urban-induced rainfall for areas downwind the city (Bornstein and Lin, 2000).

(ii) Increased energy demand due to requirements for cooling during elevated summer temperatures in cities – adding pressure to the power grid leading to increased air pollutant and greenhouse gas emissions. The pollutants released from most power plants include SO_2, NO_x, PM and CO, which also contribute to global climate change (Lourens *et al*., 2011).

(iii) Air quality, as temperature is an important factor in the proliferation of air pollution. For example, elevated temperatures have been studied to increase the rate of surface ozone production which is produced when nitrogen oxides (NO_x) react with volatile organic compounds (VOCs) in the presence of sunlight (Zunckel *et al*., 2004).

(iv) Compromised human health and comfort as the culmination of UHI and the reduced air quality can lead to the general uneasiness, respiratory difficulties, heat cramps and exhaustion, as well as heat-related deaths (Tan *et al*., 2010).

(v) Impaired water quality as pavements and rooftop surfaces reach temperatures of 27 to 50 degrees Celsius higher than air temperatures and transfer excess heat to storm water (Wong *et al*., 2011). SUHIs therefore lower water quality through thermal pollution and can impact on streams, rivers and the aquatic life contained in these by affecting metabolism and reproduction of aquatic biota (Wong *et al*., 2011).

To mitigate the effects of urban heat islands, mitigation strategies to counter the presence of SUHIs and UHIs have been suggested. A common means to reduce the effects of concreted environments is to promote green areas as an ecological measure. Vegetated surfaces have a

different Bowen ratio than bare or mineral surfaces as they convert incoming solar radiation into energy for transpiration and photosynthesis through plants – consequently reducing the sensible heat flux (Ngie *et al*., 2014). Remotely sensed Normalized Difference Vegetation Index (NDVI) is often used to estimate surface temperatures and has shown in studies that the presence of vegetation influences observed LST values (Ngie *et al*., 2014). Studies have shown that temperatures recorded over green areas are generally lower than those recorded in a built environment (Kikegawa *et al*., 2006).

Recent research has focused on the studying and the development of 'cool coloured' materials that use specifically modified colours that reflect particularly well in the infrared wavelength (Rosenthal *et al*., 2007). Such research will see products that can be dark in colour but provide a solar reflectance close to that of a white or light-coloured material (Rosenthal *et al*., 2007). The introduction of such material would mitigate against the excessive heat retention at the surface. Since the urban landscape has been manipulated and this has consequently led to the presence of urban heat islands, it is then possible to lessen the urban heat island effect by improving land use planning (Rosenthal *et al*., 2007). To quantify the relationship between the heat islands and the landscape by applying land cover indices provides insight into the behaviour of the landscape.

2.4 Relationship between LST and land cover indices

Different land cover types are noted to have different thermal properties and thus influence the spatial distribution of land surface temperature and subsequently the ambient temperatures observed above a specific area (Wong and Yu, 2005). The UHI effect has been found to be weak over areas containing water bodies such as dams, streams and high levels of vegetation while it has been observed to be stronger in built up areas and areas with a greater portion of impervious surfaces. To quantify the behaviour of land classes and land surface temperature, various land cover indices can be used. This approach has been widely used and LST has been observed to have varying relationships with land cover indices.

The relationship between LST and NDVI is one that contrasts with seasons as the greenness of vegetation varies between wet and dry seasons. On a regional basis, Li *et al*. (2011) note that the statistical relationship between mean LST over the whole range of NDVI values is highly nonlinear. However, a strong negative linear relationship is observed between mean LST and positive NDVI due to the presence of vegetation. Li *et al*. (2011) show a heightened variation in the relationship between LST and NDVI in the cases of high NDVI, especially during summer. This observation has also been noted in the study by Yuan and Bauer (2007).

It is often argued that fractional vegetation cover (FVC) better represents the abundance of vegetation than NDVI even though they are closely related (Song, 2004). This is due to the likelihood of NDVI saturating at high FVC when the background is dark. Li *et al*. (2011) found that FVC had a slightly stronger relationship with LST than NDVI where an R^2 value of 0.9957 was recorded for the summer period; however, variations do exist between seasons. The investigation of LST and percent impervious surface (ISA) sees LST generally increasing with percent ISA (Li *et al*., 2011). Li *et al*. (2011) also observe that a substantial variance in LST usually occurs for areas with high percent ISA. Generally, in their study, a strong linear relationship between LST and ISA was observed based on regional mean values in early spring and summer giving R^2 values of $R^2 = 0.8545$ and $R^2 = 0.9843$, respectively.

Built-up areas serve as major trappers of heat within urban areas. Chen *et al*. (2006) provide a qualitative and quantitative analysis between land use/land cover (LULC) and UHI where they also analyse the relationship between LST and the normalised difference built-up index (NDBI). In their study, mean values of NDBI and linking temperature intervals were used. From this analysis, an R^2 value of 0.9848 ($r = 0.995$) was observed between LST and NDBI – indicating a statistically significant positive relationship. As land cover can be seen to influence surface temperature observation, the subsequent increase of ambient temperatures and the formation of urban heat islands can also impact significantly on local pollution.

2.5 Impact of inversions and urban heat islands on local atmospheric pollution

The phenomenon of UHIs is influenced largely by urbanisation which is closely related to increasing pollutant emissions. Within the space of an urban area, the consequences of combined urban heat and pollution islands call for the concern to explore and understand the strong interactions between urban micrometeorology and air pollution (Sarrat *et al*., 2006). A case for local impacts of urban heat island on atmospheric pollution in South Africa can be drawn from the city of Pietermaritzburg.

Records of reports have often noted the air pollution problem in Pietermaritzburg, dating back to the 1980s. The city of Pietermaritzburg offers a unique combination of the causes that usually lead to sustained periods of air pollution episodes. Firstly, the city is located in a deep basin – causing it to experience regular down-valley advection of cold air which induces the effect of the pronounced valley inversion (Tyson *et al*., 1972). Secondly, bad town planning has resulted in all its main industries and the landfill site being located in the city's bowl – resulting in the worsening of air pollution. In addition, the N3 major highway dissects the city, which carries an ever-increasing number of large trucks and vehicles which contribute to emissions. The routine burning of timber plantations on the escarpment of the city's basin and the famous sugar plantations on the hilltops, also adds to the pollution problems of the municipality (Msunduzi SDF, 2009).

The above situation plays out in the following manner: the city's location in a valley causes a temperature inversion to occur, which on its own is not a normal phenomenon. This effect may worsen during the winter season where cold air sinks down and remains at the base of the valley where frost may also occur. As cold air is deposited at the base of the valley, it causes the warm air, with pollutants, to rise above the cold air mass to form a thermal belt (Tyson and Preston-Whyte, 2000). It is this belt that then traps pollutants above the city – heightening their adverse properties and inducing the negative health impacts associated with the various pollutants which cannot escape (Tyson and Preston-Whyte, 2000). These stable layers created by urban heat islands and inversion layers then trap hazardous smog over the city centre, where an increase in temperature leads to the proliferation of pollutants, especially secondary pollutants such as surface ozone. It is therefore in these situations where temperature and wind are seen

to be very important factors in air pollution concentrations as they impact on the concentration, composition and transportation of air pollutants.

The emission of pollutants in cities from human activities can be mainly propelled by thermodynamic processes involved in the cities as seen in the case of Pietermaritzburg. The down-valley advection of cold air as mentioned above, would ideally promote cool conditions at the base of the city, with the pronounced valley inversion having greater temperature impacts in the higher altitudes of the city. In this instance, it is therefore seen and with little doubt, possible to conclude that recorded increased temperatures associated with the central city and the floor of the basin, are a result of urban warming (Tyson *et al*., 1972).

The presence of urban heat islands above cities, influenced by surface urban heat islands below, leads to the concentration of pollutants in a dust dome due to the convection that lifts pollution into the air (Tyson and Preston-Whyte, 2000). The pollution remains trapped in the atmosphere due to the somewhat stable air masses created by the presence of urban heat islands and inversion layers. The inversion conditions provide the capping of dust and other particulates at a lower than usual level in the atmosphere where in the absence of winds, the layer of pollution remains intact and can have adverse impacts the environment and human life (Tyson and Preston-Whyte, 2000).

These thermodynamic processes found in the cities mainly determine the spatial distribution and temporal evolution of air pollutants in the city. A comparison of the distribution of UHIs and PM_{10} values was done by Feizizadeh and Blaschke (2013) where a cross-comparison (LST vs PM_{10} concentration) indicated a high correlation between highly air-polluted areas and UHI zones in Tabriz city, Northwestern Iran. In addition, the UHI zone with LST of 25-27 degrees Celsius was identified as the highest temperature zone in the central part of the city and coincided with the highest air pollution (Feizizadeh and Blaschke, 2013). The overall study showed evidence for a high correlation between LST, UHI and air pollution in the Tabriz city.

2.6 The detection and studying of urban heat islands

To study urban heat islands requires their detection which is done through the measuring surface or air temperatures. Rao (1972) first pioneered the study of urban climates by demonstrating that the identification of urban areas is possible from the analyses of thermal

data acquired by satellite imagery. On the other hand, the measurement of UHIs has been done through the usage of different instruments and at various levels to account for the intermittent relationship between surface and air temperatures. According to Voogt (2004) substantial differences in radiative cooling between central urban areas and surroundings occur during clear and calm nights and help create conditions that allow for the best UHI observations.

The detection and studying of urban heat islands recognises that, like any other meteorological phenomenon, UHI characteristics change under different geographical locations (Ngie *et al*., 2014). The advent of satellite remote sensing has allowed the possibility of spatial mapping over larger areas, with not only measuring the magnitude of SUHI but being able to adopt multiple analysis techniques. These techniques allow for the observation of the SUHI effect, in addition, they provide for the study of its causation through the combination of remote sensing and urban micrometeorology (Voogt and Oke, 2003). Various approaches have been employed in studying the SUHI effect with the aim to measure its magnitude, extent, relationship with land cover and their impacts on micrometeorology and air quality. Yuan and Bauer (2007) found that LST provided a stronger relationship with percentage impervious surface area (ISA) than the normalised difference vegetation index (NDVI) in a quantitative measure of the SUHI effect.

Sarrat *et al*. (2006) have studied the impact of an urban land cover on local meteorology and spatial distribution of atmospheric pollutants over a region in Paris where it was found that nocturnal and diurnal urban effects, especially urban heat island induced turbulence, impact on the spatial distribution of primary and secondary regional pollutants, in particular surface ozone and nitrogen oxide. Musakwa and Van Niekerk (2015) have also carried a land cover study in Stellenbosch and found that areas with high concentrations of impervious surfaces (usually above 60% per hectare) located in the CBD, Stellenbosch University campus as well as Idasvallei can greatly increase the SUHI effect and surface water run-off.

A study by Hardy and Nel (2015) revealed through an assessment of LST data with classified Landsat data that areas with dense vegetation in the city of Johannesburg are cooler and represent lower SUHI values in contrast to less vegetated areas. Furthermore, this study reiterated the observation of higher temperatures in highly built-up and densely populated such as city centres than the surrounding areas. In addition, it was found that the SUHI effect is

strongest during the night over Johannesburg's northern suburbs and areas with high building density.

2.7 Satellite remotely sensed data

2.7.1 Remotely-sensed thermal data

Remote sensing as a tool has offered a cost-effective method to obtain information for the studying of Earth phenomena. Satellite imagery has helped overcome the limitations that come with the use of *in situ* data that often provide localised and biased data. The use of remotely sensing for observing the spatio-temporal land cover changes with a focus on the basic property of materials used on urban structures is particularly useful. These properties are related with the surface radiance and emissivity data (Joshi & Bhatt, 2012) and aid in detecting and studying UHIs. The equipment in use however should have the capabilities of detecting heat emitted by objects and the ability of producing infrared images of the object in study.

The region between 3-35 μm of the electro-magnetic is called the thermal-infrared region (TIR) (Ngie *et al*., 2014). Data used to estimate LST are currently offered by satellite TIR sensors that provide different spatial resolution and temporal coverage data. The thermal-infrared region offers advantageous spectral bands although they are limited by the intensity of radiation emitted and the atmospheric windows (Rozenstein *et al*., 2014). Between 8 and 14 μm lies an excellent atmospheric window in which most remote sensors are configured to detect the thermal radiative properties of materials on the surface (Rozenstein *et al*., 2014).

Landsat Thematic Mapper (TM) and Enhanced Thematic Mapper Plus (ETM+) thermal infrared (TIR) data with 60 m and 120 m spatial resolutions, respectively, have been applied for local-scale studies of UHIs (Chen *et al*., 2006). Landsat 8 now offers better resolution (100 m for thermal, 30 m for visible) although with less frequent TIR observations. However, MODIS and AVHRR satellites provide more frequent measurements. Therefore, the data from these satellites can be used in composition to counter the trade-offs between the spatial and temporal resolutions offered by the satellites (Rozenstein *et al*., 2014).

2.7.2 Remotely-sensed air quality data

The use of satellite remote sensing in air quality studies has been a cost effective yet powerful tool to estimate, especially Particulate Matter concentrations from the retrieved parameter of Aerosol Optical Depth (AOD) offered by sensors such as the Multiangle Imaging Spectro Radiometer (MISR) and the Moderate Resolution Imaging Spectroradiometer (MODIS) instruments. AOD data represents PM loading in the air and are non-dimensional parameters calculated as the result of light extinction by aerosols from ground-level up to the top of the atmosphere (Ghotbi *et al*., 2016). The prediction of ground-based PM and related air pollutants by satellite data is challenging especially due to the composition of particles and their various physical specifications affecting the dependency of AOD retrieval on optical properties. In addition, missing data are usually problematic due to cloud contamination in the upper atmosphere which could disturb the PM-AOD relationships (Ghotbi *et al*., 2016).

The MODIS instrument had been tasked to observe the Earth from the Terra and Aqua satellites since 2000 and 2002, respectively. From the various physical parameters derived from MODIS spectral radiances, there are a collection of products that characterise aerosol particles. The aerosol product had been delivered at a 10 km resolution retrieved through the dark target method for more than a decade (Ghotbi *et al*., 2016). The resolution of this product did not perform particularly well in urban studies. This led the NASA research team to develop and release a nominal 3 km product which was released as part of collection 6. The look up tables, inverse methods and the retrieval algorithm remained the same as the original MODIS dark target aerosol algorithm with the organisation and selection of pixels to retrieve the AOD product being the main difference.

The 3 km product is similar to the 10 km product; however, the finer resolution can resolve fine resolution features such as smoke plumes over both ocean and land (Ghotbi *et al*., 2016). It is however important to note that the retrieval of aerosols using the dark target algorithm has a limitation over bright or urban surfaces. This may cause issues of overestimation of AOD which is an issue in localised studies (Ghotbi *et al*., 2016).

The analysis of air quality and pollution concentrations with the application of AOD data has been dominated using simple linear regression as the simplest type of statistical model to characterise the relationship between AOD and PM. These have resulted in varied performances for PM predictions where correlation coefficients have usually ranged between 0.2 – 0.6 (Wang and Christopher, 2003; Engel-Cox *et al*., 2004). Further improvements have

been made to the simple-regression models with uncertain predictive power, with extensive studies exploring more dynamic and multivariate regression models. These have included other important variables such as meteorological parameters, land use data and geographical information to generate stronger and more robust relationships between AOD and PM and other pollutants (Ghotbi *et al*., 2016).

Urban atmospheres and surfaces are subject to multiple impacts, most of which are anthropogenic. This is especially seen in air pollution and the formation of urban heat islands where the interactions between urban landscapes and atmospheres result in adverse conditions as this relationship has been greatly disturbed by anthropogenic triggers. To understand these relationships and the extent to which they have been perturbed, it is important to have studies that investigate and aim to provide extensive coverage to the apparent results of anthropogenic impacts to the environment. This study offers an understanding to the urban local meteorology concerning heat island conditions and local air pollution of the Msunduzi Municipality, with a focus on the city of Pietermaritzburg.

2.8 Literature Summary

Atmospheric and surface heat islands characterise the extent to which urban atmospheres continue to be altered and impacted by anthropogenic effects. With intensifying urbanisation and the increase in pollutant emissions to the atmosphere, cities located uniquely such as Pietermaritzburg are more vulnerable to the adverse environmental impacts. The interactions between the atmosphere and the land surface are sensitive and may greatly result in modified meteorological episodes and thus rapidly influencing the climate. Remote sensing applications allow the possibilities of performing analyses on atmospheric and land surface phenomenon at a wider spatial extent, therefore offering better spatial and temporal assessments over study areas. Multiple studies have dealt with urban heat islands and pollution where land surface temperature, land cover indices and atmospheric composition products have been retrieved from satellite imagery. These data provide the necessary platform to undertake remote sensing studies to better understand the environment using cost-effective methods. Limitations are noted in the application of these data, however improvements to the accuracies of these data are becoming a fast reality.

The above literature review provides a detailed background to urban heat islands and air pollution as well as factors influencing their development and proliferation. In addition, the resulting impacts of these processes are offered. Regarding the means with which the study uses for analysis, the expected relationships between land surface temperature and land cover indices are provided with reference to previous literature. The importance of understanding the relations between atmospheric and land surface phenomena is briefly highlighted where also a detailed outline of the data applied in the study is provided.

Chapter 3: Materials and Methods

3.1 Study area

The Msunduzi Municipality of the greater Umgungundlovu District is home to the city of Pietermaritzburg, located in the KwaZulu-Natal midlands, South Africa. Of significance to the study area, the city is located relatively central at 29.6006° S, 30.3794° E in a deep valley basin which determines much of the dominant local climate (Figure 3). In general, the Msunduzi Municipality offers a favourable climate for most parts of the year. Pietermaritzburg city lies between 1000 – 1400m above sea level and experiences moderately warm temperatures where the average daily maximum is 26 degrees Celsius (Msunduzi SDF, 2009). However, temperatures of over 35 degrees Celsius are often recorded, especially during the warm months of December to May. The city also experiences cool temperatures during the cooler months where temperatures of around 11 degrees Celsius are usually observed between May and August. Its location in a deep basin means the city experiences a regular down-valley advection of cold air (Tyson and Preston-Whyte, 2000).

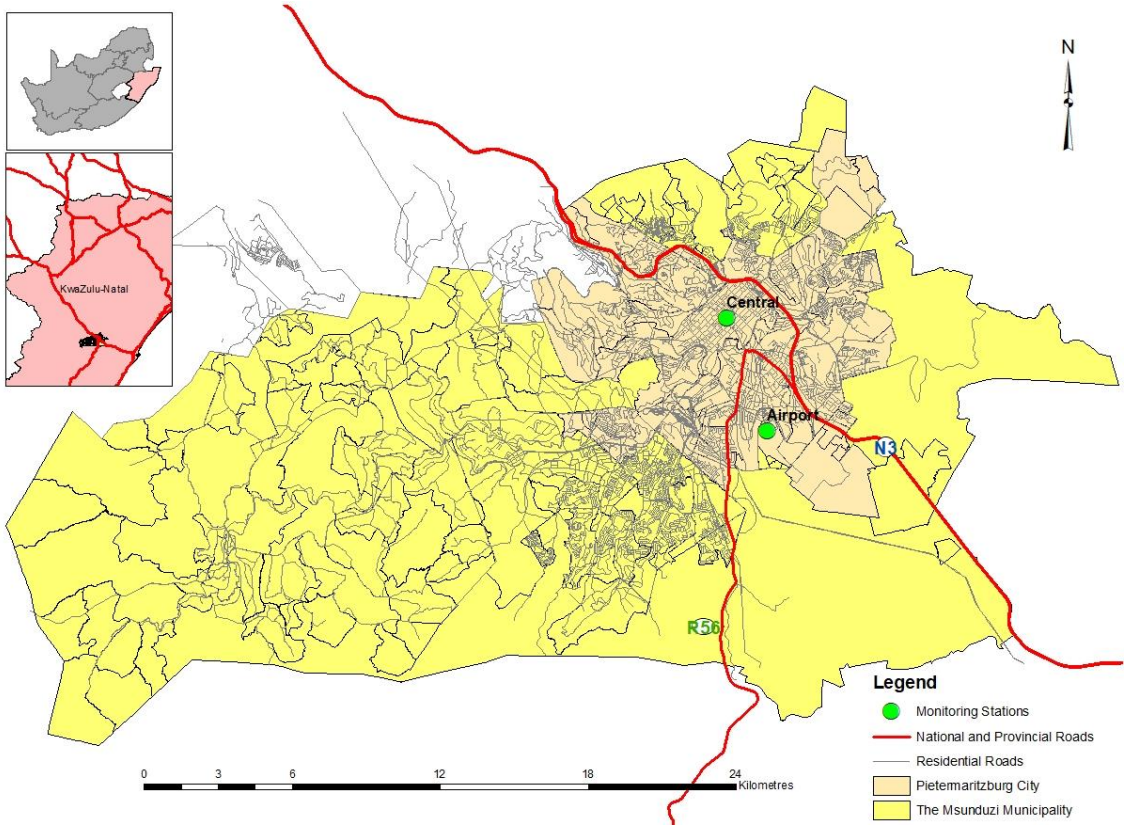

FIGURE 3. THE MSUNDUZI MUNICIPALITY WITH THE HIGHLIGHTED CITY OF PIETERMARITZBURG AND THE LOCATION OF THE MONITORING STATIONS.

It is these down-valley winds which would ideally create cool conditions during the night until early morning. This situation provides the opportunity to then study the offset of cooling through the possible warming due to heat island conditions in the city and surrounding areas within the Msunduzi Municipality. An average of 844 mm of precipitation is distributed across the year where over 138 days generally receive at least 1 mm of rain. The city's wettest periods are from January to March and from September to December. This creates a generally mildly warm climate for the city, with relatively high rainfall. These are suitable weather characteristics that have made the city attractive for human and business settlement.

The declaration of Pietermaritzburg as the administrative capital city of the province of KwaZulu-Natal in the year 2000 consequently saw the significant growth in the socio-economic status of the city as well as substantial spatial transformation. The city therefore has seen an unprecedented spatial and population growth which has resulted in the reduction of space in the city (Sutton, 2008). Due to the demand of human settlements, the city has seen a considerable decrease in the amount of its farmlands, wetlands and forests in the past 20 years.

The basic land use of the Msunduzi Municipality which includes the Pietermaritzburg Central Business District is made up of grasslands which make up a greater portion of the region, followed by settlements (formal, informal and traditional). Pietermaritzburg is situated only 80km inland from Durban along the major road route, N3, between the coastal harbour and the cities of Johannesburg and Tshwane (Msunduzi SDF, 2009). This has allowed the city to establish a strong industrial base such as the manufacturing of food and aluminium being some of the largest industries in the city (Msunduzi SDF, 2009).

The city has had a problem of air pollution since the 1980s where most of the air pollution sources were from cooking fires. The invent of factories, heavy industries, the nearby location of the New England Landfill Site, burning of timber and sugarcane plantations as well as the increase in motor vehicles and heavy-duty trucks have recently added to the toxicity of the city and surrounding areas in the Msunduzi Municipality. This has led to the residents of Pietermaritzburg complaining continuously about the state of the air where the Msunduzi Municipality has negligible efforts about the pollution levels that are usually above accepted and legal levels during most times of the year.

These heightened levels of pollution from the various sources located within the vicinity of the city's basin have been associated with the increase in the number of asthma patients in the city. It has been often suggested that the number of treated asthma patients is higher than would be expected in a town the size of Pietermaritzburg – highlighting the pollution problem in the city and its significant impact on the health of the residents.

The monitoring of pollutants in the municipality usually from stations located in Pietermaritzburg has been intermittent with the control of air pollution being a low priority due to the economic constraints of the Msunduzi Municipality. The Msunduzi Municipality have only recently (2016) recommitted themselves in the constant monitoring of the following pollutants which are contained in the city's air: PM, SO_2, NO_x, O_3, CO and various other harmful pollutants. The lack of funds due to financial neglect from the national government and a deficiency in local expertise to promote the concept of clear air has resulted in the air pollution crises of the Msunduzi Municipality. There are currently two monitoring stations located in the vicinity of the CBD and the other at the Pietermaritzburg Airport. This is still a very low spatial resolution of data capturing in the efforts to combat the air pollution problem faced by the municipality.

3.2 Materials

3.2.1 Data and data sources

To carry out the objectives outlined, satellite data collected by Landsat 8 OLI/TIRS were employed for this study. The satellite images were acquired through the Earth Explorer web portal created by the United States Geological Survey (USGS). The study set its objectives for a focused period of 5 years (2013-2017) which incorporated the consecutive seasons contained in each year (autumn; winter; spring; summer). Summer images of the year 2013 had cloud cover and were thus inaccessible for the purpose of analysis. This led to the retrieval of 19 Landsat 8 images instead of 20.

The study also made use of meteorological data in the form of hourly temperature recordings for Pietermaritzburg which were accessed through the South African Weather Services (SAWS). In addition, air quality data were requested through the Msunduzi Municipality environmental offices.

3.2.2 Landsat 8 OLI/TIRS data

Landsat 8 is the current mission from Landsat in a continuous series of land remote sensing satellites that began in 1972. It was launched successfully on the 11th of February 2013 and it deploys with it two instruments on-board: (i) the Operational Land Imager (OLI) with nine spectral bands in the visual (VIS), near infrared (NIR) and the shortwave infrared (SWIR) spectral regions; and (ii) the Thermal Infrared Sensor (TIRS) with two spectral bands in the longwave infrared region (LWIR) (Table 1). The products from this satellite are already calibrated to account for uncertainty in terms of the Top of Atmosphere (TOA) reflectance and absolute spectral radiance. They are available at no charge through the United States Geological Survey (USGS) Earth Resources Observation and Science (EROS) Centre (USGS, 2016).

TABLE 1. BAND ARRANGEMENT AND SPECIFICS OF LANDSAT 8 OLI/TIRS (AFTER USGS, 2016).

Landsat-8 OLI and TIRS bands (µm)			
Band	**Wavelength Range in (µm)**	**Band Spectrum**	**Resolution (m)**
1	0.435-0.451	Coastal/Aerosol	30
2	0.452-0.512	Blue	30
3	0.533-0.590	Green	30
4	0.636-0.673	Red	30
5	0.851-0.879	NIR	30
6	1.566-1.651	SWIR-1	30
7	2.107-2.294	SWIR-2	30
8	0.503-0.676	Pan	15
9	1.363-1.384	Cirrus	30
10	10.60-11.19	TIR-1	100
11	11.50-12.51	TIR-2	100

3.2.3 Meteorological data

The meteorological data used in the study included hourly observations of the following: temperature; humidity; wind speed and wind direction from the South African Weather Services (SAWS). Unfortunately, SAWS were only able to provide data from two stations in the Pietermaritzburg area, one located in the central business district and the other at the

Pietermaritzburg Airport. The spatial resolution of the study in terms of the position of the data sources relative to the study area has been negatively impacted.

In order to analyse the relationship between land surface temperature and air temperature, the temperature data on the day of each Landsat 8 image was extracted from the log of the temperature observations to the nearest minute. These values were lined up to match each satellite image upon where the mean LST around each weather station was compared to the air temperature observation at that particular time. The mean LST was retrieved through buffer analysis were a buffer with a radius of 1800m was created and through zonal statistics, a mean LST value from the buffer area was calculated. These data were graphed for seasonal purposes to display how land surface temperature relates to air temperature and thus highlighting the presence of heat islands in the study area.

3.2.4 Air quality data

The Msunduzi municipality are responsible for the recent monitoring of criteria pollutants as of June 2016. The locations of the two air quality monitoring stations are at the same location as the meteorological stations used in the study. However, different pollutants are measured at each station. The Central Pietermaritzburg station monitors the hourly measurements of following: Sulphur dioxide, Nitrogen oxide, Nitrogen dioxide and derivatives of Nitrogen oxides. The Pietermaritzburg Airport station monitors: Particulate matter 10 and 2.5; Nitrogen oxide; Surface ozone; Sulphur dioxide; Nitrogen dioxide and derivatives of Nitrogen oxides. Due to the difference in pollutants monitored per station, the study took an approach to continue providing an assessment of the air quality status with less emphasis on comparison between the two stations.

3.3 Pre-processing

Pre-processing is performed on data prior to analysis in order to improve its quality and to reduce errors contained in the dataset. Where applicable, data enhancement techniques are introduced for more advanced correction purposes. For this study, atmospheric correction and data calibration were applied on the retrieved Landsat 8 data. In addition, data cleaning was performed to exclude outliers and instrument/sensor failures.

3.3.1 Data Calibration

The acquisition of Landsat 8 OLI/TIRS data is retrieved as images in the form of pixels representing a byte of data with values of 0 -255 referred to as digital numbers (DN) (USGS, 2016). This format of the image requires a conversion performed on the imagery prior to any analysis. This is a process known as data calibration where digital numbers are converted into a quantity with a physical significance to retrieve information of the object in focus (Rozenstein *et al*., 2014). Data calibration uses particular parameters from the pre-launch scene in the conversion of DNs. For this study, the DNs were converted to radiance which is the radiation emitted by an object in focus under particular environmental conditions. Various methods are provided to convert digital numbers to radiance. ENVI 5.3 software provides the automatic calibration of data prior to atmospheric correction (ENVI, 2004).

3.3.2 Atmospheric Correction

The use of remote sensing as a tool to retrieve information from the Earth's surface requires the passing of solar radiation through the atmosphere before it is collected by an instrument (ENVI, 2004). As a result, remotely sensed images include signals about the atmosphere and the Earth's surface. This is associated errors especially during quantitative analysis treatments of surface reflectance. Therefore, the removal of the influence of the atmosphere is a critical pre-processing step. For the possible errors introduced by the atmosphere, atmospheric correction tools compensate for atmospheric properties and effects. The Fast Line-of-sight Atmospheric Analysis of Spectral Hypercubes (FLAASH), a first-principles atmospheric correction tool which incorporates the MODTRAN4 radiation transfer code in applying the atmospheric correction process was applied to correct wavelengths (visible, NIR and SWIR) on the Landsat 8 imagery (ENVI, 2004).

3.4 Land Cover Indices

Band manipulation in remote sensing provides the calculation of certain land cover indices from acquired satellite imagery. For this study, three land cover indices were calculated: Normalised Difference Vegetation Index (NDVI), Fractional Vegetation Cover (FVC) and the Normalised Difference Built-up Index (NDBI).

3.4.1 NDVI

The normalised difference vegetation index (NDVI) is a graphical indicator that assesses whether the target being observed contains live green vegetation or not (Chang, 2016). The process of evapotranspiration in vegetation carries a major influence in terms of the development and transformation of surface urban heat islands and thus NDVI assessments can provide an understanding between vegetation and LST relationships (Yuan and Bauer, 2007).

The band configuration of Landsat-8 imagery allows for NDVI calculation. Healthy vegetation is highly absorbent of visible light whereas it mostly reflects near-infrared light. Using bands 4 (Red) and 5 (NIR) of Landsat-8, NDVI was calculated using the equation below:

$$\boldsymbol{NDVI = \frac{Band\ 5\ (NIR) - Band\ 4\ (Red)}{Band\ 5 (NIR) + Band\ 4\ (Red)}} \quad (1)$$

3.4.2 Fractional vegetation cover

Fractional vegetation cover represents the amount and nature of vegetation cover. It is an important measure since it modulates the proportions of vegetated and non-vegetated ground visible to a sensor as the differences in radiative temperature between vegetation canopy and the ground can significantly affect the measurements of land surface temperature (Weng, 2009). The following equation was used to calculate FVC:

$$\boldsymbol{FVC = \left(\frac{NDVI - NDVI\ (min)}{NDVI\ (max) - NDVI(min)}\right)^2} \quad (2)$$

3.4.3 NDBI

The automatic detection of built-up areas using Landsat-8 data can be done through an index known as the Normalised Difference Built-up Index developed by Zha *et al*. (2003). This index uses the spectral response of built-up areas with lower reflectance in the NIR wavelength range where positive values indicate the presence of built up areas. Negative values from this index would then represent water bodies and those close to zero indicate the presence of vegetation. NDBI can be applied in assessing the contribution of built-up areas to thermal retention. The following equation was used to compute NDBI:

$$\boldsymbol{NBDI} = \frac{\boldsymbol{Band\ 6\ (SWIR1) - Band\ 5\ (NIR)}}{\boldsymbol{Band\ 6(SWIR1) - Band\ 5(NIR)}} \quad (3)$$

3.5 Land Cover Classification

Land cover classification or image classification involves the process of categorising image pixels into set or specific classes which often results in the production of a thematic map, where each class is distinctive from the other (Hodgson *et al*., 2003). It is of great importance to identify land use/cover with satellite images before the assessment of the urban heat island. There are two commonly used pixel-based classification methods namely: unsupervised classification and supervised classification methods (Hodgson *et al*., 2003). Within these broad methods, there are techniques representing each method. For this study, the Maximum Likelihood Classification technique, a form of supervised classification was used for the classification of the acquired Landsat 8 images.

For this study, the pixels were classified into 6 dominant classes in the study area, namely: Water bodies/Wetlands, Grasslands, Built-up area, Plantations, Woodlots and Indigenous forests. The Maximum Likelihood Classification technique was run through the multivariate tab of Spatial Analyst Tools in ArcMap 10.3 (ESRI, 2017). This process required the training of the study area image dataset by sampling pixels of similar characteristics into classes. 70 sampling points per class were created through desktop sampling to train the maximum likelihood classification. This resulted in 420 (70*6) training sampling points which were used to create the classified map of the study area.

An accuracy assessment was performed on the classified maps to reveal the producer and user accuracies associated with the maps using a South African National Biodiversity Institute (SANBI) land cover map (DEA, 2014) as a source for ground truthing. The values attached to the classes of the SANBI map were reclassified to match those of the classified maps. The Create Accuracy Assessment tool on ArcMap was used to create thirty (30) randomly computed test/ground truth points per class (30*6 = 180) on the SANBI land cover map. Thereafter the Update Accuracy Assessment tool was used to extract samples from the classified map in order to compare and assess the accuracies. The Compute Confusion Matrix tool was then applied to calculate the user and producer accuracies as well the Kappa coefficients of the classified maps.

3.6 Land Surface Temperature

LST is the thermal energy that is emitted in wavelengths and is given off by all surfaces. These wavelengths are identified and measured by sensors on satellites and other forms of remote sensing to observe and infer the temperature of surfaces on Earth (Voogt and Oke, 2003). The application of satellite imagery provides the observation of the energy reflected and emitted from the land surface. These surfaces include: rooftops, vegetation, water and bare ground – providing a wide range of measurements and analysis to answer questions about land use/land cover patterns (Voogt and Oke, 2003). LST can therefore be studied as a surrogate index indirectly addressing the heat island effect (Shastri and Ghosh, 2019).

3.6.1 LST processing methods

Satellite TIRS sensors measure top of the atmosphere (TOA) radiances which are a combination of three components of energy which are: (i) emitted radiance from the Earth's surface; (ii) upwelling radiance from the atmosphere and; (iii) downwelling radiance from the sky. It is from this combination where brightness temperatures are derived using Plank's law (Weng, 2009). The TOA radiances and brightness temperatures are impacted by atmospheric conditions which are corrected before the retrieval of land surface temperatures (Weng, 2009).

Satellites with a single thermal band, such as Landsat TM and ETM+ provide a challenge in obtaining LST values as they observe thermal infrared through one narrow channel. However, Landsat-8 provides a two-channel TIRS – equipped with narrower channels which can capture

finer spectral signatures from the land surface (Du *et al*., 2014). This offers the opportunity to retrieve LST by employing the widely used split-window algorithms rather than the single channel methods (Du *et al*., 2014).

The split-window algorithm does not involve the input of information about the atmospheric profiles at the time of image acquisition (Du *et al*., 2014). This method applies differential atmospheric absorption in the two adjacent thermal infrared channels where it subsequently uses the linear or nonlinear combination of brightness temperatures to calculate LST (Du *et al*., 2014). Due to this algorithm not requiring information about the atmospheric profiles, a variety of split-window algorithms have been developed for LST retrieval from numerous sensors (Du *et al*., 2014). There are however issues with the application of split-window algorithms on Landsat-8 data as the USGS have alerted users of larger uncertainty in the TIRS Band 11 values. Therefore, the attempts to employ the split-window algorithm using both TIRS Bands 10 and 11 should be done with caution as the development of a suitable model with substantial parameters is still necessary (Wang *et al.*, 2015).

The retrieval of land surface temperature for this study was computed by employing the Split-Window Algorithm adjusted for Landsat 8 data. This is a structured mathematical algorithm that uses the brightness temperature of two bands of TIR and the mean and difference in land surface emissivity as well as the atmospheric water vapour content for the estimation of LST of an area (Wang *et al.*, 2015).

The following algorithm estimates LST:

$$\boldsymbol{LST = TB_{10} + C_1(TB_{10} - TB_{11}) + C_2(TB_{10} - TB_{11})^2 + C_0 + (C_3 + C_4W)(1 - \varepsilon) + (C_5 + C_6W)\Delta\varepsilon} \quad (4)$$

Where:

LST =Land surface temperature (K)
C_0-C_6= Split-Window coefficient values (see Table 2)
TB_{10} & TB_{11}= Brightness temperature of band 10 and band 11 (K)
ε= mean LSE of TIR bands
W= Atmospheric water vapour content
$\Delta\varepsilon$= Difference in LSE

TABLE 2. SPLIT-WINDOW COEFFICIENT VALUES (SOBRINO *ET AL*., 1996 IN SKOKOVIC *ET AL*., 2014).

C_0	-0.268
C_1	1.378
C_2	0.183
C_3	54.300
C_4	-2.238
C_5	-129.200
C_6	16.400

In the computing of LST, the brightness temperature (TB) of both Landsat 8 TIR bands is a required input.

3.6.2 Brightness Temperature

Brightness temperature (TB) is the microwave radiation radiance travelling upward from the top of the Earth's atmosphere. It is the effective temperature viewed by the satellite under an assumption of unity emissivity (USGS, 2016). The calibration processes require the conversion of DN values of TIR bands to TB. Brightness temperature for both TIRS bands is calculated by the following equation:

$$\boldsymbol{TB = \frac{K2}{Ln\left[\left[\frac{K1}{L\lambda}\right] + 1\right]} - 272.15} \quad (5)$$

Where:

TB = At-satellite brightness temperature (degrees Celsius)
L_λ = TOA spectral radiance (Watts/(m^2 * sr * μm))
K_1 = Band-specific thermal conversion constant from the metadata (K1_CONSTANT_BAND_x, where x is the thermal band number)

K_2 = Band-specific thermal conversion constant from the metadata
(K2_CONSTANT_BAND_x, where x is the thermal band number)

In the process of processing TB of an area, the Top of Atmosphere spectral radiance of (Lλ) is also required as an input.

3.6.3 Top of Atmospheric Spectral Radiance

The value of Top of Atmospheric spectral radiance (Lλ) can be converted by the following equation:

$$L_\lambda = M_L Q_{cal} + A_L \quad (6)$$

Where:

L_λ = TOA spectral radiance (Watts/(m^2 * sr * μm))
M_L = Band-specific multiplicative rescaling factor from the metadata
(RADIANCE_MULT_BAND_x, where x is the band number)
A_L = Band-specific additive rescaling factor from the metadata
(RADIANCE_ADD_BAND_x, where x is the band number)
Q_{cal} = Quantized and calibrated standard product pixel values (DN)

3.6.4 Land Surface Emissivity

Land surface emissivity is defined as a proportionality factor that scales blackbody radiance also known as Plank's law. It uses this blackbody radiance to predict emitted radiance. Land surface emissivity is also the efficiency of transmitting thermal energy across the surface into the atmosphere (Sobrino *et al*., 2008). It has effects on satellite measurements which include: (i) a reduction of surface-emitted radiance; (ii) non-black surfaces reflect radiance; and (iii) the anisotropy of reflectivity and emissivity may in some cases reduce or increase the total radiance from the surface. This then requires that any retrieval of land surface temperature from multispectral TIR data should include an accurate measurement of emissivity values of the surface (Sobrino *et al*., 2008).

In estimation of LST, the calculation of LSE is necessary. LSE estimation can be done using the NDVI threshold method. These methods all result in the separation of temperature from emissivity to determine the effect emissivity has on the estimation of land surface temperature (Weng, 2009). This method requires the emissivity for soil and for vegetation for both Band 10 and Band 11. The following equation is used to calculate LSE using soil and vegetation emissivity, individually from Band 10 and Band 11:

$$\boldsymbol{LSE} = \boldsymbol{\epsilon_s}(\mathbf{1} - \boldsymbol{FVC}) + \boldsymbol{\epsilon_v FVC} \quad (7)$$

Where:

LSE = Land surface emissivity
ϵ_s= Emissivity for soil (Band 10 and 11 given as 0.971 and 0.977 respectively)
ϵ_v= Emissivity for vegetation (Band 10 and 11 given as 0.987 and 0.989 respectively)
FVC = Fractional Vegetation Cover

The resulting LSE values for both bands of TIR will be used to calculate the mean and difference LSE as, where the mean is calculated as follows:

$$\boldsymbol{\varepsilon} = \frac{\boldsymbol{LSEBand10} + \boldsymbol{LSEBand11}}{\mathbf{2}} \quad (8)$$

Whilst the difference in LSE, required for the algorithm, is given by the following equation:

$$\Delta\boldsymbol{\varepsilon} = \boldsymbol{LSE_{10}} - \boldsymbol{LSE_{11}} \quad (9)$$

Where:
$\boldsymbol{\varepsilon}$ = Mean LSE
$\Delta\boldsymbol{\varepsilon}$ = LSE difference
In Figure 4, the process of computing LST is presented as scheme to provide the steps to LST output maps. The steps in this method were all run through an ArcMap environment of ArcGIS

software (ESRI, 2017) with the usage of Raster Calculator to calculate and produce raster files from the inserted equations.

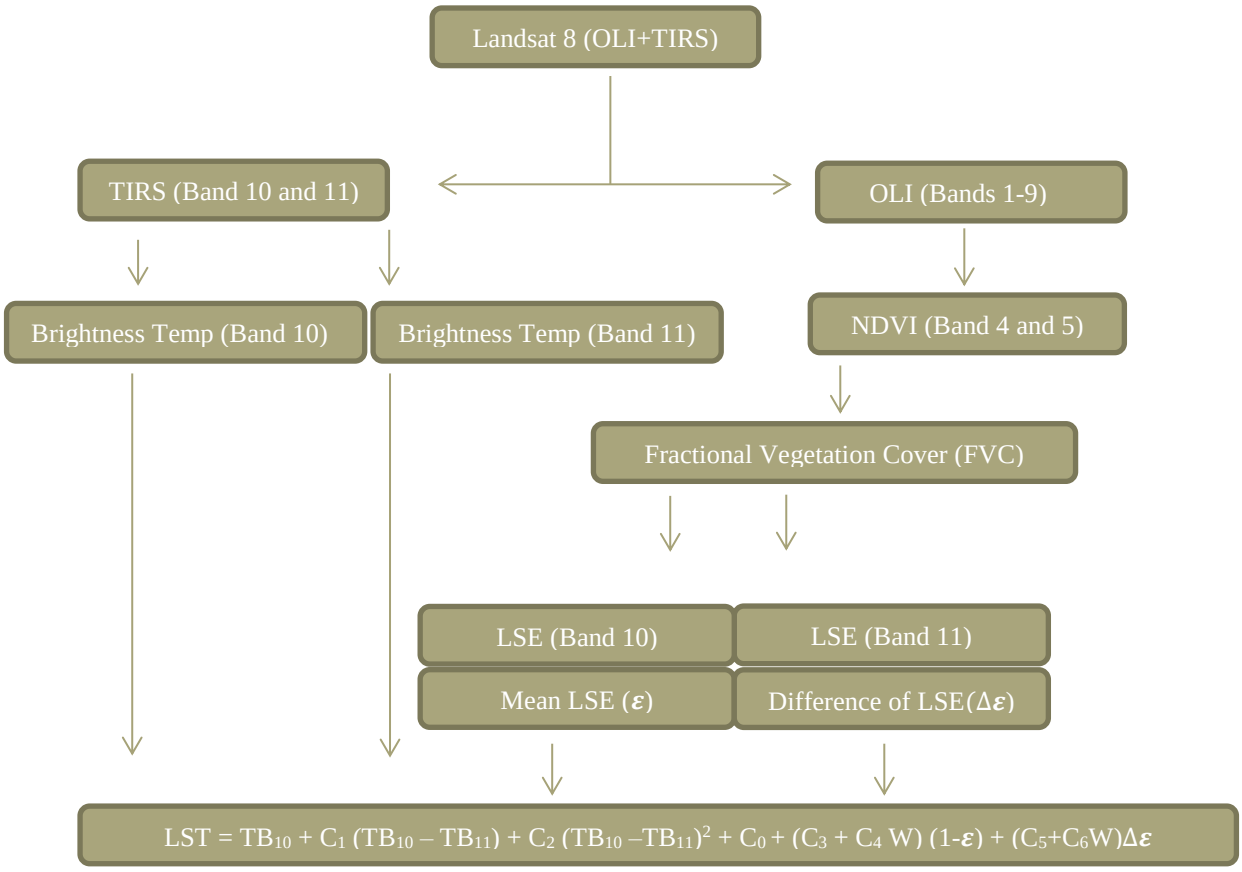

FIGURE 4. A SCHEME FOR LAND SURFACE TEMPERATURE COMPUTATION USING THE RASTER CALCULATOR TOOL ON ARCMAP SOFTWARE.

Although there are advantages in the application of remote sensing, there are several considerations that should be made when using some of these study techniques to the UHI effect (Streutker, 2002). Determining temperature from remotely sensed data should always be done in cognisance that temperatures derived as LST are surface temperatures of the emitting materials rather than those otherwise observed by *in situ* instruments. As a result, the combination of this with the variety of the surface types representing the urban fabric can cause surface temperature to demonstrate a much substantial spatial variation than the observed air temperatures above the surface itself (Streutker, 2002).

3.7 MODIS Aerosol Optical Depth

3.7.1 MODIS AOD product

The MODerate resolution Imaging Spectroradiometer (MODIS) has been observing the earth from the Terra and Aqua satellites since 2000 and 2002, respectively. Various physical parameters are derived from MODIS spectral radiances, amongst these are a variety of products characterising aerosol particles. These are retrieved through several algorithms producing aerosol products from MODIS. The MODIS Aerosol Optical Depth (AOD) 3-kilometre product is retrieved through the Dark Target algorithm, applied over land and the ocean (Remer *et al*., 2013).

The application of MODIS collection 6 level 2 AOD data from the aqua satellite (MYD04-3K) at 550 nm with a spatial resolution of 3 km were used in the study. MODIS AOD files are a product from the retrieval of light extinction estimates which can be applied in atmospheric aerosol assessments. The AOD products were retrieved in HDF format, which required conversion through the MODIS Conversion Toolkit (MCTK) as a plugin on ENVI 5.3. The conversion tool allows the projection and extraction of files from the HDF package – a process that was run to retrieve AOD files in this study. The converted files were then transferred to ArcGIS for mapping. In addition, AOD values were extracted per monitoring station to evaluate the relationships between AOD and *in situ* monitored air pollutants.

3.8 Statistical Analyses

3.8.1 Existence of SUHI in the Msunduzi Municipality

The first objective of the study aimed to investigate and analyse the presence of surface urban heat islands in the Msunduzi Municipality. This objective was reached through mapping the spatial distribution of land surface temperature using Landsat 8 thermal data per season over the study period. In addition, the relationship between land surface temperature and atmospheric temperatures observed by *in situ* monitoring stations was investigated. This was performed by creating two buffer zones with a diameter of 1800m around the two monitoring stations (Central Pietermaritzburg and Pietermaritzburg Airport). These buffer zone shapefiles were used to sample LST around the monitoring stations using the Zonal Statistics by table

tool in ArcMap. This was done per LST raster file, where a mean LST value was obtained and used as LST at the monitoring stations.

The ambient air temperature values from monitoring stations were then tested for normality using the Shapiro-Wilk test which showed a normal distribution for the values. These values were then correlated to understand the strength of the relationship between monitored atmospheric temperature and land surface temperature acquired through remote sensing techniques.

To assess the urban heat island effect, buffer zones of a diameter of 1800m between 4 urban and 4 rural areas were created. These were used to extract mean LST between the rural and urban areas to provide an indication of the difference in land surface temperatures. The comparison of the city and rural fabric with regards to land surface temperature would indicate the nature in which the natural landscape has been altered.

3.8.2 Relationship between LST and land cover indices

The second objective was set to determine the relationship between land surface temperature and different land cover indices. In addition, this objective also studied the distribution of land surface temperature per land cover class contained in the study area. Using ArcMap, LST, NDVI, NDBI and FVC were computed using the Raster Calculator tool. Performing statistical analyses on the data obtained from the study required a sample dataset that would give a representation of the population of the dataset.

Transects along the North-South and West-East directions of the municipality were created to extract samples of mean LST, NDVI, FVC and NDBI for the seasons. These sample points were used for statistical analyses. Normality tests and inferential statistics were performed on the sampled data points using SAS software package. These were done to understand the distribution of the data and the relationships between land surface temperature and the land cover indices analysed in the study.

To assess the distribution of temperature per land cover class, the study area image was classified into six main land cover classes: Indigenous Forests, Woodlots, Plantations, Built-up Area, Wetlands/Waterbodies and Grasslands. Land cover classification outputs were done for the years 2013, 2015 and 2017.

3.8.3 Assessment of impact of SUHIs on urban pollution and MODIS AOD as proxy for measured pollutants

The third objective of the study aimed to assess the impact of urban heat islands on urban pollution. Air temperature, wind speed and direction as well as air pollution observations from the two ground stations located in the study were used to illustrate and display the pattern of selected air pollutants and the selected meteorological variables between winter and spring. In addition, individual correlations between air temperature and measured air pollutants were run on the observations to test the strength and direction of the relationships. This period was chosen because of the weather phenomena during these periods which offer the intense of the inversion layer during winter and its gradual phasing out during spring. This graphical analysis was performed using the Openair R statistics package (Carslaw and Ropkins, 2012) and Microsoft Excel.

Due to the limitation of monitoring stations in the study area, MODIS AOD which is a measure of the extinction of the solar beam by dust and haze was employed in the study to provide a spatial distribution of aerosols in the Msunduzi Municipality. With the use of air pollution data from two ground monitoring stations, the objective further aimed to relate AOD values with selected measured air pollutant observations per station to test and validate the relationships between the variables for the potential application of MODIS AOD as a proxy for measured air pollutants.

Chapter 4: Results and Discussion

4.1 Results

4.1.1 Land Cover/Land Use patterns

Different land cover or land use patterns have varied thermal properties. The configuration of these land covers in a specific area of interest has been noted to influence the spatial distribution of land surface temperature and therefore the atmospheric temperature observed above the specific area. The Msunduzi Municipality has been classed into six dominant land cover types for the purpose of this study as seen below (Figure 5).

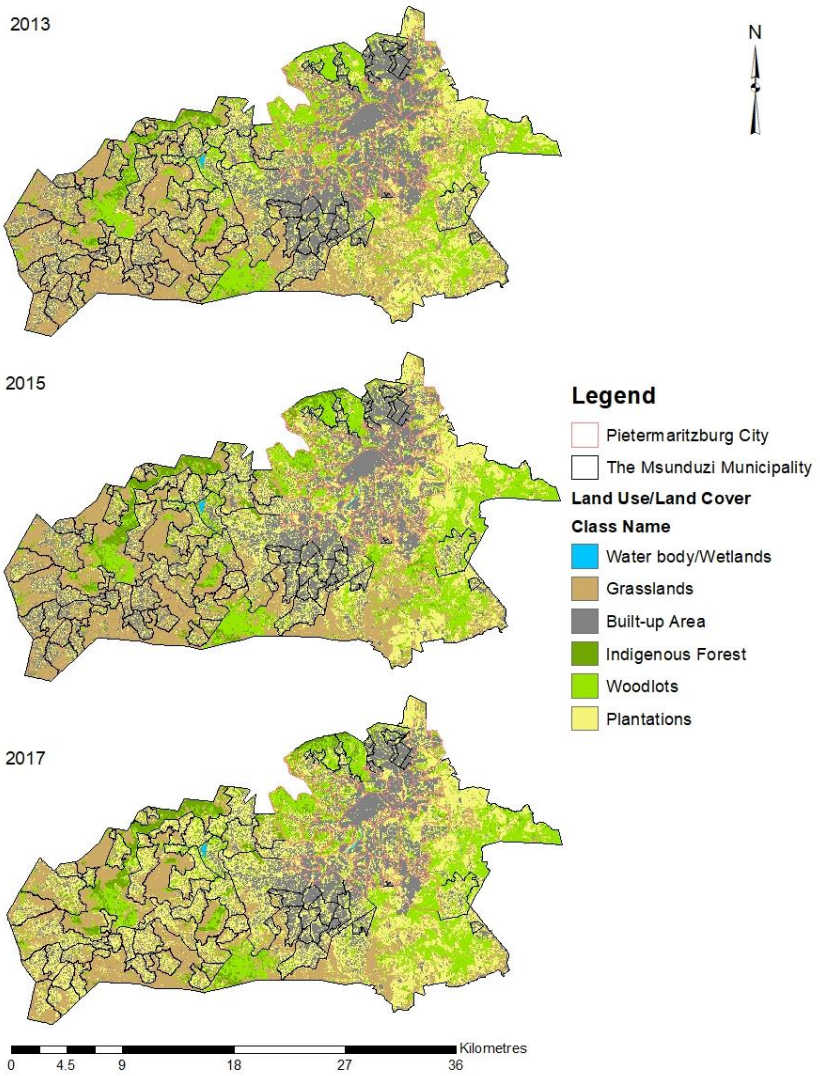

FIGURE 5. LAND USE/LAND COVER CLASSIFIED MAPS OF THE MSUNDUZI MUNICIPALITY (2013-2017)

These are: Indigenous Forests (IF), Built-up Area (BA), Grasslands (GL), Plantations (PL), Woodlots (WL) and Wetlands/Waterbodies (WW). The built-up area class includes impervious surfaces such as buildings, human settlement areas (informal and formal), roads and pavements. Plantations include the subsistence/commercial farms as well as the dominant sugarcane farms to the southern parts of the municipality, with woodlots also capturing some of the urban green spaces notable in the urban settlements of the municipality.

The land cover maps for the Msunduzi Municipality between 2013 and 2017 indicate active changes in the area of each class during the study period. This is most notable for areas associated with land clearing for the cyclical farming of crops and land remediation where ploughing and harvesting contribute significantly to the presence and absence of vegetation. Such changes may contribute to the errors associated with the classification of a series of satellite imagery (Hodgson *et al*., 2003).

It is important to note however that the area of the Msunduzi Municipality is relatively a dormant area and does not experience a significant amount of land cover changes. Therefore, it can then be accepted that during the study period, Built-up Areas have been the dominant land cover class followed by Grasslands and Plantations and Woodlots. Indigenous Forests and Water body/Wetlands occupy the least area in the Msunduzi Municipality.

Urbanisation continues to contribute significantly to the expansion of built-up areas in the Msunduzi Municipality which signals the potential of an increase in urban materials which have properties such as thermal emissivity, solar reflectance and heat capacity that can promote and influence the development of pockets of heat concentrations (Wang *et al*., 2007). This can therefore result in the formation of urban heat islands as these properties influence how incoming solar radiation is reflected, emitted and absorbed (Voogt and Oke, 2003).

An accuracy assessment was performed to provide the user, producer and overall accuracies for the classified land cover maps. It could be argued that the dates provide less consistency for analysis purposes. However, this is a limitation of the retrieval of satellite images beyond the control of the study. It is in this regard that the study provides an analysis that assesses each season as such, rather than a consistent day throughout the study period.

The overall accuracies for the land cover maps produced range between 40-61% for the years 2013 – 2017 (Table 3).

TABLE 3. CLASSIFIED MAPS ACCURACY ASSESSMENT SHOWING: PRODUCER, USER ACCURACIES; OVERALL ACCURACY AND KAPPA COEFFICIENTS (2013-2017).

	User's Accuracy						Producer's Accuracy							
Year	IF	PL	GL	WW	BA	WL	IF	PL	GL	WW	BA	WL	Overall Accuracy	Kappa
2013	78	42	14	100	14	38	35	50	20	65	10	60	40	0.28
2015	78	30	25	100	63	68	70	40	30	65	50	75	55	0.46
2017	65	52	44	100	52	61	75	58	42	74	60	55	61	0.53

The split between vegetation classes introduces substantial error to pixel classification and therefore reduces the overall accuracies of the maps. The 2017 classified map however, produced a reasonable overall accuracy (61%) which provided the possibility of analysis.

4.1.2 Urban Heat Islands

4.1.2.1 Surface Urban Heat Islands

In investigating and characterising the presence of surface urban heat islands (SUHI) in the Msunduzi Municipality, Landsat 8 thermal data were employed to compute land surface temperature observations. Maps between 2013 and 2017 were produced to characterise the nature and extent of the spatial distribution of satellite-retrieved land surface temperature between autumn, winter and spring and summer months. These maps highlight the spatial distribution of the SUHI per season during the study period.

Autumn

South Africa's autumn season falls typically between the months of March and May. For this reason, satellite images that fell between these months were selected to characterise the nature and extent of SUHIs in the study area for the autumn season (Figure 6).

What can be seen from these images in general is that higher LSTs are consistent with the presence of built-up areas in the study area during the autumn season. The location of the city centre (Pietermaritzburg CBD) and immediate urban areas are visually interpretable to be retaining excess heat when compared to the surrounding rural areas in the Msunduzi Municipality. There are instances where the surrounding grasslands also indicate higher than average temperatures and this can be attributed to burnt scars in the municipality which are known to absorb heat due to altered thermal and absorption properties. This is particularly due to the notable colour changes of the surface which influences how heat is absorbed or reflected by the surface (Rosenthal *et al*., 2007).

During the autumn season, between 2013 and 2017, higher land surface temperatures were concentrated mainly in the developed areas of the Msunduzi Municipality. The range of land surface temperature values is indicative of the different land cover types that have different thermal properties in the municipality.

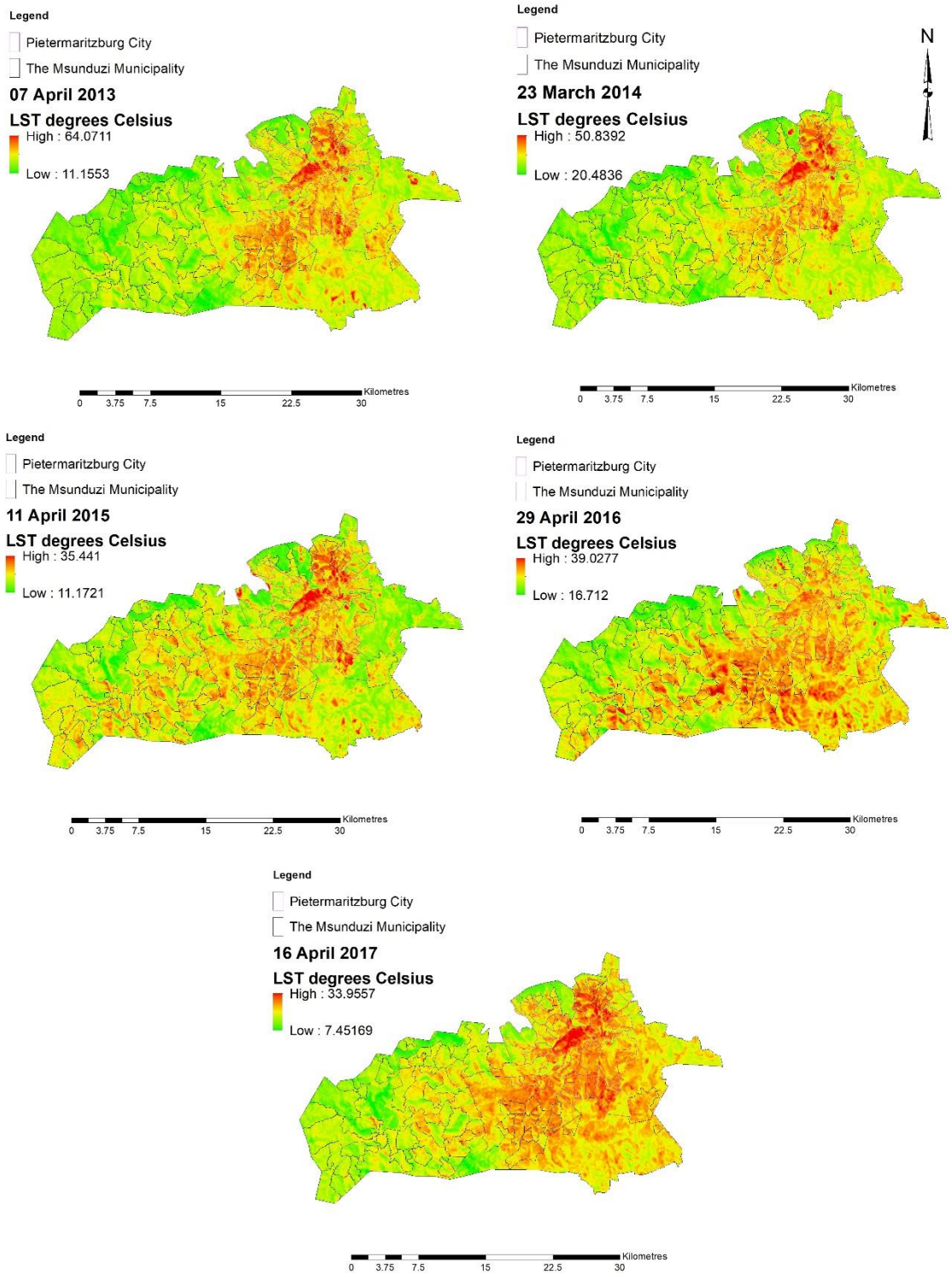

FIGURE 6. LAND SURFACE TEMPERATURE AUTUMN MAPS FOR THE MSUNDUZI MUNICIPALITY (2013-2017).

Winter

What is most notable in the assessment of heat islands in the winter season is a shift from the presence of higher temperatures being considerably concentrated in the central business district of the study area to being largely concentrated towards the rural areas that are usually vegetated for most parts of the year as seen below (Figure 7).

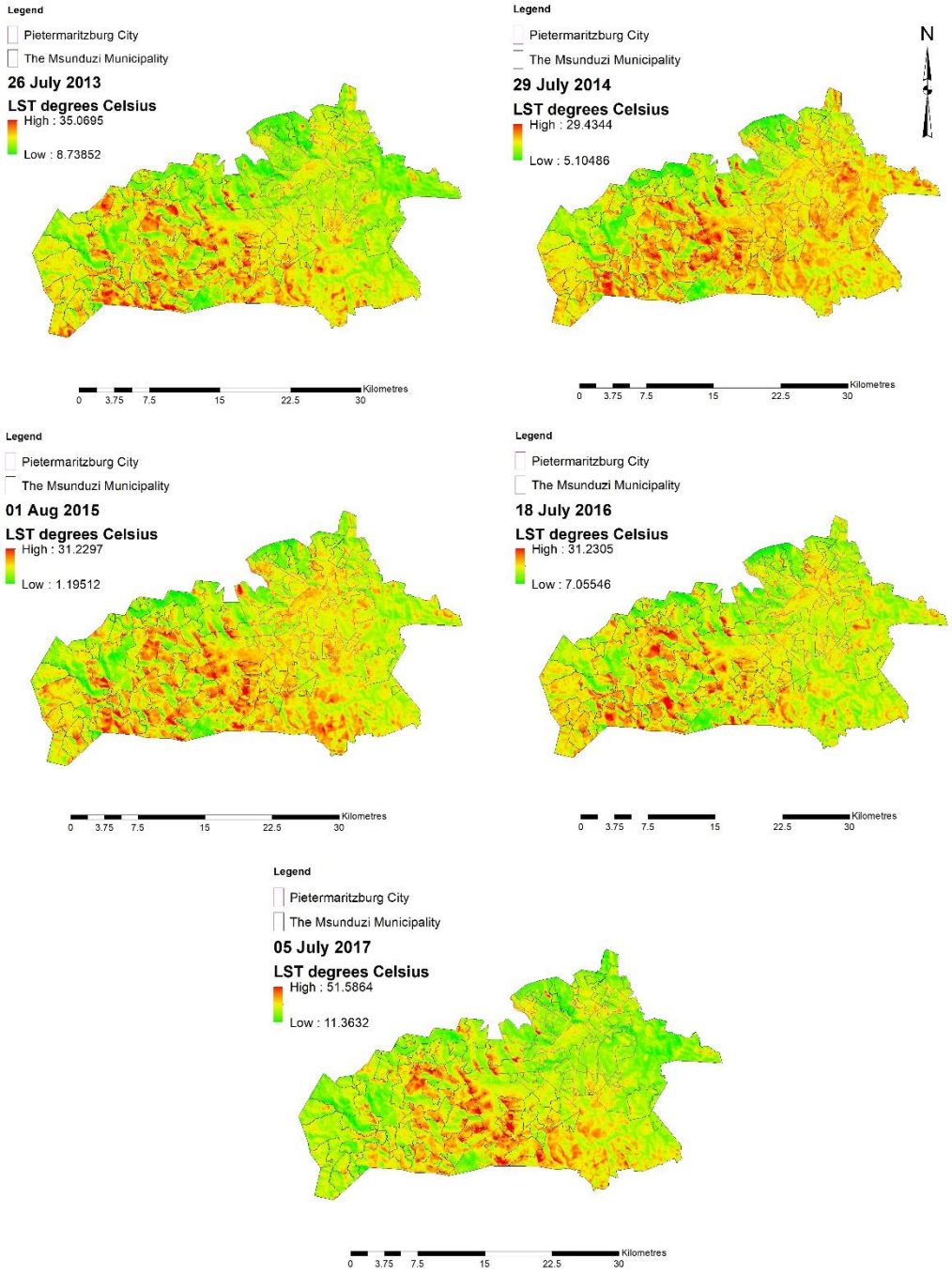

FIGURE 7. LAND SURFACE TEMPERATURE WINTER MAPS FOR THE MSUNDUZI MUNICIPALITY (2013-2017).

Much of the higher land surface temperatures during winter are spread around the regions with rural areas and grasslands of the study area. What contributes to the shift of higher temperatures from the central business district to the rural areas is likely due to unvegetated surfaces during winter. The presence of fires due to biomass burning and land clearing and the loss of chlorophyll from vegetation during winter could explain how the outcropping of bare ground contributes to higher than normal temperatures in areas that would usually be covered in green vegetation (Yuan and Bauer, 2007).

Spring

The spatial distribution of land surface temperature during the spring season is not definite as was the case during autumn (Figure 8). What is seen is that higher land surface temperatures are concentrated and tethered towards grasslands and the plantations in the municipality, with isolated sinks where built-up areas are located. What can also be noted is that patches of bare ground are seen to have higher temperatures when compared to vegetated surfaces. This could explain how land clearing in plantations through fire can result in burnt scars and bare ground absorbing more heat and therefore seen to be the cause of higher land surface temperature values than built-up areas, especially during the early morning as the land warms quicker than artificial impervious surfaces.

The map on the 07th of Sept 2017 appears to indicate extreme higher temperatures in the study area due to the presence of an active fire captured at the acquisition of the image (located south west of the CBD) which has distorted the distribution of land surface temperature. An extreme land surface temperature in the region of 140 degrees Celsius is observed. The presence of fires across the landscape are also observed to contribute to the spatial nature of temperature dynamics at the surface of the earth in this case.

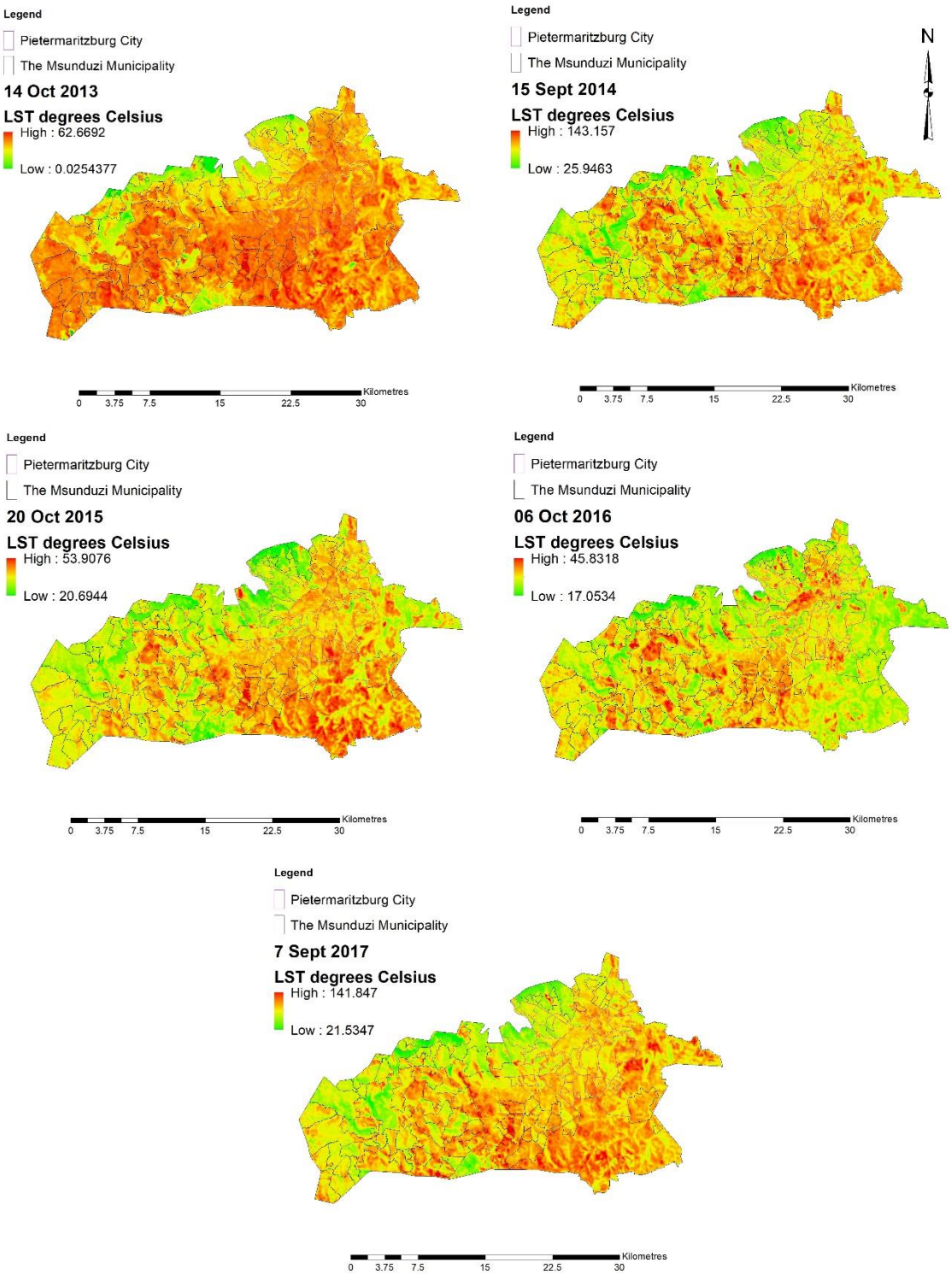

FIGURE 8. LAND SURFACE TEMPERATURE SPRING MAPS FOR THE MSUNDUZI MUNICIPALITY (2013-2017).

During the spring period, higher land surface temperature values are observed in the areas classified as plantations and woodlots, situated in southern area of the municipality. These areas that are usually dominated by plantations but due to the agricultural clearing procedures in the municipality, these areas are usually cleared to make way for new plantations in the warm seasons. During the spring season, the growths of the plantations are in their infancy and therefore have minimal influence in the reduction of land surface temperatures.

There are however visible sinks of heat in built up areas, especially the Pietermaritzburg CBD and the outlaying residential areas. The presence of heat islands is still maintained predominately in built-up areas, however during the spring areas that are cleared of vegetation absorb much more heat during this period due to the presence of burnt scars and active fires across the landscape before the rainy season.

Summer

The surface urban heat island during summer is clearly defined with the spatial pattern of the central business district and surrounding residential and industrial areas (Figure 9). Outcrops of built-up areas particularly absorb more heat than surrounding areas of different land use. The residential areas located south west of the CBD can also be clearly seen to be sinks of heat in the municipality, with areas dominated by vegetation indicating lower land surface temperatures similarly to the other seasons.

The SUHI from the 05 Nov 2015 map suggests the SUHI is not clearly defined and characterises much of how heat is distributed during the spring season. This can explain how the periodic growth of plantations in the southern parts of the municipality towards the summer sees the reduction of high land surface temperatures compared during the spring period.

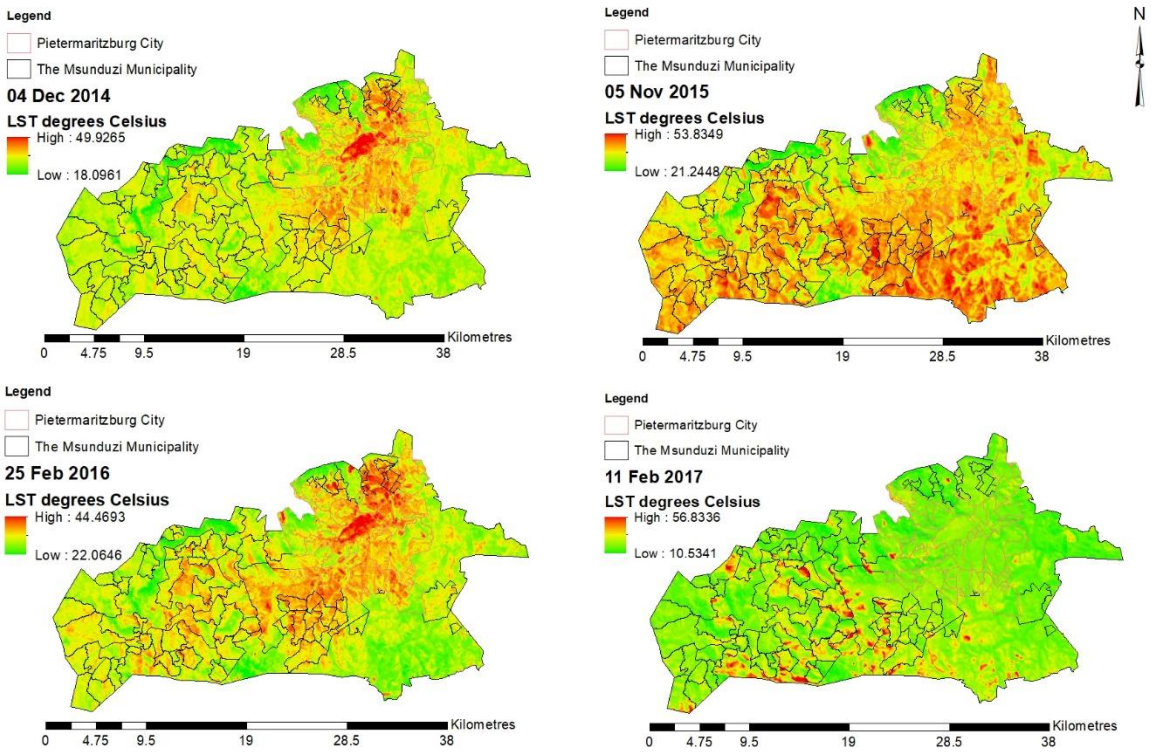

FIGURE 9. LAND SURFACE TEMPERATURE SUMMER MAPS FOR THE MSUNDUZI MUNICIPALITY (2014-2017).

Mean SUHI in Msunduzi Municipality

The mean LST maps clearly indicate the presence of heat sinks and isolated heat islands in the Msunduzi Municipality over the 5-year period (Figure 10). The parts that are dominated by built-up areas which include high-rise buildings, human settlements, industries and road infrastructure are notable sinks of heat in the study area while areas dominated by dense vegetation are noted to retain less heat. The extent and the shape of the surface heat island and the neighbouring heat sinks are consistent with the sprawling of the CBD and the development of areas of settlement as well as areas where land has been cleared in the municipality. The SUHI is seen to be better defined and therefore better observed during the autumn and summer periods in terms of the distribution of land surface temperature over the 5-year period. These are seasons where there is greater coverage of vegetated surfaces which creates distinct boundaries with non-vegetated surfaces for better distinction of the surfaces that contribute to an increase in land surface temperature.

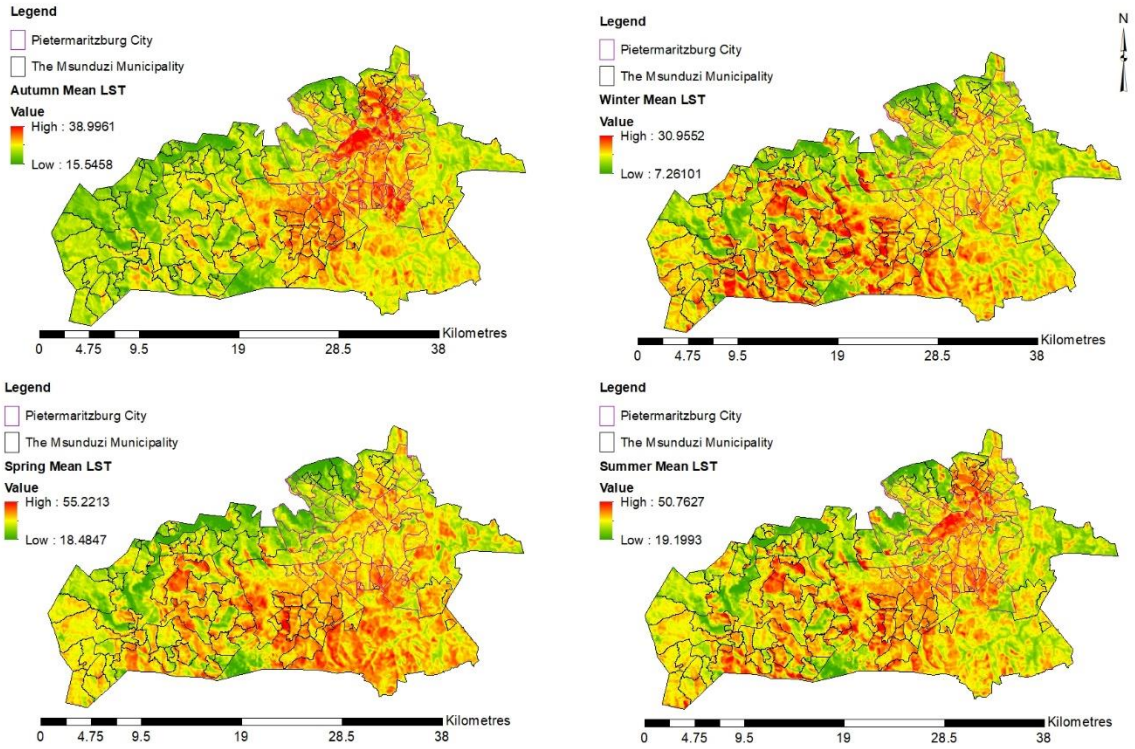

FIGURE 10. SEASONAL MEAN LAND SURFACE TEMPERATURE MAPS FOR THE MSUNDUZI MUNICIPALITY (2013-2017).

Mean spring LST indicates that areas that are dominated by dense vegetation during the spring period relatively have lower land surface temperatures due to the cooling effect of vegetation. Patches of forest in the municipality are observed to consistently contribute to the reduction of land surface temperatures. However, areas that experience systematic vegetation growth and clearing are seasonal SUHIs with relatively higher LST during the spring period compared to the developed areas such as the CBD and immediate surrounding residential areas. Over the 4-year period of SUHI analysis for the summer season, the distribution of LST is not spatially concentrated over a distinct area as in autumn, but there are isolated patches of high LST observations which differ in size. The most notable one being in the CBD with other heat sinks located in residential areas and spaces which have been cleared of vegetation in the municipality.

Land cover patterns during autumn and summer are most likely distinctive compared to winter and spring where there could be similarities between land cover classes particularly between

the spectral signatures of built-up areas and non-vegetated surfaces due the loss of vegetation. These similarities can also explain how SUHIs are spread throughout the study area where non-vegetated surfaces retain more heat during winter, especially to the southern parts of the municipality. The mean LST values were classed to further characterise the nature of SUHIs in the Msunduzi Municipality. The values were classed into below average, average and hotspot areas during each season.

4.1.3 Mean LST class distribution

The distribution of LST can be further assessed to provide details on the actual nature of the surface. By classing the observed LST values into below average, average and hotspot, it is possible to see the areas that are of concern in terms of the high land surface temperatures experienced in these areas, especially since these observations are done in the morning and are expected to increase towards the afternoon (Figure 11). Land surface temperature values were sampled from the mean land surface temperature observations per season. The numerical distribution of these sampled data was assessed and the 1st, 2nd and 3rd standard deviations were used as marks for the below average, average and hotspot classes per season, respectively.

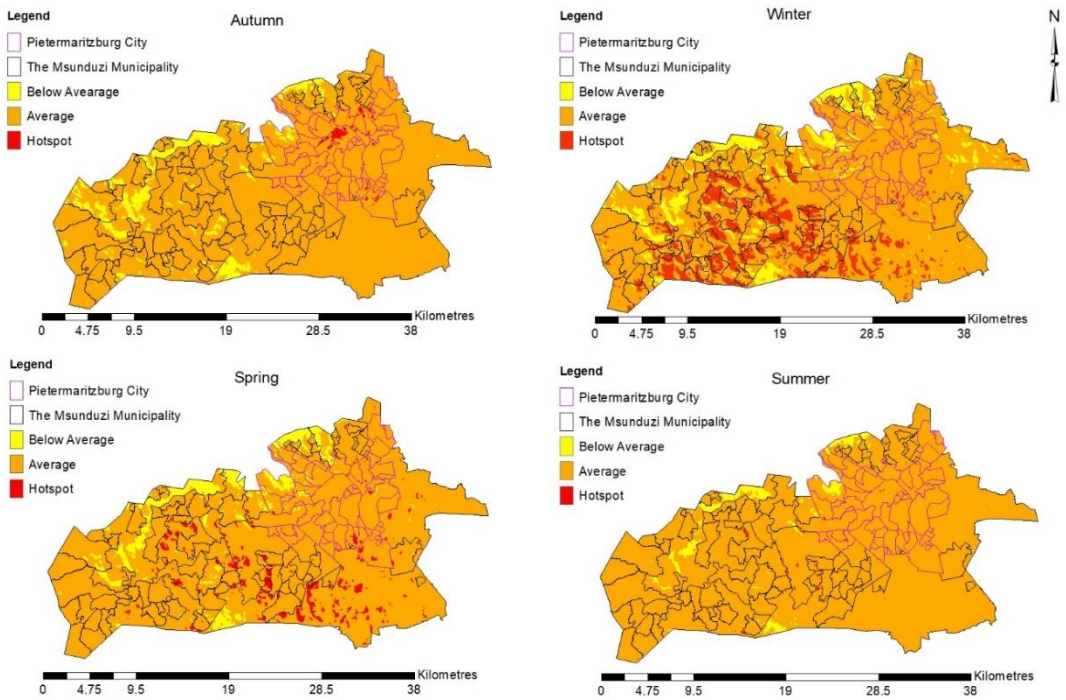

FIGURE 11. SEASONAL MEAN LAND SURFACE TEMPERATURE CLASS DISTRIBUTION (2013-2017).

During autumn, it can particularly be seen that the city centre is observed as a hotspot area for high land surface temperature values in comparison to the surrounding areas. The greater extent of the municipality is seen to have average values with areas that are dominated by dense vegetation, notably being classified as below average. This differs however for the winter period, where it is observed that the southern parts of the municipality experience higher land surface temperature values compared to the CBD. This shift in the SUHI hotspot is notable during the winter due to the changes in land cover, especially the response of grasslands and plantations to the winter period and thus exposing much of the bare ground.

The distribution of hotspots during the spring period is similar to the winter period. During the spring a reduction in the spatial extent of the areas characterised as hotspots during the winter is observed. This is could be due to the period regrowth of vegetated surfaces that had been dormant during the winter. In this we see that as these surfaces are re-vegetated, the SUHI dissipates in these areas and eventually becomes very minimal during the summer. The summer period shows a rather evened distribution of values throughout the study area. With isolated areas that can be classified as hotspots.

From these maps, it can be suggested that the distribution of LST in the Municipality is transitional during seasons and depends heavily on the land cover and its seasonal changes. During the autumn when there are distinctive boundaries in the land cover, the city centre is clearly visible to be a constant heat sink. As the seasons continue to alternate there are instances where certain land covers retain more heat than the built-up areas. This can be explained by the varying capacity to retain heat amongst land cover classes especially during the morning where dry vegetated surfaces and the exposed below surface during winter absorb incoming solar radiation much quicker than artificial surfaces. Such observations may distort the understanding of the SUHI with night-time observations often revealing a better understanding to how heat is retained at the surface.

4.1.4 Land surface temperature and ambient air temperature

The atmosphere is heated through the transfer of energy via conduction, convection and radiation. As incoming solar radiation strikes the surface of the earth and warms it, the warm ground begins to emit long wave radiation where some of it is absorbed by greenhouse gases and causes the atmosphere to warm. The ability of the surface to emit long wave radiation depends on the thermal properties of the surface (Tyson and Preston-Whyte, 2000). A changing landscape through processes such as urbanisation introduces impervious surfaces such as concrete, road networks and pavements that absorb more incoming solar radiation thus creating high land surface temperatures and consequently high ambient air temperatures (Voogt and Oke, 2003). To test this, ambient air temperature observations from *in situ* monitoring stations were tested against extracted land surface temperature values between two stations located in the Msunduzi Municipality. Figure 12 illustrates the mean LST extracted from a 1000m buffer and ambient air temperature between stations: Pietermaritzburg Central and Pietermaritzburg Airport during all seasons in the years 2013 to 2017 is seen below.

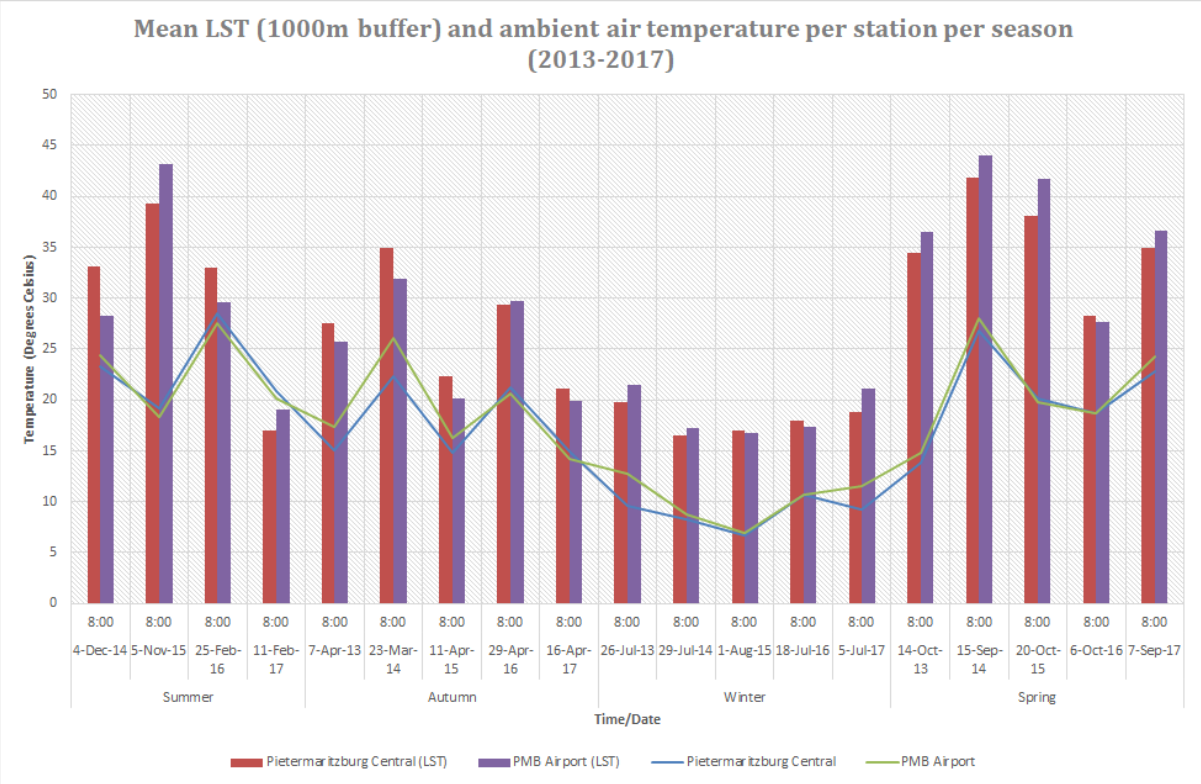

FIGURE 12. A GRAPHICAL ANALYSIS SHOWING MEAN LST EXTRACTED FROM 1000M BUFFERS AGAINST AMBIENT AIR TEMPERATURE OBSERVATIONS BETWEEN CENTRAL PIETERMARITZBURG AND PIETERMARITZBURG AIRPORT (2013-2017).

From this graph the relationship between LST and ambient air temperature is seasonal, with peaks in LST being consistent with observed peaks in ambient air temperature. LST patterns are usually higher than observed ambient air temperatures except for the 11th of February 2017. A considerable decrease is seen during the winter season throughout the years, with LST values during spring appearing to be relatively higher. The correlation between ambient air temperature and land surface temperature reveals a linear pattern where an increase in land surface temperature is positively correlated with an increase in air temperature. The relationship between these values was quantified through a Pearson correlation which expressed a score of 0.70, indicating a reasonably strong positive relationship between the two variables (Figure 13).

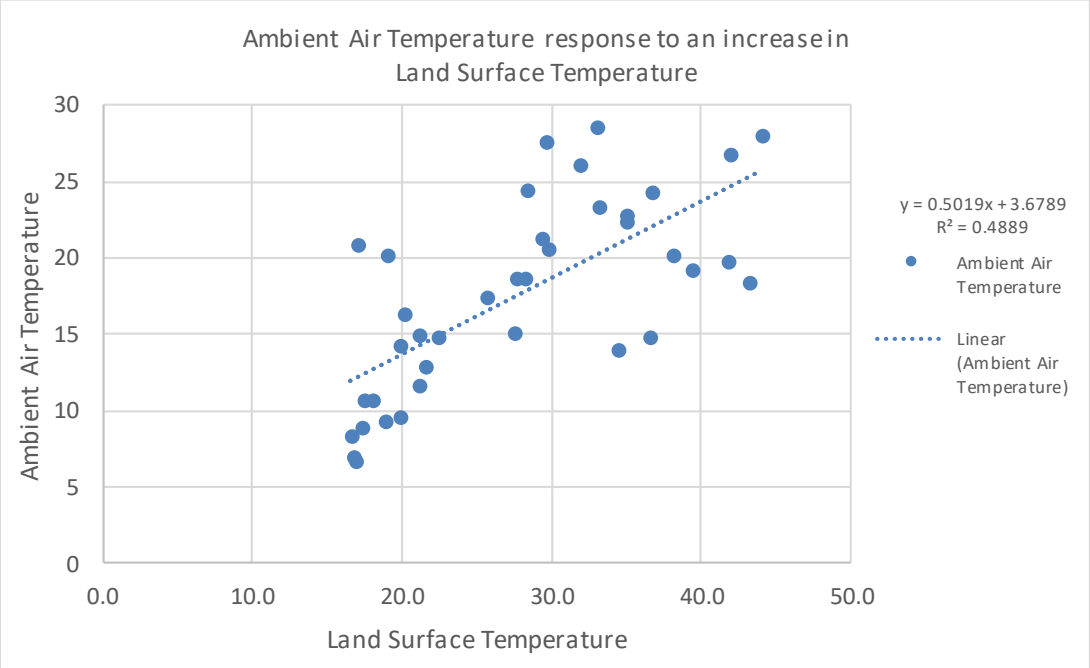

FIGURE 13. A SCATTERPLOT SHOWING THE RELATIONSHIP BETWEEN SATELLITE RETRIEVED LST AND MEASURED AMBIENT AIR TEMPERATURE AT THE LOCALITY OF MONITORING STATIONS.

From this relationship, it seen that over a space of 1000m, the temperature of the ambient air observed above is influenced by the temperature of the surface below it. This relationship ($r = 0.70$; $R^2 = 0.49$) could then highlight the possibility of the formation of urban heat islands due to a changing surface that influences the temperature of the ambient air above it. To quantify the intensity of the surface urban heat island (SUHI) effect, buffers to extract LST values over urban and rural areas were created wherein the difference in the land surface temperature values between these areas would express the intensity of the SUHI effect. Due to the absence of

weather monitoring stations in rural parts of the municipality, the assessment only used extracted LST values. Below are the locations of the buffer zones above rural and urban areas (Figure 14).

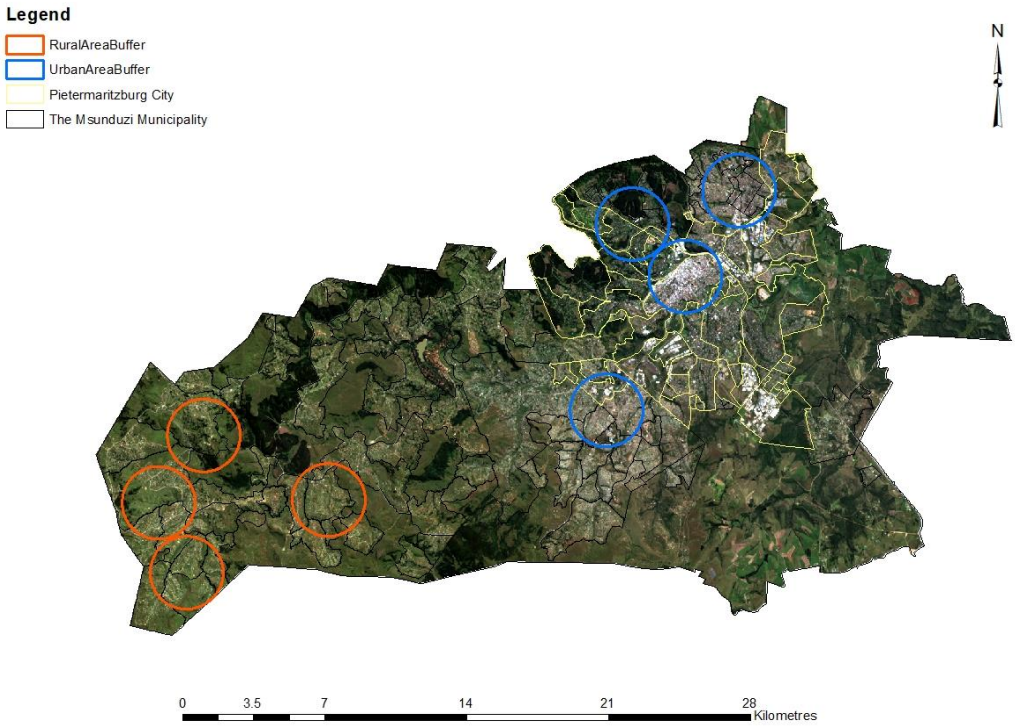

FIGURE 14. LOCATION OF BUFFER ZONES BETWEEN AREAS CLASSIFIED URBAN AND RURAL IN THE MSUNDUZI MUNICIPALITY.

The difference in LST values between urban and rural areas per season indicates that it is not always consistent that urban areas are warmer than rural areas with regards to surface temperatures. There are instances were areas classified as rural are warmer than those classified as urban as seen below (Figure 15).

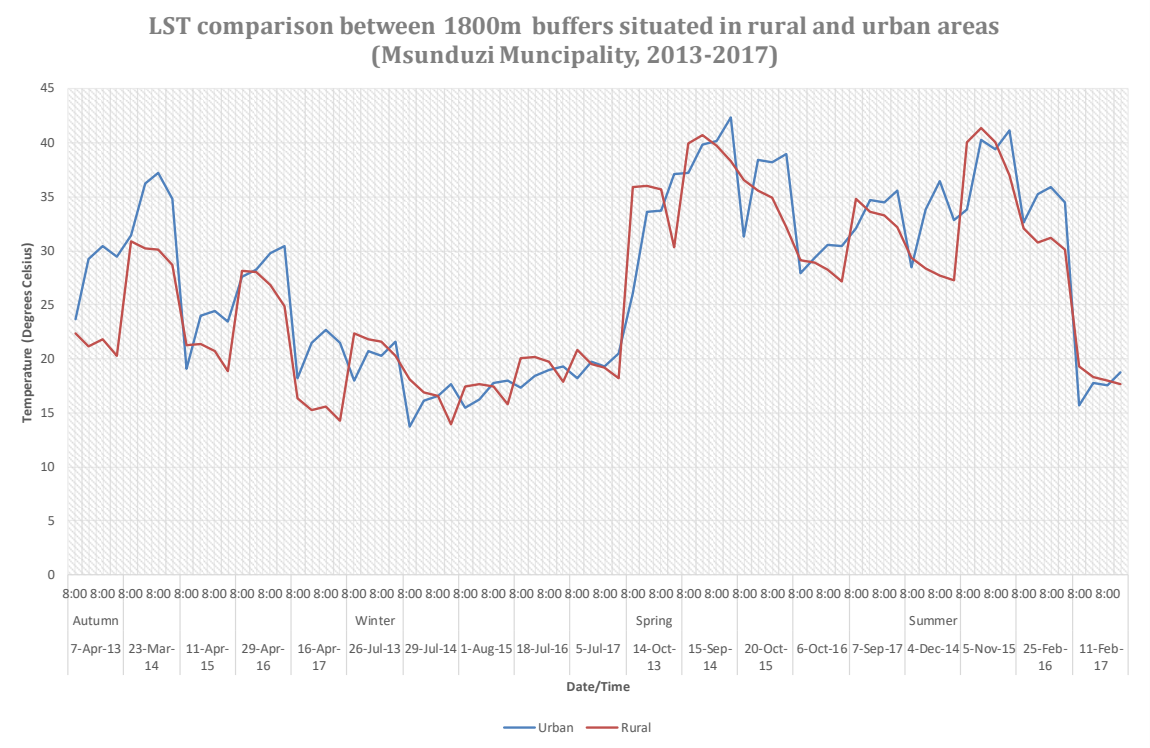
LST comparison between 1800m buffers situated in rural and urban areas
(Msunduzi Muncipality, 2013-2017)
Temperature (Degrees Celsius)
45
40
35
30
25
20
15
10
5
0
8:00 8:00 8:00

The mean differences are seen in Figure 16 , where the highest difference is visibly during the autumn season.

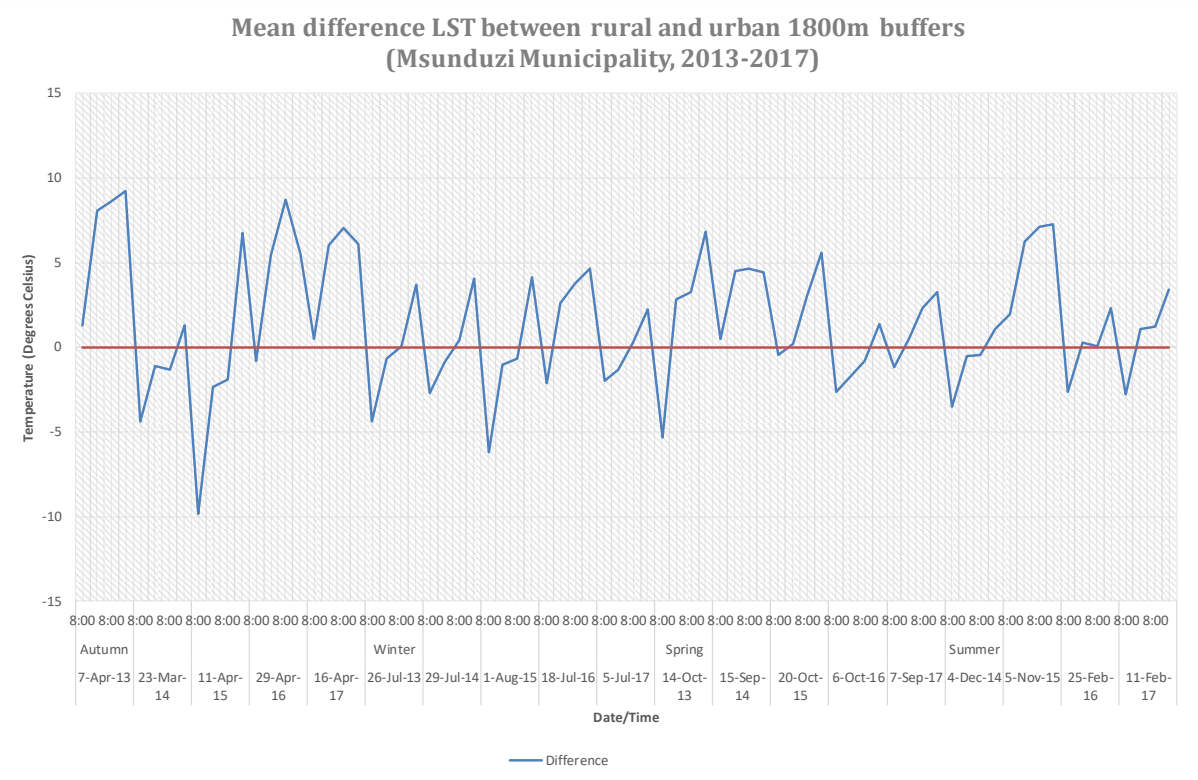

FIGURE 16. A GRAPH SHOWING THE MEAN DIFFERENCES OF LST BETWEEN SUHI BUFFERS LOCATED IN RURAL AND URBAN AREAS IN THE MSUNDUZI MUNICIPALITY.

It is demonstrated that there is a positive relationship between land surface temperature and air temperature. The heating up of the ambient air is influenced by the type of surface below as urban areas tend to be warmer than rural areas. The SUHI effect is present in the Msunduzi Municipality and is most intensive during autumn between 2013 and 2017. The distribution of LST as a result of dominant land cover patterns creates definite discontinuities between rural and urban areas in the municipality.

4.2.5 Spatial Autocorrelation

A spatial autocorrelation analysis was performed on the sampled LST data for each season between the years 2013 and 2017. This analysis expresses the distribution of LST values from the sampled data which would then infer on the spatial spread of both high and low LST values. A Moran's Index value quantifies the spatial correlation of the distribution. In addition, this would indicate whether the values are distributed in the following manner: dispersed, random or clustered. The illustration below shows the schematic representation of the distribution of values.

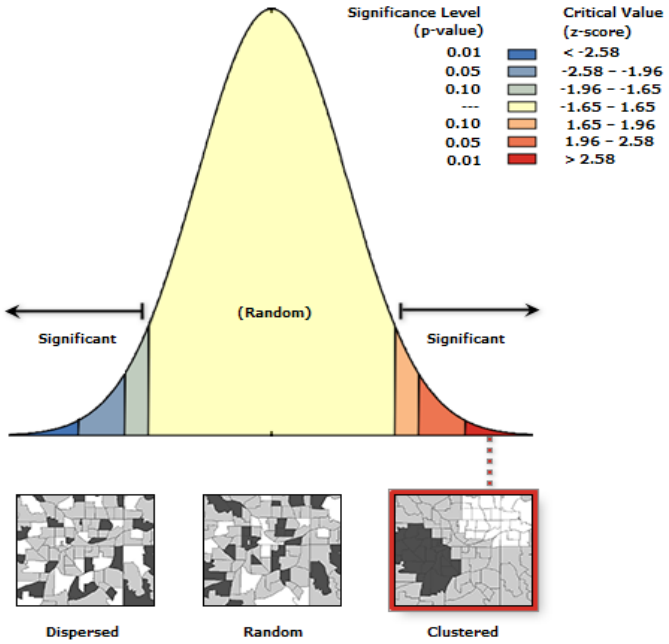

FIGURE 17. A SCHEMATIC REPRESENTATION OF VALUE DISTRIBUTION ON SPATIAL AUTOCORRELATION (ESRI, 2017).

Autumn has the highest Moran's Index (0.48) indicating that most of the highest LST value are clustered close together, with the lower values also clustering closer to each other. This demonstrates that during the autumn season, the SUHI effect is most pronounced in the Msunduzi Municipality. The spring season follows closely after autumn, also indicating that there is a clustered distribution of LST values. Summer and winter have lower Moran's Index values with, 0.33 and 0.29; respectively. The distribution of values in these seasons is nevertheless clustered. This could explain that although high and low values of LST are moderately clustered together during summer and winter, the response of the distribution of

LST values in terms of how the land surface changes during seasonal transitions is slow (Table 5).

TABLE 5. OUTPUT RESULTS FROM SPATIAL AUTOCORRELATION ANALYSIS

Season	Critical Value (z-score)	p-value	Moran's Index	Distribution
Autumn	86.563699	0.000	0.479292	Clustered
Winter	44.917888	0.000	0.248164	Clustered
Spring	82.131872	0.000	0.454431	Clustered
Summer	59.542156	0.000	0.329224	Clustered

From the analysis, it is observed that the land surface temperature values were consistently clustered, suggesting separate clusters between warm and cool areas in the Msunduzi Municipality. The large disparity between warm and cool areas in the municipality inevitably leads to strong heat island conditions. In further assessing the SUHI's dependency on LULC, the use of vegetation and built-up area parameters are studied with LST to understand the contribution of LULC to increases and decreases of LST in the Msunduzi Municipality.

4.1.5 Land surface temperature and land cover indices

The use of remotely-sensed satellite data arranged in various band combinations allows for the computation and calculation of indices which are products of mathematical calculations. For the second objective of the study, the Normalised Difference Vegetation Index (NDVI), Fractional Vegetation Cover (FVC) and the Normalised Difference Built-up Index (NDBI) were used in the analysis to quantify the relationship between land cover/land use and land surface temperature. These indices were calculated per image where then the mean values of each season were calculated. Below are NDVI map outputs for autumn, winter, spring and summer between 2013 and 2017 (Figure 18).

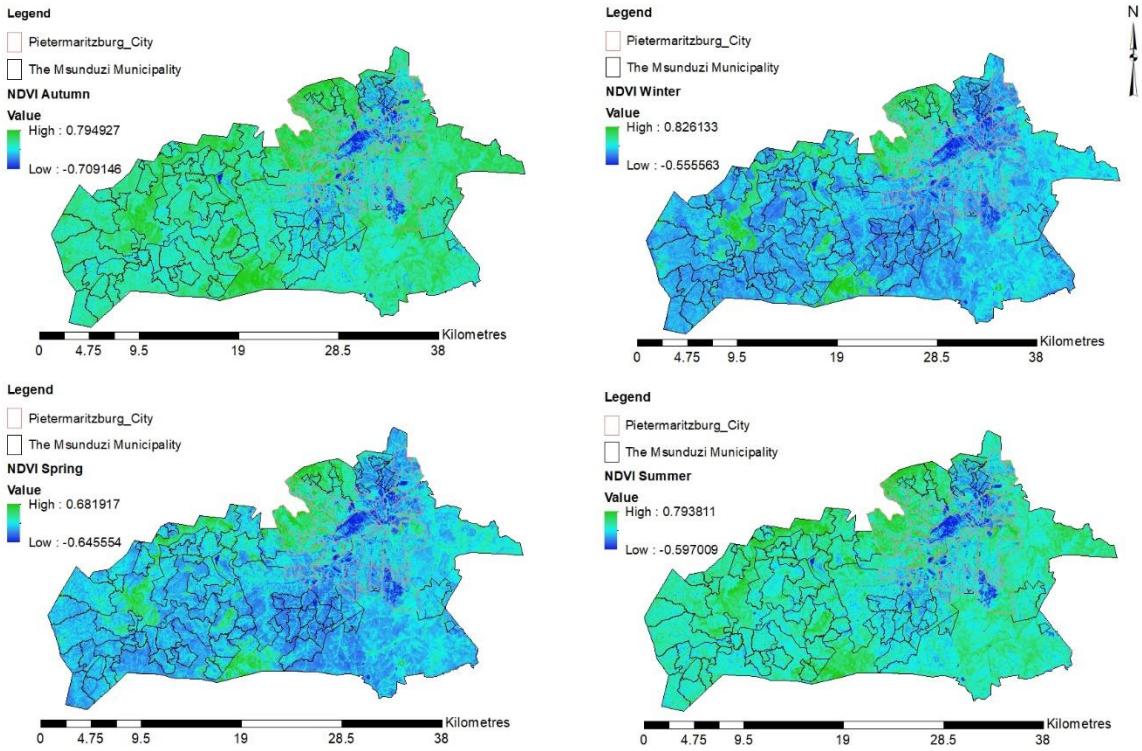

FIGURE 18. SEASONAL MEAN NDVI MAPS FOR THE MSUNDUZI MUNICIPALITY (2013-2017).

The NDVI is a graphical indicator that reveals whether the target being observed contains live green vegetation or not (values closer to 1, indicate live green vegetation). During autumn, large parts of the municipality appear to be covered in live green and healthy vegetation with outcrops of built up areas being observed to indicate a low NDVI values. Areas covered by dense forest appear the healthiest as during this season. This differs for the winter season, where it is observed that large parts of the municipality are dry, and this is represented by a widespread of low NDVI values with only dense forests remaining in a decent state – a pattern that is also observed during spring.

It is visible that during winter and early spring, much of the municipality is covered by dry and sparsely vegetated surfaces. It is only during summer where larger parts of the municipality start appearing to be regaining their health, signalling that land cover classes are becoming distinct. Similar patterns are observed in the analysis of FVC in the Msunduzi Municipality (Figure 19). Fractional Vegetation Cover indicates the amount of vegetation contained over the surface of the earth. The map outputs below reveal the FVC patterns per season in the Msunduzi Municipality during the study period.

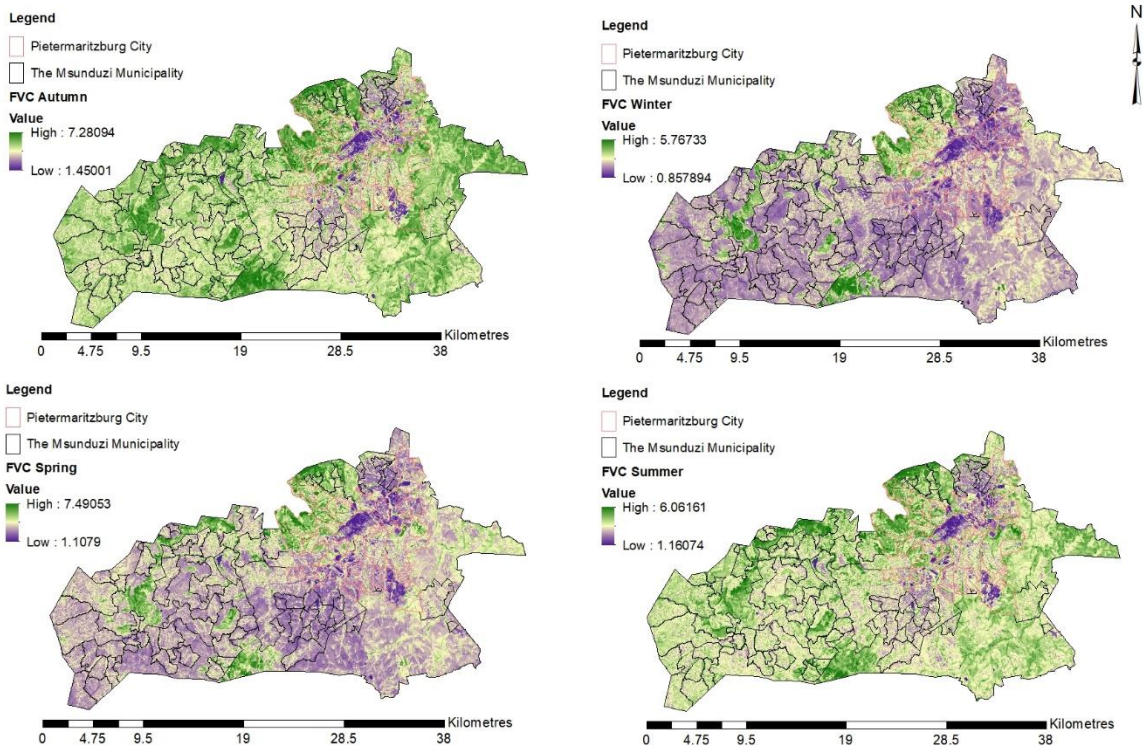

FIGURE 19. SEASONAL MEAN FVC MAPS FOR THE MSUNDUZI MUNICIPALITY (2013-2017).

During the autumn season, much of the surface of the Msunduzi Municipality is well vegetated, with only parts that are dominated by built up areas indicating a deficiency in vegetation cover. As winter approaches, there is a significant decrease in vegetation cover, as similarly noted in the winter NDVI where there was a notable decrease in vegetation greenness. A gradual increase in vegetation cover during spring can be seen to continue into the summer season – where much of the area classified as grasslands are rejuvenated by the meteorological conditions associated with the warmer season.

The anticipated changing land cover patterns as a response to the changing meteorological and climatic conditions associated with each season can be observed (Yuan and Bauer, 2007). This change would then influence the thermal dynamics of the Msunduzi Municipality, especially the ability of the surface to absorb or reflect incoming solar radiation. The changing vegetated surface, especially during the winter, exposes much of the underlying bare ground which may cause more heat retention in these areas than during the warm season. This can be seen in the mapping of the NDBI (Figure 20), where much of the grasslands have a similar spectral signature to built-up areas due to their reduced greenness and liveness.

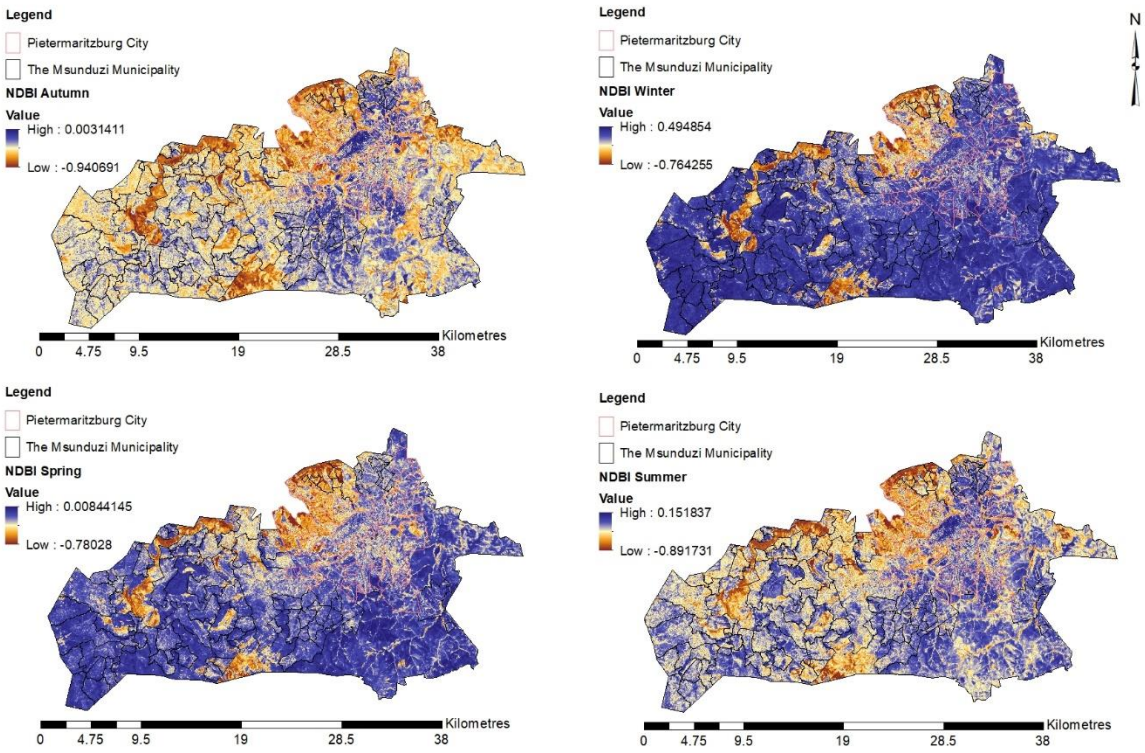

FIGURE 20. SEASONAL MEAN NDBI MAPS FOR THE MSUNDUZI MUNICIPALITY (2013-2017).

The NDBI reveals the outcrop and extent of built up areas in an area, in this instance, built up areas in the Msunduzi Municipality. During autumn, the extent of the built-up areas is distinctly visible due to well-defined and spectrally-distinct land cover classes in the municipality. This makes it possible for the built-up areas to be identified. As the winter approaches, it is seen that the changing spectral signatures of the grasslands due to the reduction of greenness are observed as built-up areas. This is due to the spectral signatures of the grasslands tethering towards the wavelengths like those of built-up areas (Yuan and Bauer, 2007). The dryness and colour change of the vegetation during the winter significantly impacts on the thermal characteristics of the surface. It is for this reason that the southern parts of the municipality are observed to retain additional heat during the winter season.

As spring approaches, much of the surface is still in recovery from the winter with larger parts of the municipality still maintaining the spectral signatures associated with built-up areas. Only parts dominated by dense forest retain their greenness and vegetation status throughout the seasons. During the summer period, it is seen that much of the surface that was classified as built-up areas is significantly changing and is represented by higher NDBI values, representing non-built-up areas. The rejuvenation of the grasslands can be attributed to prevailing wet and warm conditions in the municipality.

4.1.6 LULC influences on land surface temperature

The configuration of land use or land cover patterns has been noted to influence the surface thermal dynamics of a given area. To further characterise these influences, two transects along the north-south and west-east directions of the municipality were used to extract mean LST and NDVI, FVC and NDBI data points for the summer and winter seasons between 2013 – 2017. These transects capture the dominant land cover classes where the north-south transect bisects the Pietermaritzburg CBD and the surrounding settlements and the vegetation discontinuities between them. The west-east transect captures segments of the rural areas, dominant plantations as well as portions of woodlots present within the municipality. These transects are illustrated in the map below (Figure 21).

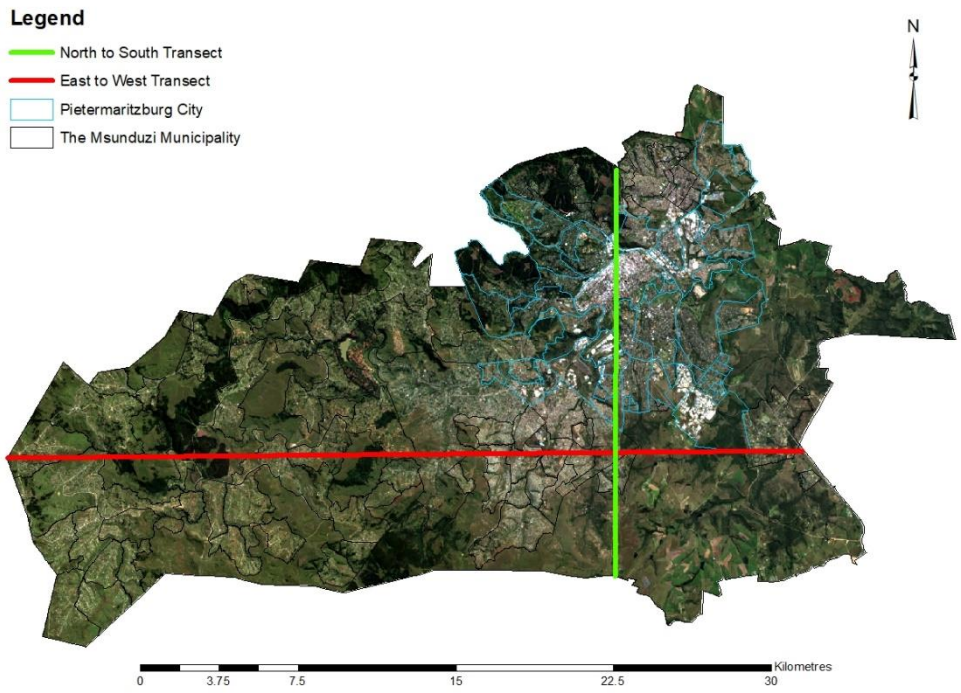

FIGURE 21. LOCATION OF THE NORTH-TO-SOUTH AND WEST-TO-EAST SAMPLING TRANSECTS.

The transects of mean LST and land cover indices extracted for the summer and winter seasons indicate the influences of land cover on land surface temperatures. With the application of remote sensing land cover indices, the graphs below illustrate the patterns in the changing of LST across different LULC configurations in the Msunduzi Municipality. In the North-South transect it is observed that LST increases substantially within the CBD during both seasons (Figure 22). These increases are associated with the presence of built-up areas as indicated by the simultaneous increase in NDBI and decreases in NDVI and FVC during both winter and summer. In sections dominated by vegetation and water bodies, clear decreases in LST are noted with subsequent increases in NDVI and FVC. These patterns suggest a cooling effect by the presence of vegetation in the municipality during both seasons.

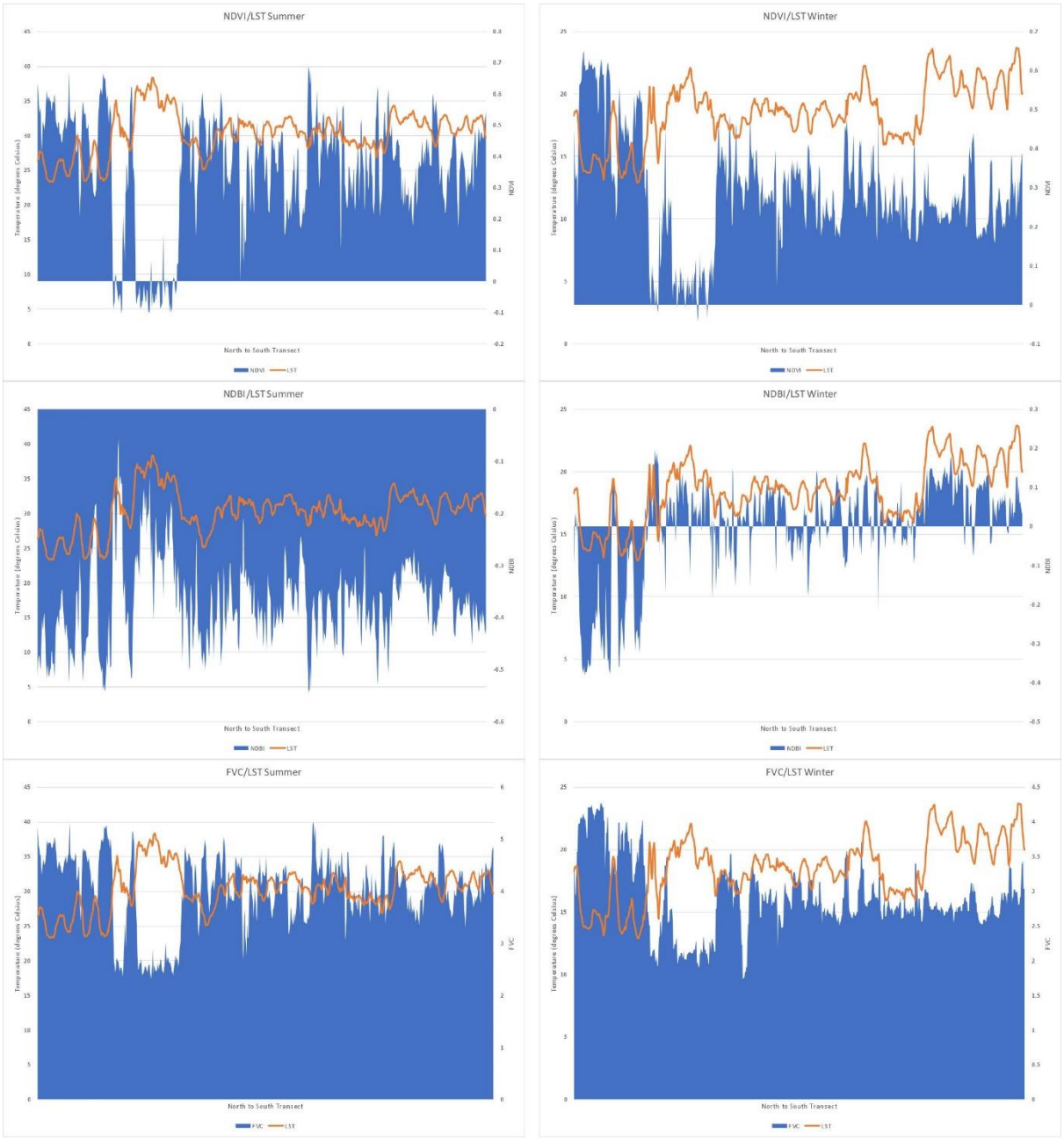

FIGURE 22. NORTH-TO-SOUTH SECTIONAL COMPARISON BETWEEN MEAN LST, NDVI, NDBI AND FVC FOR SUMMER AND WINTER.

Similar trajectories between LST and land cover indices are observed along the West-East transect where settlements and bare ground areas are observed to be warmer than areas dominated by vegetated surfaces (Figure 23). The discontinuities of differing LULC patterns along the transect are clearly observed in the LST response signal where vegetated surfaces predominately act as coolants in the municipality relative to artificial surfaces. The relationships between LST, NDVI and FVC differ only in terms of magnitude between the seasons with similar signal trajectories being observed for both seasons. What seems to change

drastically between the seasons is NDBI, where the signal is interrupted by the presence of vegetation and therefore not being a suitable measure as an index for built-up areas. However, values closer to zero are still associated with increases in LST during both seasons along the transects.

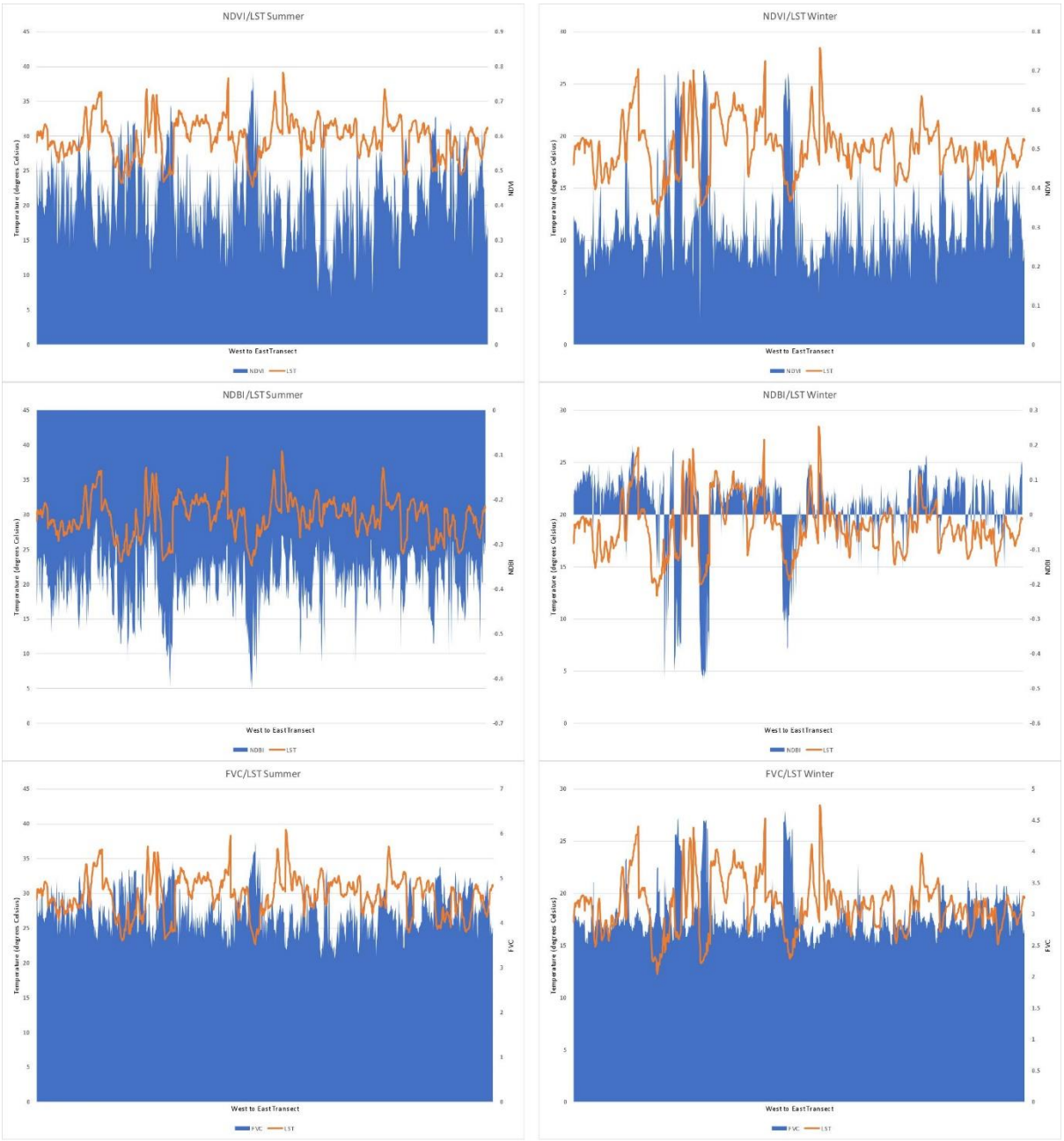

FIGURE 23. WEST-TO-EAST SECTIONAL COMPARISON BETWEEN MEAN LST, NDVI, NDBI AND FVC FOR SUMMER AND WINTER.

The seasonality of LST over different land cover classes is provided below (Figure 24). The surface is visibly warmer during summer compared to winter, with the built-up area class observed to substantially absorb incoming solar radiation compared to other classes. During winter however, the grasslands class is observed to be slightly higher than the built-up areas class. Woodlots weaken the SUHI effect than plantations, with indigenous forests indicating much more efficiency amongst the land cover classes. The presence of plantations within the urban areas indicate a potential for the weakening of the SUHI effect where the presence of vegetation and particularly trees improve the ability of cities to reduce surface temperature.

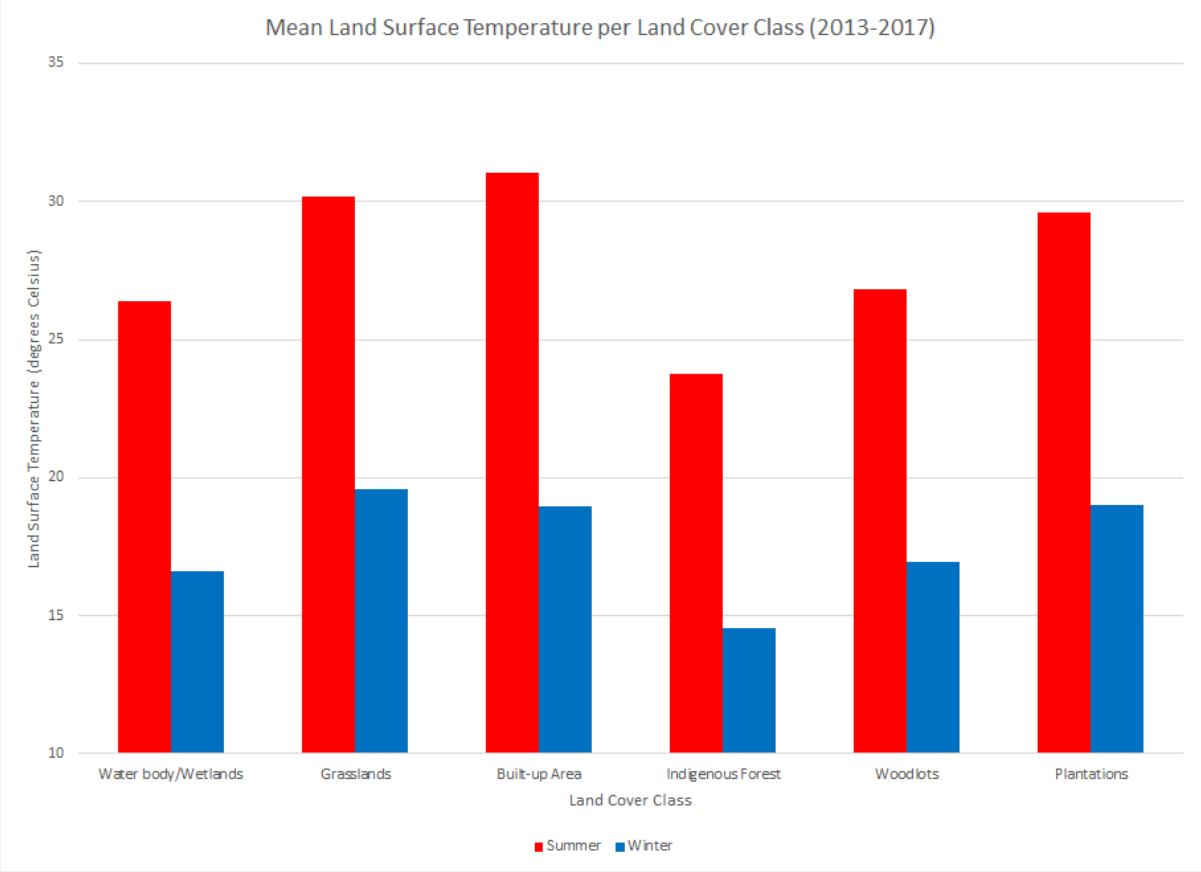

FIGURE 24. MEAN LAND SURFACE TEMPERATURE PER LAND COVER CLASS BETWEEN SUMMER AND WINTER (2013-2017).

To substantiate the relationships between LST and the land cover indices, a correlation analysis provides an indication of the strength and direction of these observed patterns.

4.1.7 Correlation analysis

The summary statistics as well as outputs from the computation of a correlation analysis between LST, NDVI, NDBI, FVC for the four seasons along the N-S and W-E transects are provided below (Table 6).

TABLE 6. SUMMARY STATISTICS FOR CORRELATION ANALYSIS BETWEEN LST, NDVI, NDBI AND FVC FOR N-S AND W-E TRANSECTS

				North-South				
Statistics	**LST**				**NDVI**			
	Autumn	**Winter**	Spring	**Summer**	Autumn	**Winter**	Spring	**Summer**
Mean	26.075	18.529	35.469	30.272	0.339	0.287	0.122	0.357
Min	19.556	12.883	26.078	23.333	-0.214	-0.044	-0.191	-0.105
Max	36.555	23.735	42.736	38.406	0.692	0.649	0.450	0.689
Standard deviation	3.305	0.139	3.763	3.069	0.220	0.122	0.139	0.186

	NDBI				**FVC**			
	Autumn	**Winter**	Spring	**Summer**	Autumn	**Winter**	Spring	**Summer**
Mean	-0.576	-0.002	-0.456	-0.371	5.088	2.919	3.013	4.011
Min	-0.757	-0.381	-0.633	-0.544	2.875	1.745	1.980	2.313
Max	-0.313	0.197	-0.278	-0.054	6.736	4.276	4.219	5.330
Standard deviation	0.084	0.517	0.061	0.081	0.944	2.395	0.492	0.700

				West-East				
Statistics	**LST**				**NDVI**			
	Autumn	**Winter**	Spring	**Summer**	Autumn	**Winter**	Spring	**Summer**
Mean	24.164	18.867	35.719	29.693	0.420	0.308	0.152	0.430
Min	17.617	12.241	25.304	22.641	0.074	0.061	-0.039	0.130
Max	29.975	28.432	43.431	39.152	0.756	0.703	0.544	0.778
Standard deviation	2.547	2.608	3.453	2.822	0.124	0.104	0.105	0.108

	NDBI				**FVC**			
	Autumn	**Winter**	Spring	**Summer**	Autumn	**Winter**	Spring	**Summer**
Mean	-0.597	0.019	-0.441	-0.388	5.422	2.987	3.117	4.281
Min	-0.788	-0.486	-0.681	-0.624	3.924	2.444	2.498	3.179
Max	-0.438	0.203	-0.338	-0.240	7.075	4.655	4.645	5.808
Standard deviation	0.061	0.117	0.059	0.062	0.577	0.382	0.390	0.445

North-South

	LST/NDVI				LST/NDBI			
Statistics	Autumn	**Winter**	Spring	**Summer**	Autumn	**Winter**	Spring	**Summer**
Correlation	-0.839	-0.554	-0.636	-0.735	0.836	0.748	0.751	0.671
R^2	0.704	0.307	0.405	0.540	0.698	0.560	0.564	0.451

LST/FVC

	Autumn	**Winter**	Spring	**Summer**
Correlation	-0.838	-0.547	-0.639	-0.735
R^2	0.702	0.299	0.409	0.540

West-East

Statistics	LST/NDVI				LST/NDBI			
	Autumn	**Winter**	Spring	**Summer**	Autumn	**Winter**	Spring	**Summer**
Correlation	-0.634	-0.409	-0.706	-0.659	0.702	0.563	0.659	0.668
R^2	0.402	0.167	0.498	0.434	0.493	0.317	0.434	0.446

LST/FVC

	Autumn	**Winter**	Spring	**Summer**
Correlation	-0.636	-0.421	-0.709	-0.672
R^2	0.404	0.177	0.503	0.451

The correlation analysis between LST, NDVI, NDBI and FVC substantiates the relationships observed in the transect analysis. NDVI and FVC are negatively correlated with LST. This is notably observed during autumn (-0.839) and summer (-0.735) along the N-S transect, and between spring (-0.706), summer (-0.659) and autumn (-0.634) along the W-E transect. The strength of these relationships decreases during the winter along both transects indicating that the SUHI effect is less intense. The relationship between LST and NDBI clearly contrasts with that of vegetation parameters where positive correlations are observed. This reveals that the presence of built-up areas is consistent with increases in heat retention and subsequently the observed increases in LST. This relationship was observed to be strong along both transects throughout the seasons, particularly during autumn where 0.836 and 0.702 are observed along the N-S and W-E transects, respectively.

These observed relationships are however moderately explained by the individual vegetation and built-up area parameters along both transects throughout the seasons. It is seen that although relatively strong correlations are observed, there are variables unaccounted for that contribute to the observed LST fluctuations between seasons. In some instances, considerable variance (70%) of LST is predictable from NDVI and FVC during autumn. This predictive capacity considerably decreases during winter, suggesting weaker dependencies between LST and vegetation parameters during the other seasons as observed along the N-S transect. Furthermore, a weaker predictive capacity is observed along the W-E transect for FVC and NDVI compared to the N-S transect, however these relationships still respond similarly between all the seasons.

4.1.8 UHIs and Air Quality

Measured air pollutants and ambient air temperature

The impact of urban heat islands on air pollution is observed in how ambient air temperature remains a significant factor in the production and concentration of air pollutants in the lower layers of the atmospheric boundary layer, especially that of secondary pollutants such as surface ozone (Zunckel *et al*., 2004). Apart from definite trends in affecting surface ozone concentrations, temperature profiles in the lower atmosphere are a contributing factor in the retention of various pollutants, especially during inversion conditions.

Inversion conditions are most significant during the night where they can particularly affect pollution distribution by trapping pollutants through the above thermal layer opposing any movement and subsequent dissipation of pollutants. It is only during the midmorning period, when the inversion conditions dissipate, that the movement of pollutants occurs, thus dramatically reducing pollutant concentrations during noon and the afternoon period (Tyson and Preston-Whyte, 2000). The study assessed a time variation of pollution concentrations between winter and spring – seasons where pollution episodes are considerably pronounced. This was done in order to understand the patterns associated with pollution concentrations during the day and the night. In doing so, this would also bring clarity on the relationships and the possible impacts between temperature and various air pollutants.

The selection of the period of analysis was arbitrary between the seasons of winter and spring although it was guided by the intensity of inversions during the winter in Pietermaritzburg and the lifting of the inversion layer due to an increase in instability of the atmosphere during spring and towards the summer season. The air pollution data in use were from two monitoring stations located in the vicinity of the Pietermaritzburg CBD and the other, located at the Pietermaritzburg Airport. Each station monitored different pollutants and the specifics are listed below (Table 7).

TABLE 7. MONITORED POLLUTANTS PER STATION LOCATED IN THE MSUNDUZI MUNICIPALITY

	Monitoring Station	
	Pietermaritzburg CBD	Pietermaritzburg Airport
Pollutants	Sulphur dioxide (SO_2)	Particulate Matter (10 & 2.5)
	Nitric oxide (NO)	Sulphur dioxide
	Nitrogen dioxide (NO_2)	Nitric oxide
	Nitrogen oxides (NO_x)	Nitrogen dioxide
		Surface ozone (O_3)
		Nitrogen oxides

It is important to highlight the limitation in the lack of direct comparison for some of these pollutants due to the difference in the parameters monitored by the stations as their usually associated with the specifications of the area of location thus influencing the capabilities of the monitoring instrumentation. The constant monitoring of air pollutants in the Msunduzi Municipality is also relatively in its infancy as it only began in June/July 2016; therefore, it is currently not feasible to conduct lengthy studies for air pollution related assessments with the freely available air quality dataset provided by the municipality.

The Msunduzi Municipality has a variety of pollution sources, with most of them located in and around the vicinity of the city of Pietermaritzburg. The location of the monitoring stations offers a low spatial resolution and therefore the assessment of pollutants was only restricted to the neighbouring areas of the city centre and the Pietermaritzburg Airport. The variation of air pollutants concentrations and their related patterns to increases and decreases in air temperature during the winter season was assessed for the winter and spring seasons (July-August and September-October). The assessment evaluated a time series and variation of concentrations of SO_2, NO, NO_x and NO_2, PM_{10}, $PM_{2.5}$ and O_3 observations for the central Pietermaritzburg and Pietermaritzburg airport stations. In addition, Pearson correlations were computed to assess the linear correlation between each pollutant and ambient air temperature.

Over a period of two winter months, the oscillations in the concentrations of pollutants in the Msunduzi Municipality are observed. A summary statistics table for monitored pollutants and selected meteorological variables during July and August 2017 is provided below (Table 8). During this period, mean pollutant concentrations for the central station were observed. NO_x concentrations peak at 81 ppb with 16 ppb observed for SO_2. NO_x concentrations are considerably lower at the airport station (34 ppb) whereas SO_2 concentrations have remained unchanged. Mean Particulate Matter concentrations are observed at 42 and 29 ppb for PM_{10} and $PM_{2.5}$, respectively.

Assessing the mean concentrations for criteria pollutants against the National Ambient Air Quality Standards hourly limits for SO_2 set at 134 ppb, with NO_2 at 106 ppb, indicates that these are below the set limits. However, with a mean of 16 ppb at the central station, there are concerns especially with the constant trend of SO_2 that it may exceed the 19 ppb annual limit. Similarly, NO_2 concentrations at a mean of 23 and 29 ppb for the stations, may signal potential exceedances of the yearly limit set at 21 ppb. PM_{10} concentrations average at 42 ppb, below the set hourly limit of ~ 61 ppb with O_3 concentrations registering 24 ppb, also observed to be well below the 8 hours running limit of 61 ppb.

TABLE 8. TABLE SHOWING THE SUMMARY STATISTICS FOR MONITORED POLLUTANTS AND SELECTED METEROLOGICAL VARIABLES (JULY-AUGUST 2017) AT THE PMB CENTRAL AND AIRPORT STATIONS.

Pietermaritzburg Central (Winter) [ppb]											
	PM_{10}	**$PM_{2.5}$**	**NO**	**SO_2**	**O_3**	**NO_x**	**NO_2**	**Tair**	**Rh**	**WS**	**WD**
Min			0	8		1	1	4	7	0	1
1st Qu			3	15		16	12	11	44	0	118
Median			12	16		35	20	14	62	0	217
Mean			58	16		81	23	15	59	1	199
3rd Qu			77	16		113	30	18	78	1	270
Max			426	26		481	92	31	96	4	360
NA's			1	1		1	1	1	1	1	1
Pietermaritzburg Airport (Winter) [ppb]											
Min	3	2	0	0	0	0	3	4	7	0	0
1st Qu	31	18	1	0	14	11	13	12	39	1	20
Median	40	26	2	1	25	23	24	14	60	2	110
Mean	42	29	11	2	24	34	29	15	59	2	127
3rd Qu	51	36	7	2	33	44	40	19	80	3	30
Max	188	358	393	12	68	384	105	31	98	11	360
NA's	27	23	130			32	25				

The pollution oscillation and wind rose graphs between the two stations are provided below.



FIGURE 25. TIME PLOT SHOWING HOURLY POLLUTANT CONCENTRATIONS (PPB) VERSUS WIND SPEED AND AMBIENT AIR TEMPERATURE, PMB CENTRAL STATION (JUL-AUG 2017).

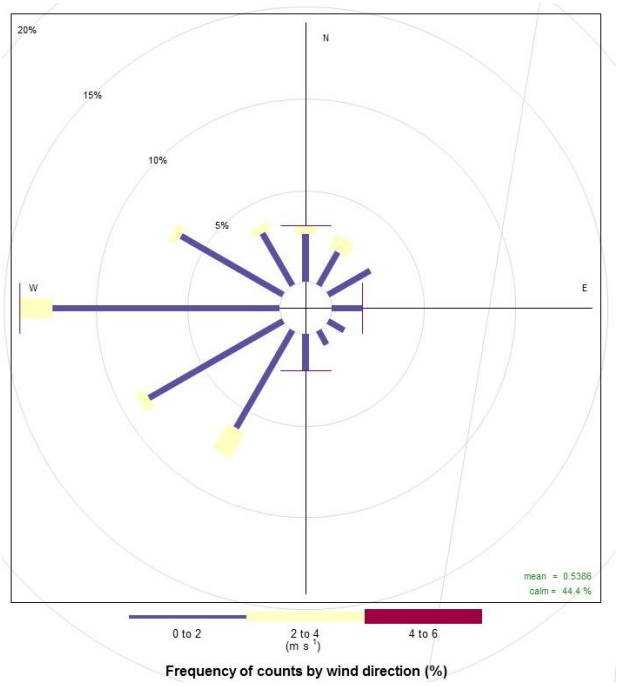

FIGURE 26. WINDROSE INDICATING WIND SPEED FREQUENCY COUNTS BY PERCENTAGE WIND DIRECTION, PMB CENTRAL STATION (JUL-AUG 2017).

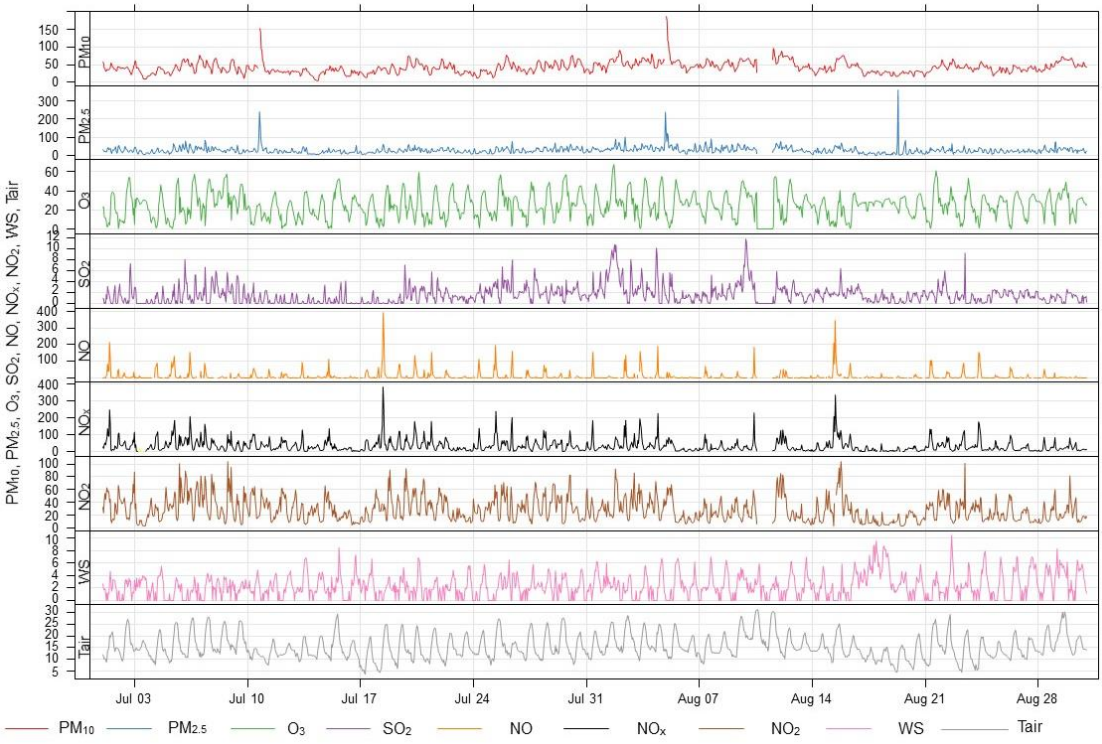

FIGURE 27. TIME PLOT SHOWING HOURLY POLLUTANT CONCENTRATIONS (PPB) VERSUS WIND SPEED AND AMBIENT AIR TEMPERATURE, PMB AIRPORT STATION (JUL-AUG 2017).

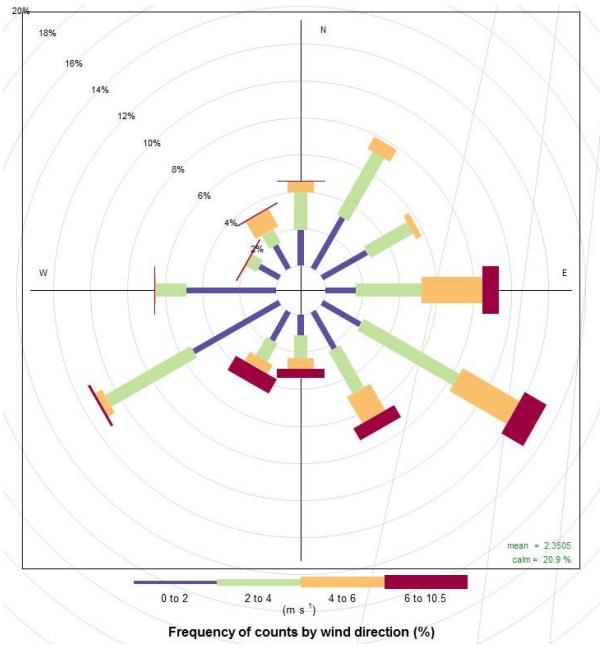

FIGURE 28. WINDROSE INDICATING WIND SPEED FREQUENCY COUNTS BY PERCENTAGE WIND DIRECTION, PMB CENTRAL STATION (JUL-AUG 2017).

The pollutant concentrations during winter in the Msunduzi Municipality are generally within limits, however the possibility of these trends running throughout the year, suggests that the municipality is close to exceeding the set limits for criteria pollutants. It can also be seen with how meteorological conditions may contribute to pollution concentration changes where between the 7th and 21st of August (Figure 25 and Figure 27), the increased wind speeds and reduced ambient air temperature indicates the passage of fronts that have caused the breaking of stable layers, thus causing increases in observed pollutants that may otherwise be trapped (Tyson and Preston-Whyte, 2000). In addition, situations of pollutant recirculation due to dominant synoptic circulation may also be attributed to the rapid increases in concentrations.

The dominant wind direction during winter differs between the stations, where the central station indicates slower wind speeds with a dominant westerly direction (Figure 26), compared to quicker wind speeds recorded at the airport station, with dominant south east winds (Figure 28). The differences in these wind speeds and direction are likely due to the altitudes of the monitoring stations, as well their locations where the central station is within the geologic basin where winds may be weakened during winter, in contrast to the airport station where the surroundings have a lesser impact on the observed wind speeds and directions.

To further assess the patterns of the measured air pollutants, a time variation analysis was run on the hourly concentrations to understand the weekly and mean diurnal cycles for the study periods. In the case of the central station, it seen that pollutant concentrations generally increase between 6:00 am and 12:00 noon. It is during this period where NO_x concentrations generally increase as a response to traffic levels along the N3 highway that are seen to peak during the morning period (Figure 29). This contrasts with the afternoon, where it may be expected that the traffic conditions may cause heightened pollution levels, however it is seen that pollution levels reach a constant period after the decrease from the morning period. There are instances where pollutant concentrations are seen to slightly increase during midnight. The general peaks are consistent between Mondays and Saturdays, with Sundays being an exception. The weekend effect is particularly seen in both stations, where there are lower pollutant concentrations, especially with regards to NO_x – associated with vehicle emissions. The time variation plots also indicate a standard deviation, where substantial concentration variation is observed for nitrogen oxides.

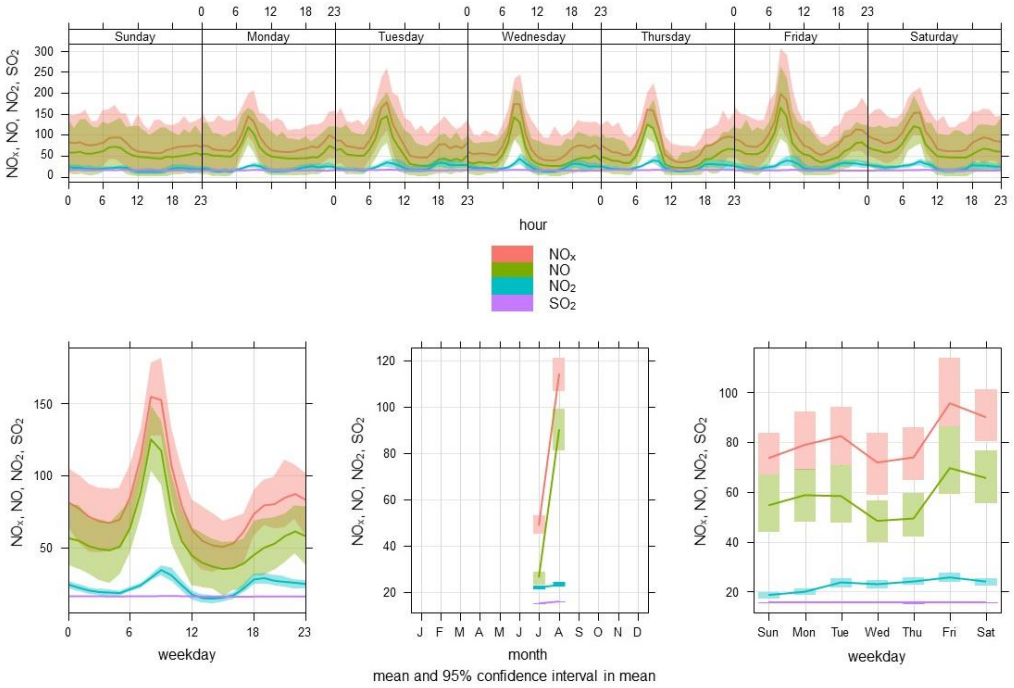

FIGURE 29. TIME VARIATION ILLUSTRATING POLLUTANT MEAN DIURNAL, WEEKLY AND MONTHLY CYCLES FOR NOX, NO, NO2 AND SO2 (PPB), PMB CENTRAL STATION (JUL-AUG 2017).

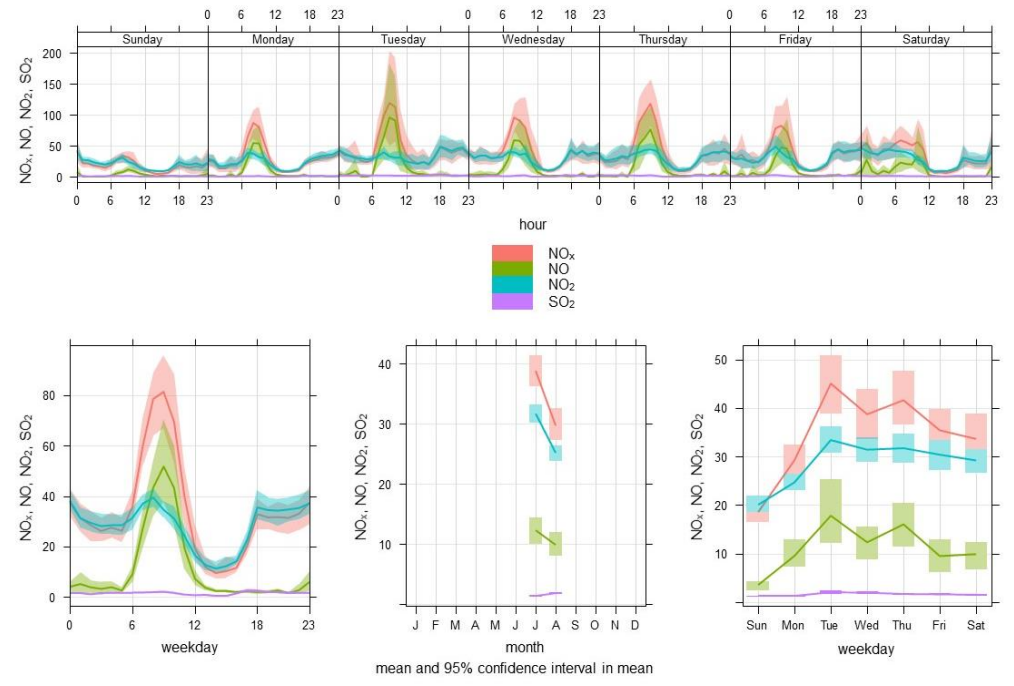

FIGURE 30. TIME VARIATION ILLUSTRATING POLLUTANT MEAN DIURNAL, WEEKLY AND MONTHLY CYCLES FOR NO_x, NO, NO_2 AND SO_2 (PPB), PMB AIRPORT STATION (JUL-AUG 2017).

NO_x cycles at the airport station differ compared to the central station, where they are considerably lower, although peaks are still observed between 6:00 and 12:00 (Figure 30). Concentrations are seen to decrease heading into the spring period at the airport station, which considerably contrasts to what is observed at the central station. In terms of the pollution peaks for the days of the week, these are generally scattered between the two stations, with Tuesdays and Fridays normally registering higher peaks than other days. Particulate matter concentrations indicate no definite cycles throughout the week, however O_3 cycles are generally following a diurnal cycle that shares similar characteristics to temperature cycles where surface ozone concentrations peak in the afternoon and recede towards the evening (Figure 31). The monthly concentrations indicate increases towards the spring season, which may be attributed to the burning of the grasslands and plantations as well as biogenic chemicals released by vegetation which sees the emission of aerosols and pollutants in the form of particulate matter into the atmosphere.

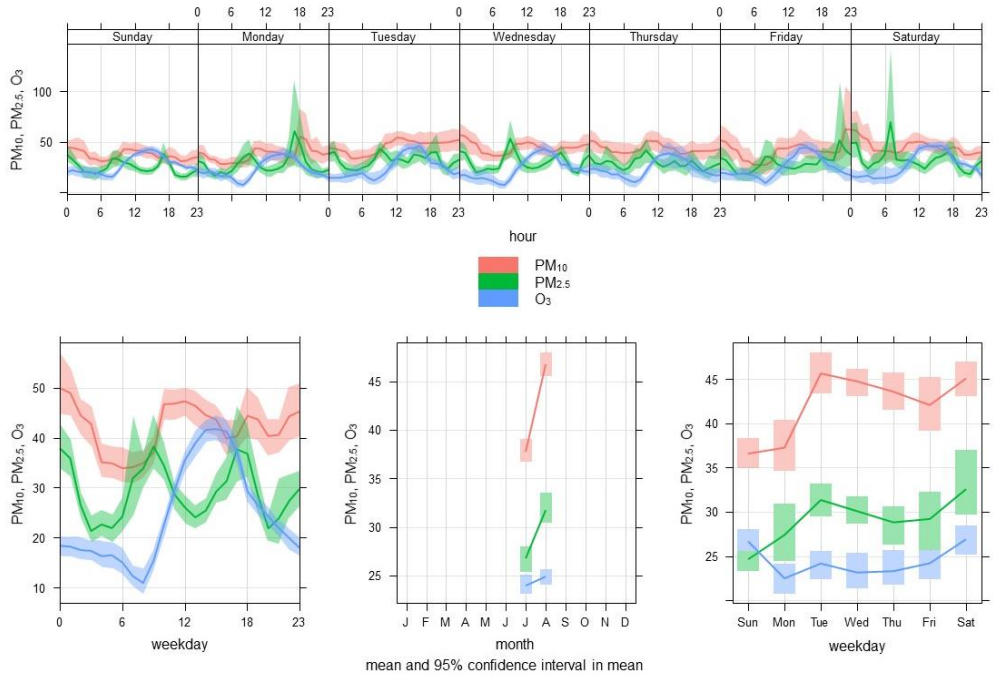

FIGURE 31. TIME VARIATION ILLUSTRATING POLLUTANT MEAN DIURNAL, WEEKLY AND MONTHLY CYCLES FOR PM_{10}, $PM_{2.5}$ AND O_3 (PPB), PMB AIRPORT STATION (JUL-AUG 2017).

The pollutant concentrations are relatively lower during spring, when compared to the observations during winter at both stations in the municipality. Diurnal cycles are also observed during spring, with NO_x concentrations being relatively lower than during winter. The central station however still shows slightly higher pollutant concentrations compared to the airport station during spring. The summary statistics for observed pollutants during spring are provided below (Table 9).

TABLE 9. TABLE SHOWING THE SUMMARY STATISTICS FOR MONITORED POLLUTANTS AND SELECTED METEROLOGICAL VARIABLES (SEPTEMBER-OCTOBER 2017) AT THE PMB CENTRAL AND AIRPORT STATIONS.

Pietermaritzburg Central (Spring) [ppb]											
	PM_{10}	**$PM_{2.5}$**	**NO**	**SO_2**	**O_3**	**NO_x**	**NO_2**	**Tair**	**Rh**	**WS**	**WD**
Min			0	12		0	0	7	4	0	1
1st Qu			2	15		10	5	14	54	0	188
Median			6	16		14	9	16	73	1	261
Mean			8	16		19	10	18	67	1	230
3rd Qu			9	17		21	13	20	85	1	286
Max			132	20		176	64	38	96	5	360
NA's			6	6		6	6	6	6	6	6
Pietermaritzburg Airport (Spring) [ppb]											
Min	3	1	0	0	0	0	1	8	6	0	0
1st Qu	16	10	1	0	18	6	8	14	55	2	80
Median	23	15	2	1	25	12	14	17	76	3	110
Mean	27	18	5	3	27	19	18	18	69	3	129
3rd Qu	35	22	4	4	34	23	23	21	89	4	180
Max	130	297	161	22	79	173	167	41	99	15	360
NA's	25	23	100	19	19	86	27	217	19	217	217

Pollutant concentrations are seen to decrease heading into the mid-spring period, with the highest concentrations recorded at the beginning of the spring period. This is visible at both stations in the municipality where pollutants are within reasonable limits during the spring period. During the spring season, air temperatures have notably increased, whilst the dominant wind directions have remained similar to the winter period between the two stations. What contrasts is the observed absence of the substantial passage of fronts during the spring season.



FIGURE 32. TIME PLOT SHOWING HOURLY POLLUTANT CONCENTRATIONS (PPB) VERSUS WIND SPEED AND AMBIENT AIR TEMPERATURE, PMB CENTRAL STATION (SEPT-OCT 2017).

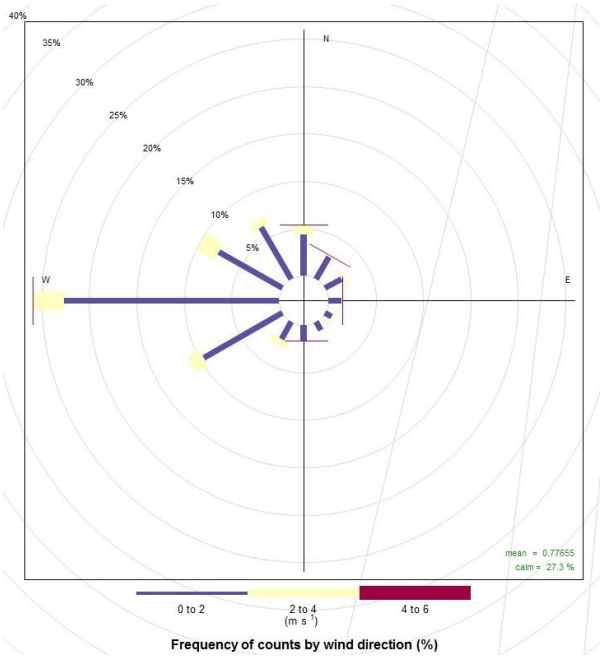

FIGURE 33. WINDROSE INDICATING WIND SPEED FREQUENCY COUNTS BY PERCENTAGE WIND DIRECTION, PMB CENTRAL STATION (AUG-SEPT 2017).

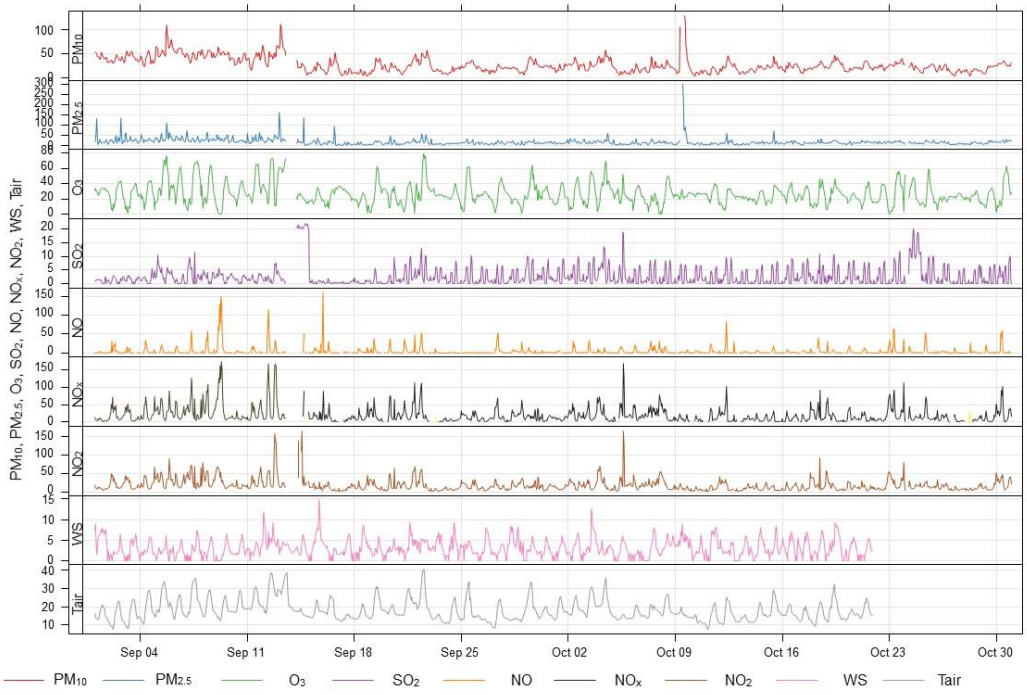

FIGURE 34. TIME PLOT SHOWING HOURLY POLLUTANT CONCENTRATIONS (PPB) VERSUS WIND SPEED AND AMBIENT AIR TEMPERATURE, PMB AIRPORT STATION (SEPT-OCT 2017).

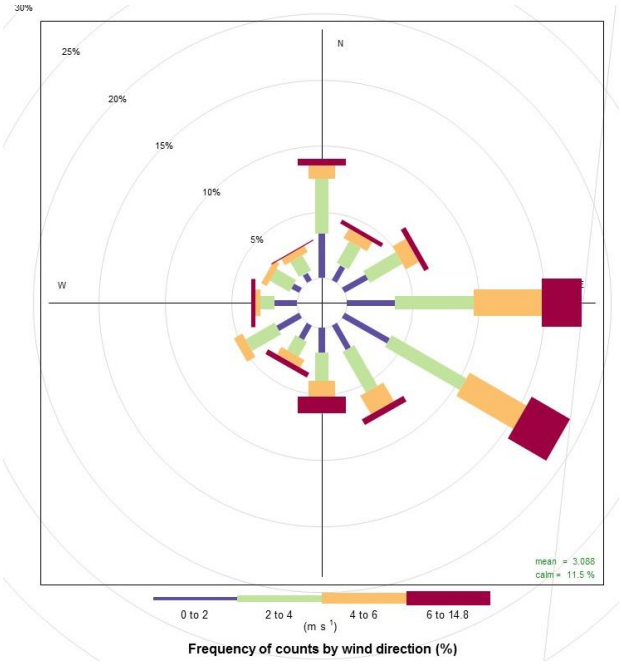

FIGURE 35. WINDROSE INDICATING WIND SPEED FREQUENCY COUNTS BY PERCENTAGE WIND DIRECTION, PMB AIRPORT STATION (AUG-SEPT 2017).

The time variation cycles of pollutants during spring indicate similar patterns to those in winter except for concentration levels, where they are substantially lower during spring. The weekend effect is still dominant. During the study period, Tuesdays and Thursdays are observed to register higher pollutant concentrations, especially NO_x concentrations, compared to other days of the week. The diurnal cycles of these pollutants are consistent between both seasons where increases are generally observed between 6:00 and 12:00, followed by a decrease during the afternoon and a slight increase towards the evening is also observed during spring. This trend is followed by all measured pollutants except for O_3, which still maintains its highest concentrations during the afternoon with decreases into the evening.

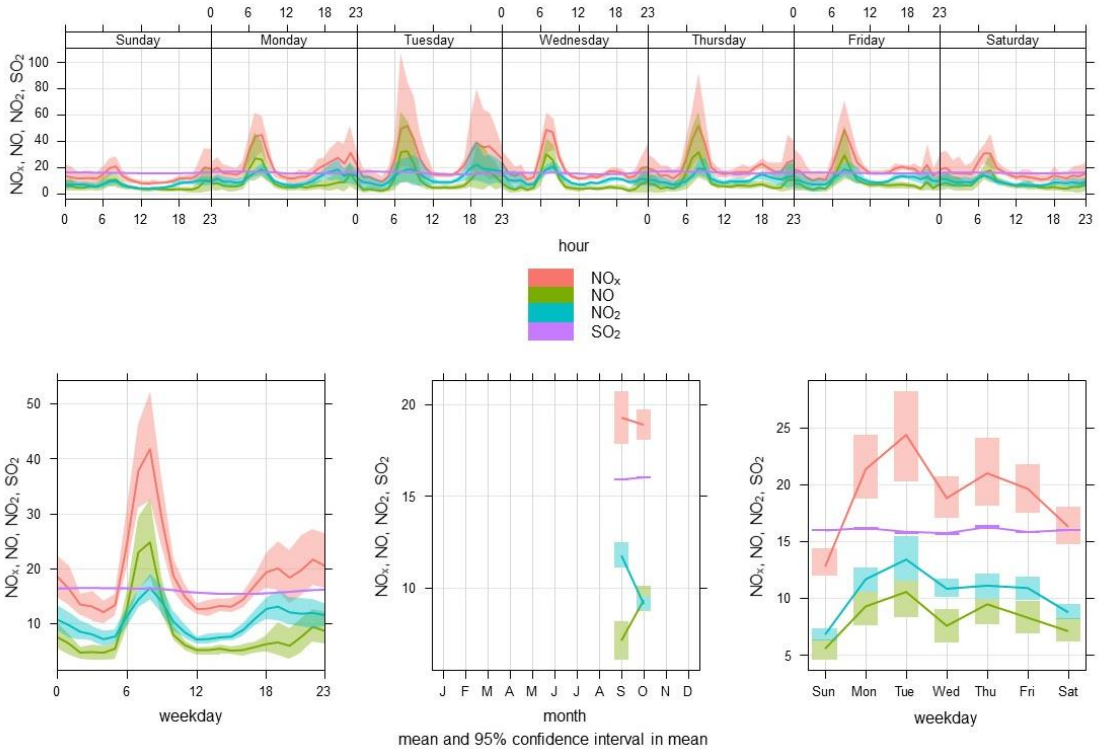

FIGURE 36. TIME VARIATION ILLUSTRATING POLLUTANT MEAN DIURNAL, WEEKLY AND MONTHLY CYCLES FOR NO_X, NO, NO_2 AND SO_2 (PPB), PMB CENTRAL STATION (AUG-SEPT 2017).

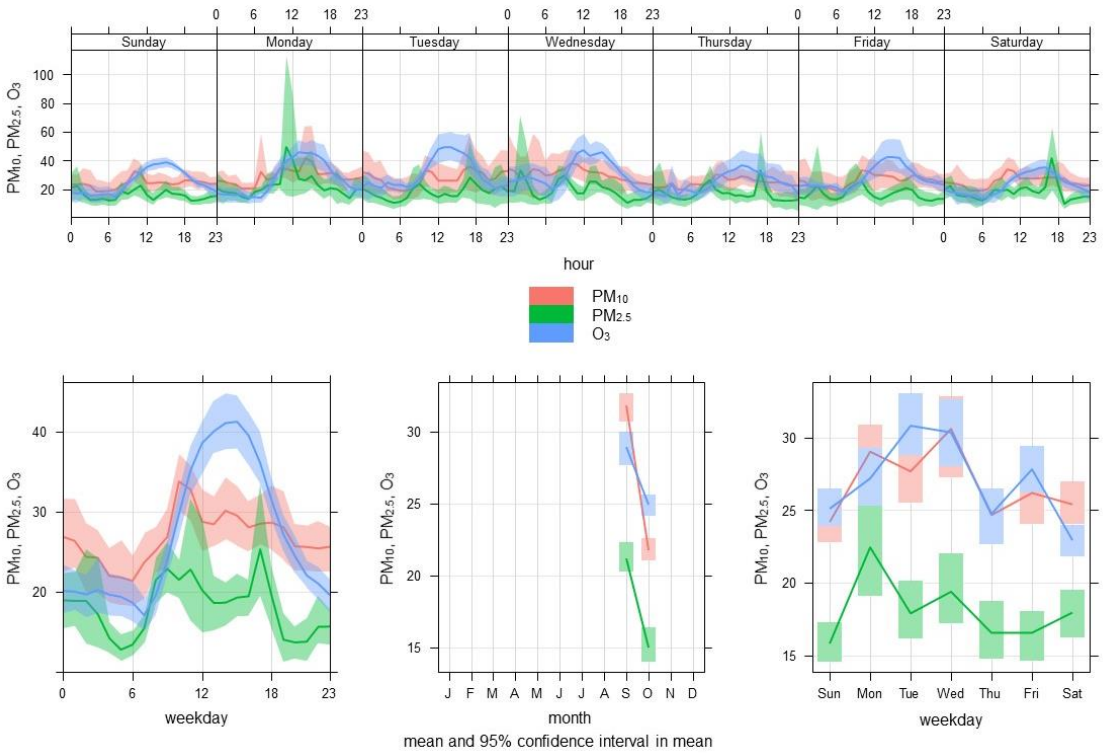

FIGURE 37. TIME VARIATION ILLUSTRATING POLLUTANT MEAN DIURNAL, WEEKLY AND MONTHLY CYCLES FOR PM_{10}, $PM_{2.5}$ AND O_3 (PPB), PMB AIRPORT STATION (AUG-SEPT 2017).

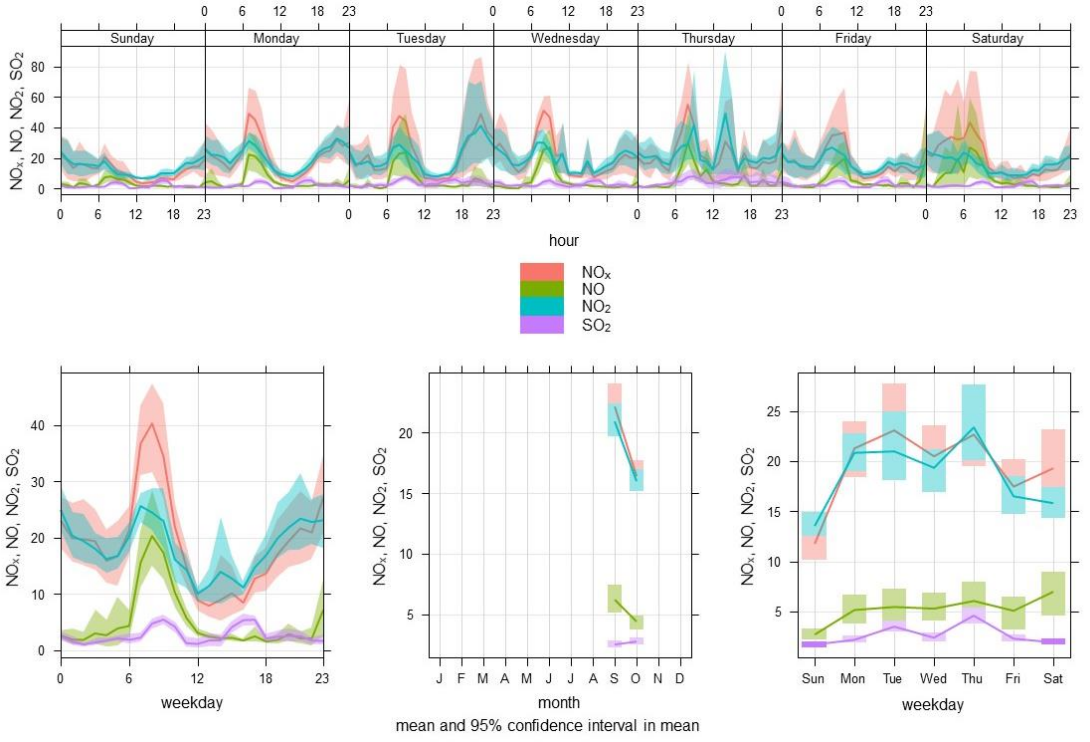

FIGURE 38. TIME VARIATION ILLUSTRATING POLLUTANT MEAN DIURNAL, WEEKLY AND MONTHLY CYCLES NO_X, NO, NO_2 AND SO_2 (PPB), PMB AIRPORT STATION (AUG-SEPT 2017).

With regards to particulate matter concentrations, PM_{10} levels are considerably higher than $PM_{2.5}$ levels at the airport station however, their mean concentrations are substantially lower compared to winter. Monthly pollutant concentrations are seen to decrease heading into the spring period except for NO and SO_2 at the central station indicating slight increases. In order to further understand how these pollutants are impacted by ambient air temperature and the development of urban heat islands, it was necessary to assess the mean hourly concentrations with mean hourly air temperature observations during the spring and winter periods. This would provide an illustration on how pollution concentrations are impacted by the dominant hourly temperature patterns and the urban heat island in the Msunduzi Municipality.

The assessment of hourly pollutant concentrations with hourly ambient air temperature observations during winter and spring indicate the following patterns between the two monitoring stations. During winter NO_x concentrations are observed to be consistent at both stations where rapid increases are notable during the early morning period, where air temperature is also observed to be increasing. The rapid increase in these pollutants has been linked to the exacerbated motor vehicle traffic emissions, which occur during the same period of the general increase in ambient air temperature. As air temperature continues to increase when approaching the afternoon period, these pollutants are seen to significantly decrease (Figure 39).

Increases in PM_{10}, $PM_{2.5}$ and O_3 concentrations are most notably at their highest during the afternoon period as observed from the airport station (Figure 40). O_3 concentrations are strongly correlated with temperature observations, where it can be observed that the dominance of the urban heat island effect can proliferate surface ozone concentrations, especially with the presence of nitrogen oxides in the atmosphere. During night time conditions, it is observed that the decrease in air temperature, is consistent with the increase in NO_x as was observed before sunrise conditions. This may suggest that, during conditions of lower air temperature, such as is the case during early morning and during the night NO_x concentrations are observed to increase. During the afternoon, there are then considerable increases of particulate matter and surface ozone during conditions of increased air temperature observations, during the winter period.

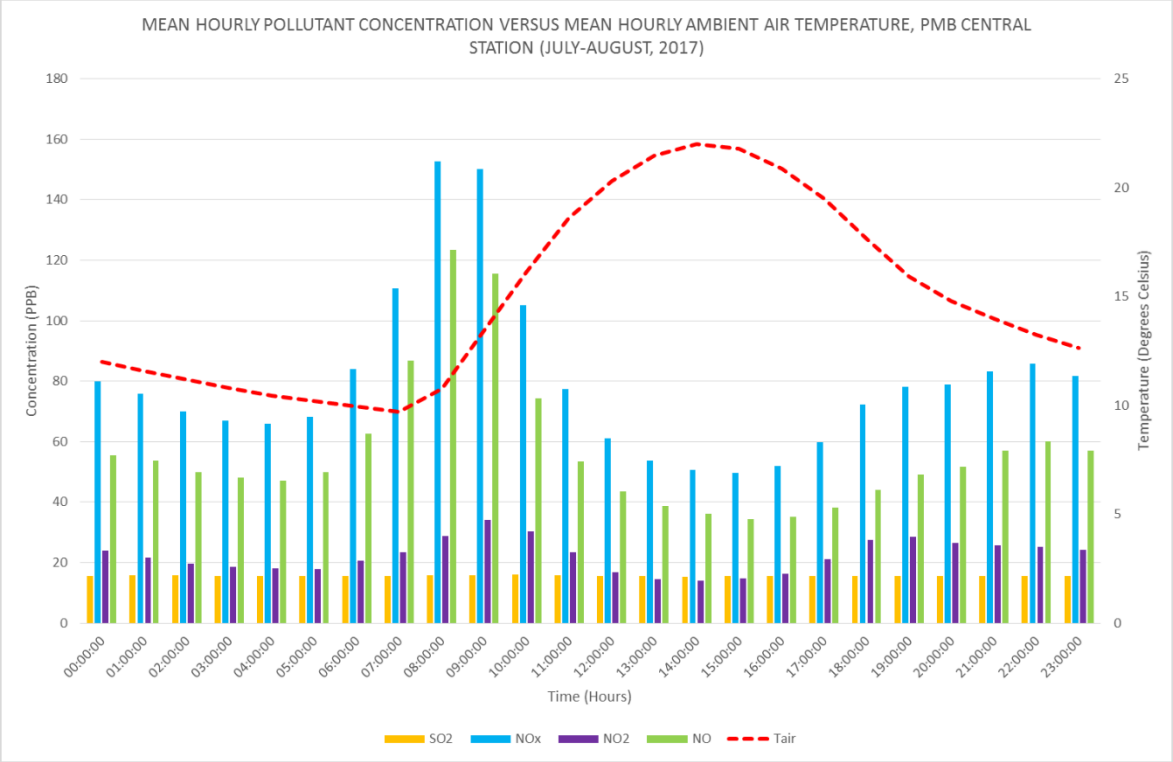

FIGURE 39. MEAN HOURLY POLLUTANT CONCENTRATION VERSUS MEAN HOURLY AMBIENT AIR TEMPERATURE DURING WINTER (PMB CENTRAL STATION).

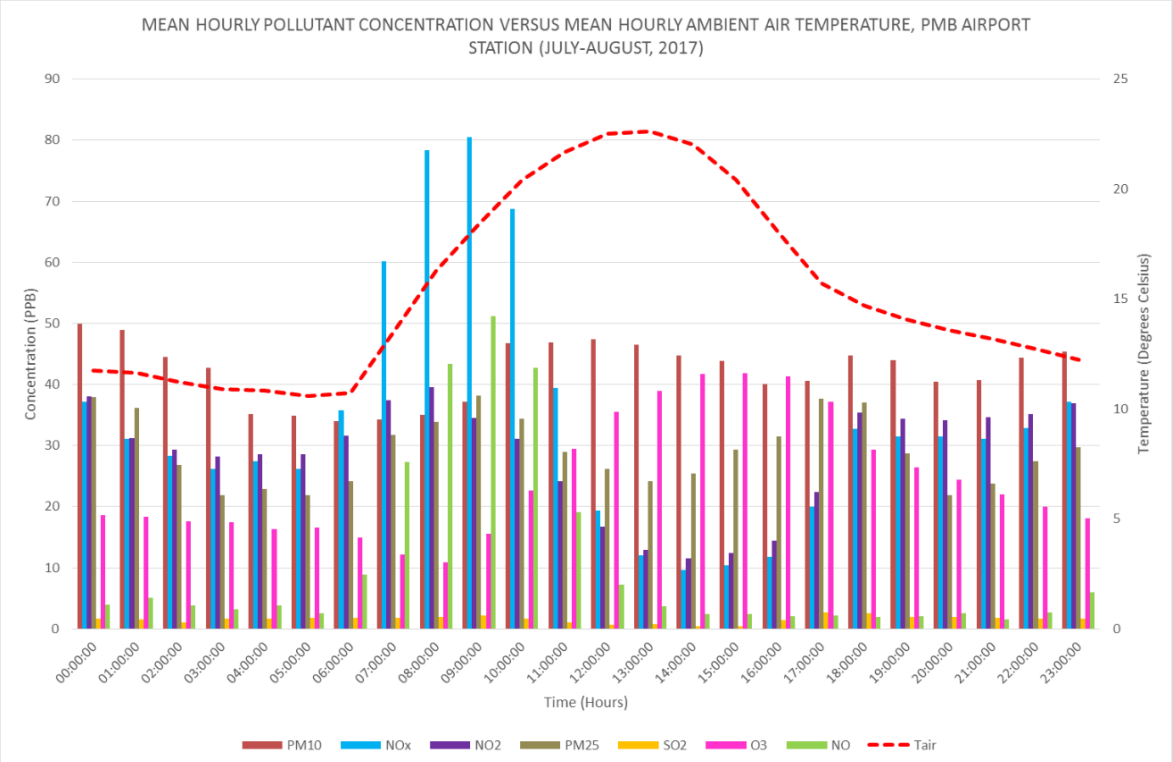

FIGURE 40. MEAN HOURLY POLLUTANT CONCENTRATION VERSUS MEAN HOURLY AMBIENT AIR TEMPERATURE DURING WINTER (PMB AIRPORT STATION).

During spring, similar patterns between air temperature and NO_x are observed as they were during the winter at the central station (Figure 41). However, there are greater differences between air temperature and pollutant concentrations. In addition, pollutant concentrations are lower than during winter and air temperatures are significantly higher during the spring season. It still seems however that NO_x concentrations are diurnal like temperature, with SO_2 concentrations remaining stable throughout the assessment.

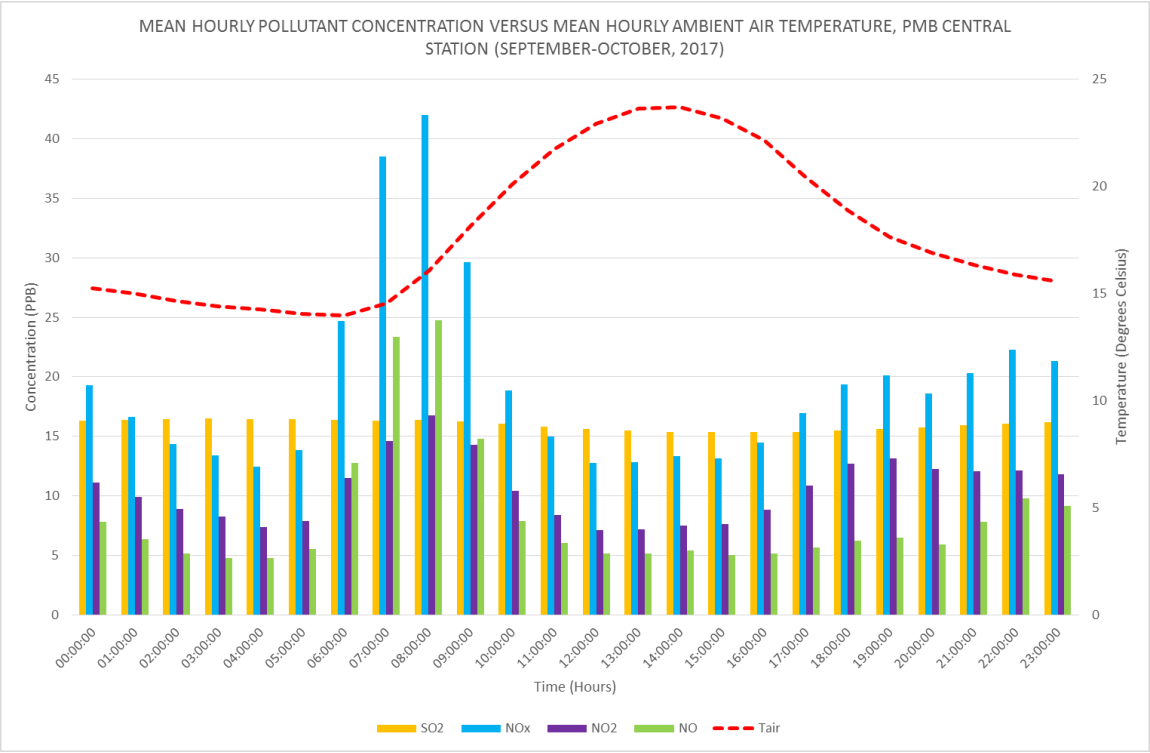

FIGURE 41. MEAN HOURLY POLLUTANT CONCENTRATION VERSUS MEAN HOURLY AMBIENT AIR TEMPERATURE DURING SPRING (PMB CENTRAL STATION).

The airport station provides more information on pollutant patterns and air temperature during the spring period, especially with surface ozone episodes (Figure 42). It is clearly illustrated that the heightened ambient air temperatures are directly contributing to the production and proliferation of surface ozone concentrations, particularly during the afternoon.

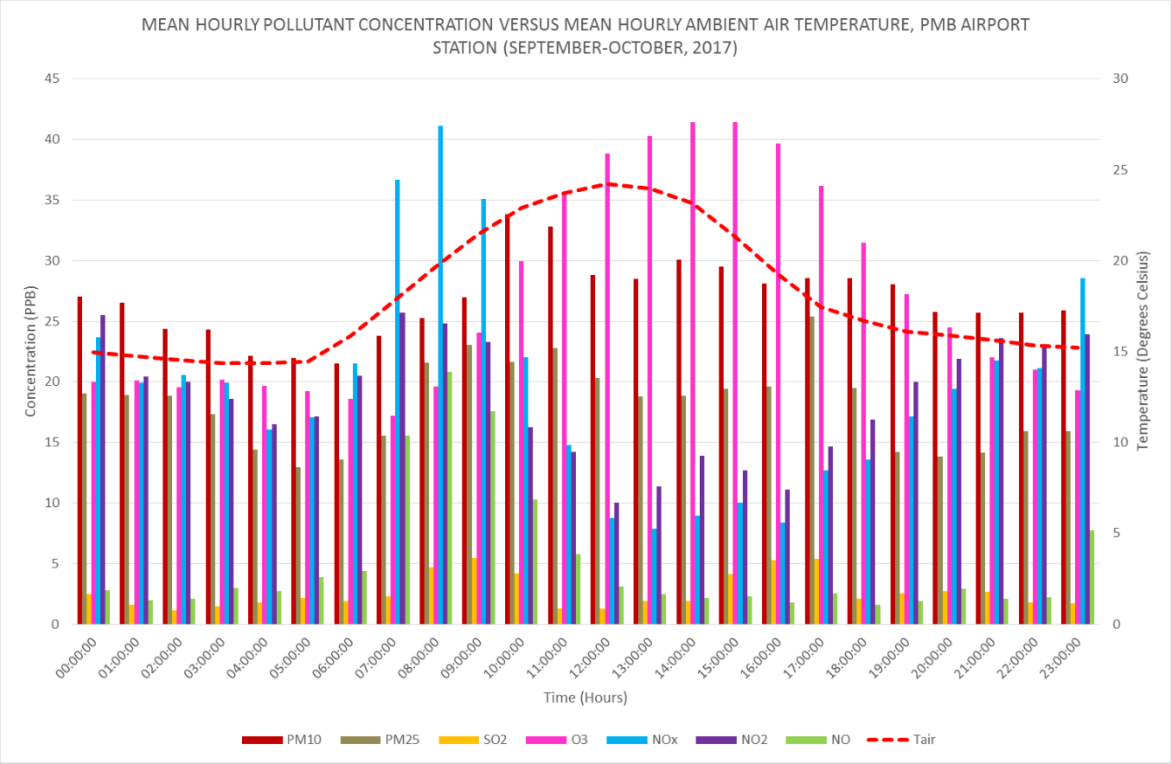

FIGURE 42. MEAN HOURLY POLLUTANT CONCENTRATION VERSUS MEAN HOURLY AMBIENT AIR TEMPERATURE DURING SPRING (PMB AIRPORT STATION).

A Pearson correlation analysis was run between the selected air pollutants and ambient air temperature observations (Table 10). Increases of surface ozone are indicated to follow an increase in ambient air temperature during both winter and spring where r = 0.71 and 0.76 are observed, respectively. There are positive correlations between air temperature and Particulate Matter, particularly stronger during spring than during winter. It is observed however that there are moderately strong negative correlations between air temperature and nitrogen oxides during winter at the airport station compared to the central station.

TABLE 10. PEARSON CORRELATION COEFFICIENTS BETWEEN SELECTED AIR POLLUTANTS AND AMBIENT AIR TEMPERATURE OBSERVATIONS.

	Pearson Correlation						
	PM_{10}	**$PM_{2.5}$**	**NO**	**SO_2**	**O_3**	**NO_x**	**NO_2**
Winter Central			-0.51	-0.56		-0.50	-0.36
Spring Central			-0.33	-0.87		-0.37	-0.40
Winter Airport	0.33	0.13	0.28	-0.54	0.71	-0.07	-0.66
Spring Airport	0.73	0.59	0.26	0.25	0.76	-0.26	-0.58

Moderately strong negative correlations are observed between air temperature and sulphur dioxide during both seasons, with an exception during spring at the airport station. It is observed that concentrations of surface ozone share a similar pattern to air temperature patterns. The mean concentrations of O_3 are not substantially different between winter and spring, although they are reasonably higher compared to other measured pollutants at the airport station.

In understanding the pollution patterns in the Msunduzi Municipality, it is important to understand the usually dominant inversion conditions, especially where the central station is located. The concentrations of nitrogen oxides at the central Pietermaritzburg station suggest that the impacts of temperature inversion conditions during spring are less intense and therefore impact less on the trapping of pollutants than during winter, where it is seen that pollutants are generally observed to have higher mean concentrations.

What is similar to the winter season, however, is the peak in nitrogen oxide concentrations during the morning in spring, thus expressing the contribution of traffic emissions especially along the N3 highway where the central monitoring station is closely located. This is seen to be a consistent source of emissions throughout the seasons. This effect is further observed at the airport station during the spring, where concentrations of nitrogen oxides are also notably higher in the early hours of the morning.

Pollutant concentrations in the municipality are as a response to source contributions into the atmosphere, especially in the case of nitrogen oxides and their heightened levels in the early morning. Although this can be clearly attributed to traffic congestions along the N3 highway, it can also be suggested that the slight lifting of inversion conditions may cause the proliferation of pollutant concentrations as cool valley conditions are reduced, especially during winter

where the trapping of pollutants from the preceding day may only get released as the inversion layer lifts during the next morning. These processes are consistent with a considerable increase in numerous pollutant concentrations and the pollutant patterns characterising the Msunduzi Municipality.

During the afternoon where observed ambient air temperature is at its highest, it is seen that usually pollution concentrations are low, except for surface ozone. This indicates that heat island conditions are favourable to pollutants that require temperature for their secondary production in the atmosphere, especially in the lower atmosphere (canopy) where most monitoring instrumentations are located – thus such observations may not fully indicate all processes occurring in the atmospheric boundary layer. To further characterise pollution distribution in the Msunduzi Municipality, an assessment of MODIS Aerosol Optical Depth provided a spatial variation component as a proxy to pollutant concentrations.

4.1.9 MODIS Aerosol Optical Depth as proxy for pollutants

To further assess the extent of pollution during the early hours of the morning in the Msunduzi Municipality, MODIS Aerosol Optical Depth products were mapped to illustrate the extent and distribution of aerosols in the municipality (Figure 43). The passing of the MODIS Terra and Aqua satellites over the study area was usually between 07h50 and 09h00. To show the distribution of aerosols over the Msunduzi Municipality, available AOD products were retrieved between the 10th of July and the 10th of September 2017. These are provided below.

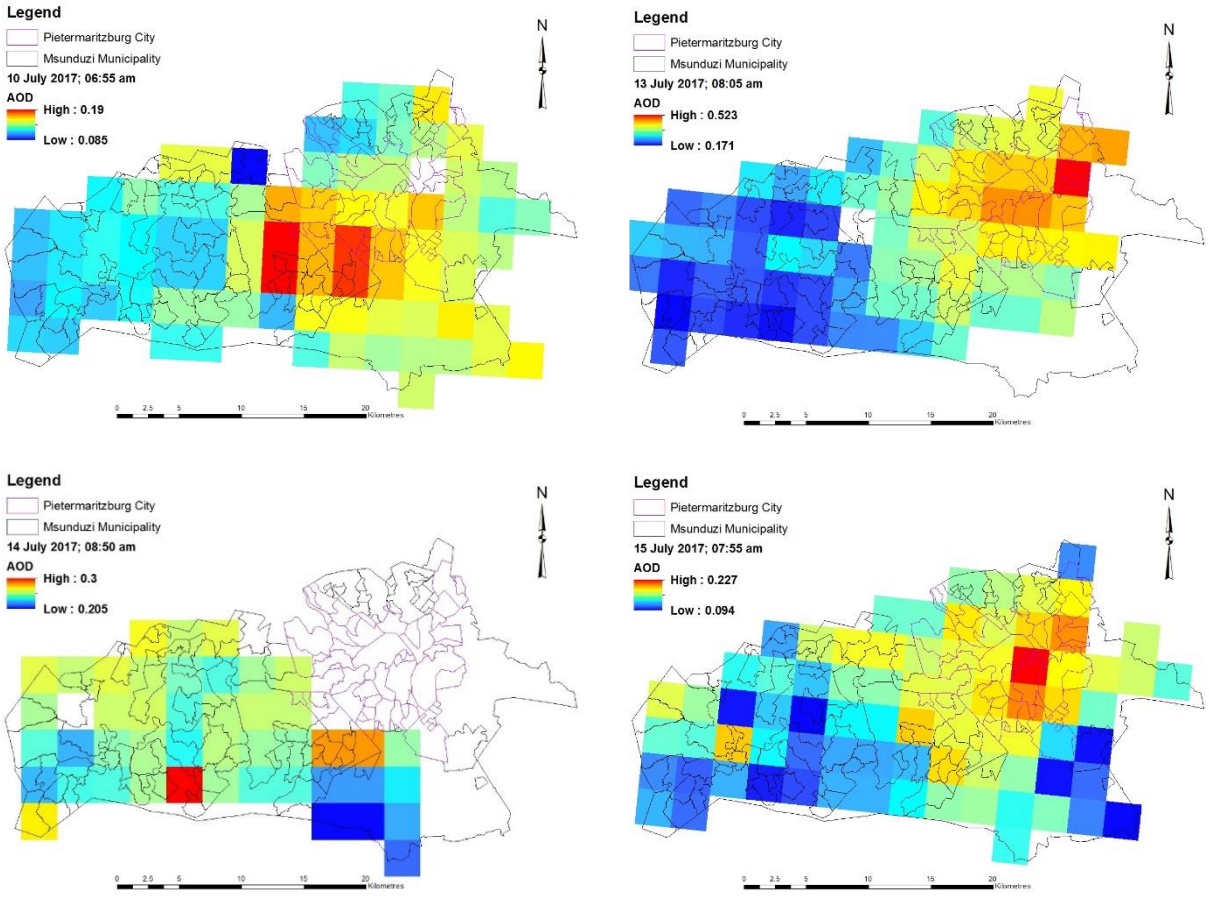

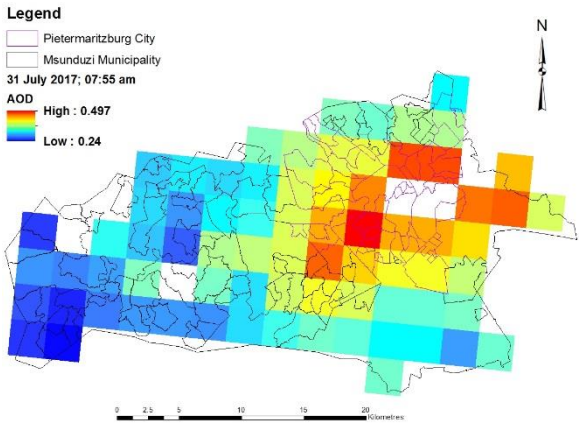
Legend
Pietermaritzburg City
Msunduzi Municipality
31 July 2017; 07:55 am
AOD
High : 0.497
Low : 0.24
N
0 2.5 5 10 15 20
Kilometres

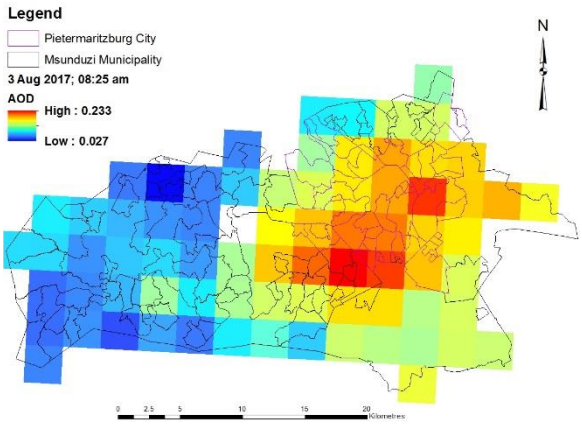
Legend
Pietermaritzburg City
Msunduzi Municipality
3 Aug 2017; 08:25 am
AOD
High : 0.233
Low : 0.027
N
0 2.5 5 10 15 20
Kilometres

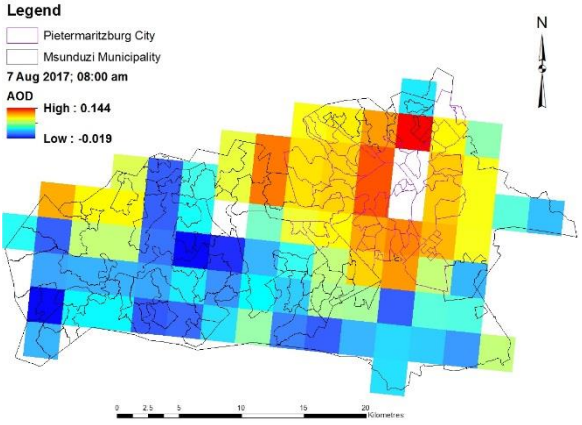
Legend
Pietermaritzburg City
Msunduzi Municipality
7 Aug 2017; 08:00 am
AOD
High : 0.144
Low : -0.019
N
0 2.5 5 10 15 20
Kilometres

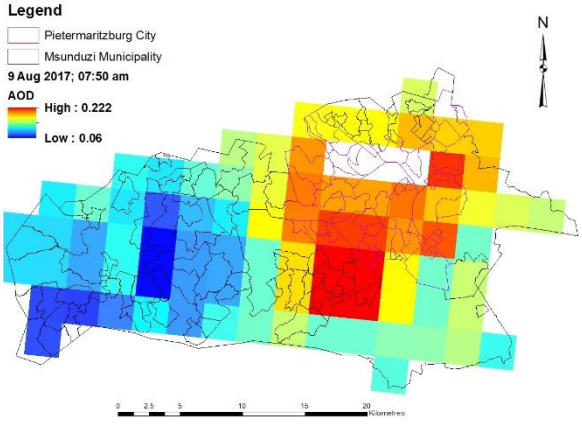
Legend
Pietermaritzburg City
Msunduzi Municipality
9 Aug 2017; 07:50 am
AOD
High : 0.222
Low : 0.06
N
0 2.5 5 10 15 20
Kilometres

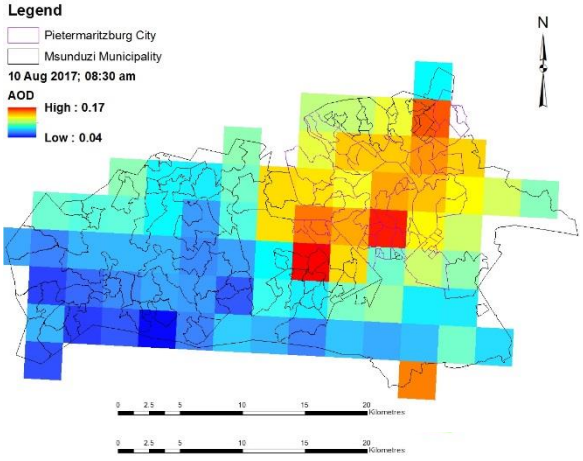
Legend
Pietermaritzburg City
Msunduzi Municipality
10 Aug 2017; 08:30 am
AOD
High : 0.17
Low : 0.04
N
0 2.5 5 10 15 20
Kilometres

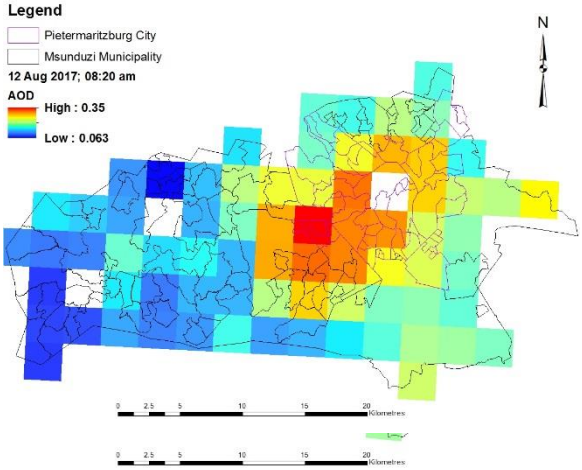
Legend
Pietermaritzburg City
Msunduzi Municipality
12 Aug 2017; 08:20 am
AOD
High : 0.35
Low : 0.063
N
0 2.5 5 10 15 20
Kilometres

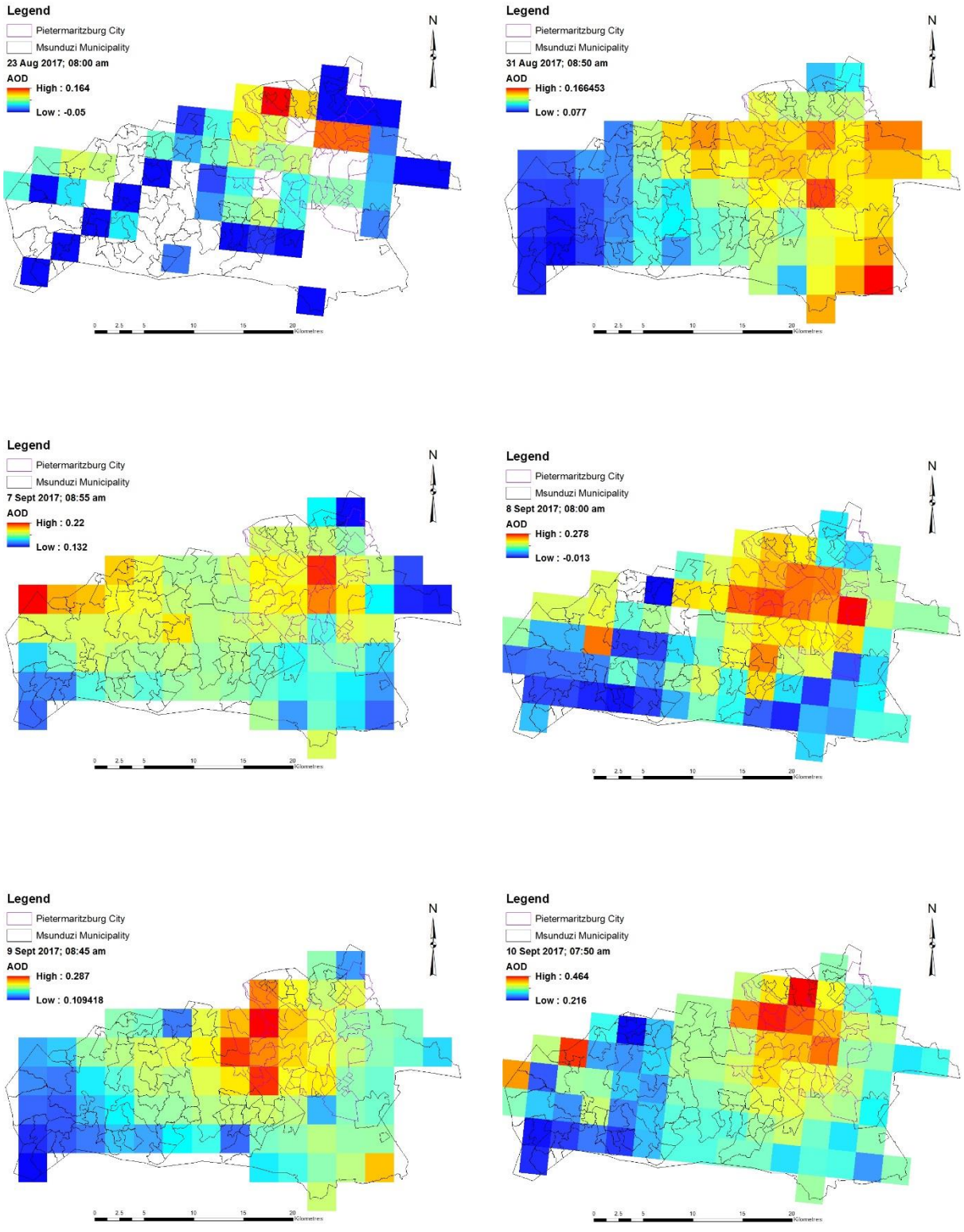

FIGURE 43. MODIS AEROSOL OPTICAL DEPTH SPATIAL VARIATIONS BETWEEN JULY 10TH, 2017 TO SEPTEMBER 10TH, 2017 DURING THE MORNING PERIOD, 07H00 TO 09H00, IN THE MSUNDUZI MUNICIPALITY.

The extent and distribution of aerosols in the Msunduzi Municipality during the selected days (the 10th of July to the 10th of September) is seen to remain consistent over the period in study. The higher AOD values, representing a measure of the extinction of the solar beam by dust and haze, are concentrated to the northwest of the municipality where the Pietermaritzburg City is located. This is the region of the municipality that is within the geologic basin that impacts much of the local meteorology and air pollution characterising the area. It is seen that high aerosol concentrations are dominant above the city of Pietermaritzburg during the early hours of the morning, which is also accompanied by higher concentrations of air pollutants which hover above the city.

The possible deepening of the inversion layer during the night potentially traps pollutants and aerosols over the city of Pietermaritzburg in contrast to the surrounding areas (Tyson and Preston-Whyte, 2000). As a result, the areas surrounding the city centre are relatively observed to show lower AOD readings due to the differing land surface characteristics pertaining to topography. The surrounding areas are located at a much higher altitude than the Pietermaritzburg City, wherein this may influence the drainage of pollutants into the basin, especially during the flow of katabatic winds at night (Tyson and Preston-Whyte, 2000).

The MODIS AOD values were extracted and compared with air pollutant concentrations to the nearest minute to assess the reliability and relationship of AOD and measured air pollutant concentrations. The resulting illustrations are provided below between the central Pietermaritzburg (Figure 44) and Pietermaritzburg Airport stations (Figure 45).

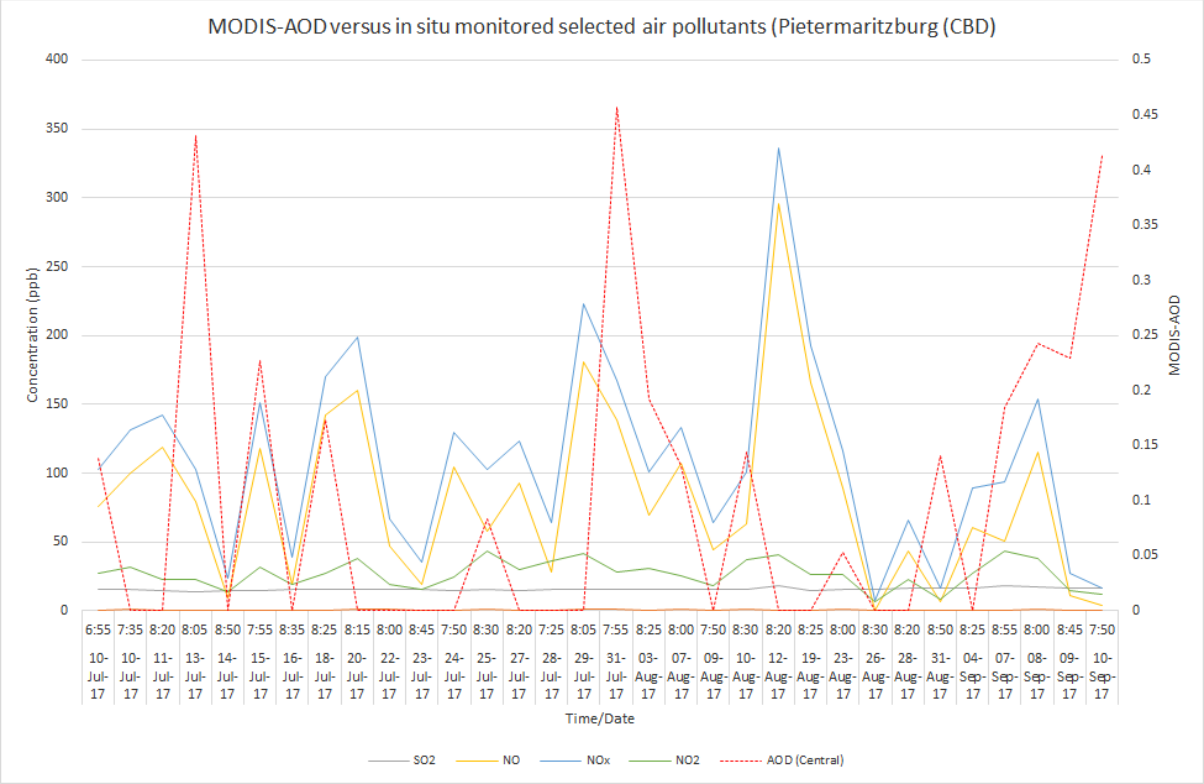

FIGURE 44. EXTRACTED MODIS AOD IN RELATION TO MONITORED SELECTED POLLUTANTS IN THE PIETERMARITZBURG CBD (10 JULY 2017 – 10 SEPT 2017)

Aerosol Optical Depth values and monitored air pollutants at the central Pietermaritzburg station indicate similar patterns where increases in pollutant concentrations are consistent with increases and decreases in AOD values. Although there are time lags and inconsistencies, there is reasonable evidence that dust and haze (represented by AOD) are within the atmospheric layer that is dominated by notable concentrations of air pollutants. It can then be suggested that during the early morning period, dust and haze as well as air pollutants are a conglomeration that creates the haze layer that is generally present and hovers above the city centre.

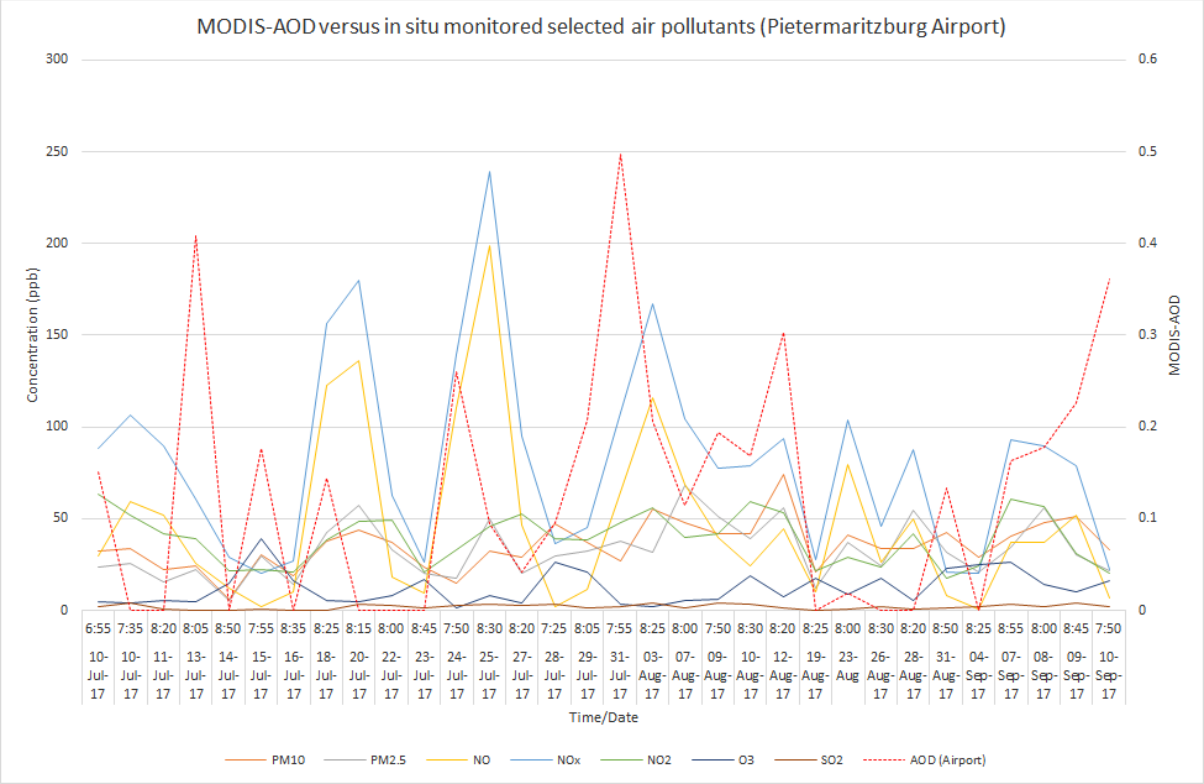

FIGURE 45. EXTRACTED MODIS AOD IN RELATION TO MONITORED SELECTED POLLUTANTS AT THE PIETERMARITZBURG AIRPORT (10 JULY 2017 – 10 SEPT 2017)

The patterns between AOD values and air pollutants at the Pietermaritzburg Airport indicate similar trajectories with the central Pietermaritzburg station. There are instances where increases in AOD values are simultaneously consistent with increases in nitrogen oxides, with similar patterns occurring at other points along the study period. To further quantify the possibility of using AOD as a proxy for measured air pollutants, a Pearson correlation analysis was performed on retrieved AOD values and pollutant concentrations between the two monitoring stations (Table 11).

TABLE 11. TABLES SHOWING THE RETURNS OF CORRELATION COEFFICIENTS BETWEEN AOD AND MEASURED AIR POLLUTANTS (A) CENTRAL PIETERMARITZBURG, (B) PIETERMARITZBURG AIRPORT

a)

SO_2	NO	NO_x	NO_2
0.039	0.191	0.145	-0.234

b)

PM_{10}	$PM_{2.5}$	NO	NO_x	NO_2	O_3	SO_2
-0.146	-0.142	-0.192	-0.189	-0.041	-0.158	-0.156

This showed very weak correlations between the variables, with individual signals between AOD and air pollutants revealing contrasting relationships between the stations. Weak negative correlations are returned at the airport station, with positive returns recorded at the central station, except for NO_2. This apparent difference in correlations is unclear, but it could suggest that increases in pollutants subsequently creates a haze layer above central Pietermaritzburg and this relationship is closely related to increases in AOD than it is at the Pietermaritzburg Airport, precisely due to the influence of the geologic location of the city of Pietermaritzburg. These weak correlations could also explain the time lags associated with the recording of the data by *in situ* stations and satellite sensors. In addition, remote sensing products represent measurements at the top of the atmosphere compared to *in situ* measurements observed near the surface which may introduce a measure of error during analysis. In a dynamic atmosphere, especially during the early morning, these relationships may be unclear. However, the time series does give an impression of existing situations where increasing AOD values are occurring at relatively the same time with increasing pollutant concentrations.

On whether AOD is a proxy for pollutant concentrations, it remains unclear in terms of the correlations of AOD and measured air pollutants. However, in terms of the spatial variation of pollutants and aerosols, AOD estimates would generally provide considerable information although their application should be cautious of over and underestimation of pollutant concentrations.

4.2 Discussion

This discussion provides the link between the three objectives outlined in fulfilling the aims of the study. In addition, results retrieved from this study are compared with similar studies to provide further insight on issues concerning urban climates.

The application of mid-resolution thermal datasets for the evaluation of the urban heat island phenomenon in South African cities has been minimal, which is a limitation towards the comparison and status of SUHIs in the country. However, similar assessments have been performed elsewhere, where comparable results have been achieved. In this study it is observed that the SUHI phenomenon and effect is most intense during autumn and summer and is consistent with the presence of built-up areas and isolated patches of seasonally unvegetated surfaces in the Msunduzi Municipality. Water bodies in the region have the lowest LST due to the cooling effect as a result of the process of evaporation over water surfaces. The CBD and suburban areas are consistently observed to be warmer than indigenous forests, plantations and woodlots. A hotspot analysis reveals sustained heat over the CBD and immediate surrounding areas – characterising these areas as a consistent heat island shaped by the spatial configuration of the sprawling built-up areas especially during autumn.

During winter and spring where the grassland layer is lower and much of the ground surface is exposed along with the presence of burnt scars, these surfaces are observed to be warmer than built-up areas. A seasonal shift of areas of high LST in the municipality is notable, however this may not substantiate the notion that the SUHI moves between seasons. It suffices to say nonetheless, that observing the SUHI during the early hours of the morning provides an understanding of how the surface responds to incoming solar radiation during the expected seasonal changes in land cover in the Msunduzi Municipality. Furthermore, the analysis of LST with LULC configuration of the urban fabric does well in highlighting the possibilities of areas susceptible to the formation of heat islands. Where in this case, areas dominated by built-up areas and seasonally unvegetated surfaces are seen to contribute substantially to the retention of heat in the municipality.

The LST difference between the developed and rural areas is most intense during autumn, with a difference of ~2.7 degrees Celsius. Although mean LST during autumn ranges between 15 – 39 degrees Celsius, the extremes are considerably lower compared to spring and summer where

55 and 51 degrees Celsius are observed, respectively. The mean LST autumn range observed in the study is comparable to the values reported by Sithole and Odindi (2015) for Pietermaritzburg where a high of 37 and a low of 22 degrees Celsius are observed along a rectangular strip, respectively. In their study, they make similar observations where high density built-up areas are areas of high thermal intensity, with areas dominated by vegetation and water bodies indicating a general decrease in thermal values. In their assessment of the rectangular strip on a rural-urban gradient, there is a clear decline in temperature from the CBD to the periphery, indicating increased thermal retention by urban areas.

The distinctiveness of the SUHI during the autumn season indicates that although the surface is generally warmer during spring and summer, the SUHI effect is not dependent on the magnitude of heat observed but rather on the observed differences in the spatial distribution of LST between rural and urban areas. The type of land cover and land use patterns dominant in these areas contribute substantially to the SUHI effect. There are instances where rural areas are observed to be warmer than urban areas where the contribution of urban green spaces considerably reduces LST in urban areas heading into spring and summer – significantly decreasing SUHI intensity.

With the heating of the surface during the early morning contributing significantly to the subsequent heating of the lower layers of the atmosphere, the configuration of land cover and land use patterns is observed to play a substantial role in how the surface absorbs and dissipates incoming solar radiation. The application of NDVI, FVC and NDBI as quantitative land cover parameters indicates a practical way to assess the dependency of LST on land cover/land use patterns. The results indicated that the correlation between LST and NDVI/FVC is negative, suggesting that vegetated green spaces in the municipality can weaken the urban heat island effect while the positive correlations between LST and NDVI infer that the built-up surfaces can strengthen and accelerate the urban heat island effect, especially during the autumn season (Kumar and Shekhar, 2015).

LST, NDVI and FVC tend to be low along water bodies. The evaporation capacity of the water plays a major role in reducing heat rather than the role of vegetation in this instance. In spaces dominated by unvegetated surfaces as in the case during winter and spring, it is seen that LST is often high. This suggests that the calorific capacity of these spaces is constituted by material that has a non-evapotranspiration and dry nature – causing the surface thermal conductivity to

increase. Such is a similar case where the N-S and W-E transects reveal that LST is usually high along residential areas and the city centre which can be referred to as the scope of the urban heat island. These are spaces usually dominated by low NDVI/FVC and high LST and NDBI. The formation of heat islands therefore is influenced by the unique urban heat distribution conditions which enlarge and deepen thermal energy intensity particularly through the building structure and materials.

Kumar and Shekhar (2015) report similar observations applying a Landsat 7 dataset. They report strong links between LST, and built-up area indices indicating the strengthening of the SUHI, while high NDVI due to the presence of vegetation weakens the effect in the city of Kalaburagi, India. Chen *et al*. (2005) observed a scattered pattern of the UHI in the Guangdong Province, China; which similarly explains the patters of the UHI in the Msunduzi Municipality where this is also related to certain land cover types. In quantifying this relationship between SUHI and land cover changes, they report of negative correlations between NDVI and LST and observed positive correlations between NDBI and LST. This continues to show that the SUHI effect becomes more prominent in areas of rapid urbanisation. In their study they note that the spatial distribution of heat islands had changed from a mixed pattern, where bare land, semi-bare land and land under development were warmer than other surfaces to an extensive SUHI over a 10-year period due to rapid urbanisation. This may well suggest that continued urbanisation and expansion of the city of Pietermaritzburg may lead to a much more defined and intense SUHIs and UHIs.

What often couples the adverse impacts of UHIs is air pollution, which is a critical issue for most cities in South Africa. The much-publicised consistent layer of haze above the city of Pietermaritzburg continues to threaten public human health and the surrounding environment. A variety of sources of pollution are present in the municipality with the prominent ones being the N3 highway, Pietermaritzburg airport, industries, mines and emissions from agricultural burning of sugarcane farms. These contribute to the concentration of pollutants in the local atmosphere. Unique also to the Msunduzi Municipality is the inversion layer that forms in the geologic basin of Pietermaritzburg trapping pollutants and sustaining the haze layer.

The assessment of pollutants in the municipality indicates that early morning periods between 6:00 and 9:00 am are critical times in terms of pollutant concentrations. This is regarded as a delicate period in the assessment of pollutants where from the overnight accumulation of

pollutants, dominant inversion conditions and the increase in pollutants as well as the warming of the Earth's surface in the following morning – result in atmospheric conditions where the prominent haze layer which is characteristic of the city of Pietermaritzburg's upper atmosphere during 6:00 and 9:00 am is present (Tyson and Preston-Whyte, 2000). NO_x concentrations increase during these times due to the surge in traffic along the N3 highway, with O_3 concentrations notably increasing immediately thereafter with peak periods in the afternoon consistently with the increase in ambient air temperature. There are concerning concentrations of Particulate Matter during both winter and spring which undoubtedly contribute to the haze layer during the early hours of the morning period.

The spatial distribution of pollutants and aerosols indicates the CBD area as a concern. AOD assessments reveal constant heightened pollution and aerosol presence over this area during winter and spring – the area dominated by the presence of the SUHI. Feizizadeh and Blaschke (2013) provide an assessment of LULC and LST revealing areas that contribute largely to the formation of UHIs. Industrial sites and construction zones are observed to contribute more to heat retention at the surface. The CBD is also notable UHI zone where LSTs of about 24-27 degrees Celsius are observed. These are considerably lower to those observed in the Msunduzi Municipality, where such values are observed during the winter. They further classify UHI zones and analyse an interpolated surface of PM_{10} indicating that areas of higher LST observations are consistent with those of higher concentrations of PM_{10} in the city of Tabraiz, Iran. High correlations between LST, UHI and air pollution are reported in general where urbanisation transforms natural land surfaces and increases artificial LULC such as buildings and impervious surfaces. These make urban landscapes fragmented and complex, thus affecting the habitability of cities.

In the Msunduzi Municipality, during the early morning it can be deduced that generally incoming solar radiation heats up the surface with the CBD and immediate residential areas absorbing more of the radiation. It is seen that land surface temperatures influence the air temperatures directly above the Earth's surface ($r = 0.70$). In the case of urban areas, the dense layout of artificial surfaces would then initiate the extended heating of the atmosphere from below which subsequently increases the ambient air temperatures. The presence of an isolated heat retention parcel above the city, helps create heat island conditions (it is important to note that land surface temperature is not the sole guiding principle to heat island formation) (Tyson

and Preston-Whyte, 2000). The continued presence of pollutants in the atmosphere from the previous night are heavily retained in this area by the inversion layer. It is only after 9:00 that the inversion layer subsides, and a dissipation of pollutants is observed. What would then dominate the local atmosphere in the city of Pietermaritzburg, would be a conglomeration of heightened temperatures and levels of pollution, especially due to its location in a basin.

The urban heat island however is seen to particularly affect the concentrations of surface ozone. Firstly, the retention of heat at the surface and subsequently by the atmosphere sees the secondary production of O_3 amidst the presence of volatile organic compounds and NO_x concentrations. As ambient temperature increases so do O_3 concentrations where correlations of 0.71 and 0.76 are observed between these two variables during winter and spring, respectively. This suggests that intense UHI conditions would strengthen the production of O_3. Secondly, with the dominant haze layer and pollution concentrations in the CBD area, these contribute to the heating of the atmosphere by re-radiation of longwave radiation by a polluted atmosphere and effectively increasing urban temperatures (Streutker, 2002). In such instances, the possibility of a positive feedback between temperature and pollution is suggested. However, it is important to note that the atmosphere is dynamic and to investigate relationships of such nature would require a study purposefully investigating the micrometeorology of the Msunduzi Municipality.

To the lengths of this study, the relationship between LULC, land surface temperature and the formation of heat islands and their contribution to air pollution have been highlighted. It is observed through the application of Landsat 8 OLI/TIRS and air pollution data that there are reasonable agreements between these relationships that the anthropogenic effects of urbanisation and land use change and degradation have adverse impacts on the environment, especially regarding the retention of heat by urban spaces. In addition, the contribution of vegetated spaces to the reduction of heat within urban areas and the fringes of urban areas is illustrated in the assessment of vegetation indices and LST. Although this is minimal within the Pietermaritzburg CBD, there is potential to maximise on heat reduction through vegetated spaces. With the observed influence of built-up areas on heat retention and increase in LST, polluted cities are susceptible to the reality of increased temperature and high pollution concentration – ultimately comprising human and environmental health in the municipality.

Chapter 5: Conclusion and Recommendations

5.1 Conclusion

The objectives guiding the study were: a) to investigate and characterise the nature and extent of the surface urban heat island effect in the Msunduzi Municipality, b) to quantify the relationship between land surface temperature and different land cover classes using remote sensing land cover indices and c) to assess the impact on pollutant concentrations with the development of the atmospheric urban heat island whilst briefly evaluating MODIS Aerosol Optical Depth as a potential proxy for measured air pollutants in the Msunduzi Municipality. The first objective revealed that a notable presence of a surface urban heat island is dominant in the Msunduzi Municipality where the increased concentration of heat is consistent with the location of the Pietermaritzburg central business district and the widespread isolated pockets of residential and industrial establishments in the study area. This retention of heat is seen to be heavily influenced by the configuration of LULC patterns in the municipality where the concentration of built-up areas promotes the formation of SUHIs.

The second objective provides indication of the strength and direction of the relationships between LST and LULC characteristics. In quantifying these relationships, it is seen that land cover characteristics have an influence on land surface temperatures. It is clearly indicated that vegetated surfaces weaken the SUHI effect in the study area with NDVI and FVC maintaining negative correlations with LST. In contrast, the presence of built-up areas is noted to strengthen the SUHI effect as NDBI maintains positive correlations with LST. These relationships are generally strong and describe the dependency of LST on LULC patterns.

The profiling of the response of LST over different land cover segments indicates marked changes in LST over different land cover and land use patterns. Areas dominated by artificial surfaces are constant sinks of heat, with areas dominated by water and vegetation generally indicating less retention of heat. What is particularly interesting are the rapid changes in LST over differing surfaces, indicating that the contribution of processes that induce land cover change, such as urbanisation and agriculture have a direct and an immediate impact to thermal dynamics. This may well and truly suggest that active surfaces such as in urban areas constantly introduce new land-atmosphere interactions.

In reaching the third objective, it is shown that air pollution is a concern in the Msunduzi Municipality, especially in the city of Pietermaritzburg particularly during early morning conditions with inversion conditions and the timing of the release of pollutants from their sources contributing substantially to the pollution oscillations observed in the study area. In investigating the potential impacts between UHIs and air pollution, it is seen that land surface temperature influences the ambient air temperatures in the study area which then leads to the evidence that sustained increases of LST can potentially influence increased heating of the surface layer where most of the pollutants are concentrated. Surface ozone is observed to be the most responsive pollutant to the increases in ambient temperature and sustained heat island conditions due to its secondary production. In this situation, it is visible that areas where much of the pollutants and aerosols are concentrated as seen on MODIS AOD products, are consistent with areas of high LST due to the concentration of built-up areas. There seems to be enough to suggest that the residents of the city are exposed to a complexity of increased air and land surface temperatures, compared to the surroundings, with a conglomeration of air pollutants and aerosols hovering above the city being a dominant feature particularly during the morning period.

5.2 Recommendations

The study provides an illustration of land and atmosphere interactions and the associated impacts. These are important processes that occur at differing scales. In the context of this study, it is seen that urban areas are actively changing which then suggests that the associated land-atmosphere interactions are rapidly being modified. To understand these modifications, additional studies would provide necessary information by providing thorough and simultaneous analyses between the linkages of land surface temperature, the development of urban heat islands and air pollution for South African cities. One of the shortcomings of the study that can be improved is the use of in situ LST data to better characterise the relationship between ambient air temperature and LST in describing the land-atmosphere interactions leading to the formation of urban heat islands. The *in situ* measurement of LST with the same overpass of satellites for the calibration and validation of the LST distribution can refine the analysis of the UHI effect for urban climate studies. Such information would aid the ability to better assess the impacts of climate change and creating climate-resilient cities.

In the context of the Msunduzi Municipality, the city of Pietermaritzburg and its unique local environment is a challenge. Mitigation requires the introduction of stricter land use policies and active plans that are not ignorant to the contribution of geologic basin to the unique atmospheric conditions in the municipality, particularly for Pietermaritzburg. This study may not provide concrete linkages between land and atmosphere interactions; however, it does explore relationships that signal potential environmental threats especially during periods where excessive heat is coupled with heightened levels of pollution during conditions that are predominately controlled by the persistent inversion conditions in the city. The use of remote sensing therefore will continue to provide the necessary tools towards the understanding and mitigation of environmental phenomena and anthropogenic impacts that exacerbate adverse conditions for inhabitants of cities and their local environment.

References

Abutaleb, K., Adeline, N., Ahmed, F., Ahmed, M.H., Elkafrawy, S.B., Arafat, S.M. and Darwish, A., 2014, October. INVESTIGATION OF URBAN HEAT ISLAND USING LANDSAT DATA. In *Proceedings of the 10th International Conference of AARSE* (p. 223).

Arnfield, A.J., 2003. Two decades of urban climate research: a review of turbulence, exchanges of energy and water, and the urban heat island. *International Journal of Climatology*, *23*(1), pp.1-26.

Baker, L.A., Brazel, A.J., Selover, N., Martin, C., McIntyre, N., Steiner, F.R., Nelson, A. and Musacchio, L., 2002. Urbanization and warming of Phoenix (Arizona, USA): Impacts, feedbacks and mitigation. *Urban Ecosystems*, *6*(3), pp.183-203.

Berrisford, S., 2011, September. Unravelling apartheid spatial planning legislation in South Africa. In *Urban Forum* (Vol. 22, No. 3, pp. 247-263). Springer Netherlands.

Bornstein, R. and Lin, Q., 2000. Urban heat islands and summertime convective thunderstorms in Atlanta: three case studies. *Atmospheric Environment*, *34*(3), pp.507-516.

Carslaw, D.C. and Ropkins, K., 2012. Openair—an R package for air quality data analysis. *Environmental Modelling & Software*, *27*, pp.52-61.

Chen, X.L., Zhao, H.M., Li, P.X. and Yin, Z.Y., 2006. Remote sensing image-based analysis of the relationship between urban heat island and land use/cover changes. *Remote Sensing of Environment*, *104*(2), pp.133-146.

Department of Environmental Affairs, 2014. DEA National Landcover (TIFF) 2014 [Raster]. Available from the Biodiversity GIS website, downloaded on 06 May 2019. http://bgis.sanbi.org/SpatialDataset/Detail/496

Du, Z., Li, W., Zhou, D., Tian, L., Ling, F., Wang, H., Gui, Y. and Sun, B., 2014. Analysis of Landsat-8 OLI imagery for land surface water mapping. *Remote Sensing Letters*, *5*(7), pp.672-681.

Engel-Cox, J.A., Holloman, C.H., Coutant, B.W. and Hoff, R.M., 2004. Qualitative and quantitative evaluation of MODIS satellite sensor data for regional and urban scale air quality. *Atmospheric Environment*, *38*(16), pp.2495-2509.

ENVI, 2004. ENVI User's Guide. Research Systems. Available from: http://aviris.gl.fcen.uba.ar/Curso_SR/biblio_sr/ENVI_userguid.pdf (accessed 14 June 2017).

ESRI, 2017. Environmental Systems Research Institute. ArcGIS 10.5.

Feizizadeh, B. and Blaschke, T., 2013. Examining urban heat island relations to land use and air pollution: multiple endmember spectral mixture analysis for thermal remote sensing. *IEEE Journal of Selected Topics in Applied Earth Observations and Remote Sensing*, *6*(3), pp.1749-1756.

Ghotbi, S., Sotoudeheian, S. and Arhami, M., 2016. Estimating urban ground-level PM10 using MODIS 3km AOD product and meteorological parameters from WRF model. *Atmospheric Environment*, *141*, pp.333-346.

Hardy, C.H. and Nel, A.L., 2015. Data and techniques for studying the urban heat island effect in Johannesburg. *The International Archives of Photogrammetry, Remote Sensing and Spatial Information Sciences*, *40*(7), p.203.

Hodgson, M.E., Jensen, J.R., Tullis, J.A., Riordan, K.D. and Archer, C.M., 2003. Synergistic use of lidar and color aerial photography for mapping urban parcel imperviousness. *Photogrammetric Engineering & Remote Sensing*, *69*(9), pp.973-980.

Joshi, J.P. and Bhatt, B., 2012. Estimating temporal land surface temperature using remote sensing: A study of Vadodara urban area, Gujarat. *International Journal of Geology, Earth and Environmental Sciences*, *2*(1), pp.123-130.

Kikegawa, Y., Genchi, Y., Kondo, H. and Hanaki, K., 2006. Impacts of city-block-scale countermeasures against urban heat-island phenomena upon a building's energy-consumption for air-conditioning. *Applied Energy*, *83*(6), pp.649-668.

Kumar, D. and Shekhar, S., 2015. Statistical analysis of land surface temperature–vegetation indexes relationship through thermal remote sensing. Ecotoxicology and environmental safety, 121, pp.39-44.

Lee, T. and Hughes, S., 2016. Perceptions of urban climate hazards and their effects on adaptation agendas. *Mitigation and Adaptation Strategies for Global Change*, pp.1-16.

Li, F., Jackson, T.J., Kustas, W.P., Schmugge, T.J., French, A.N., Cosh, M.H. and Bindlish, R., 2004. Deriving land surface temperature from Landsat 5 and 7 during SMEX02/SMACEX. *Remote Sensing of Environment*, *92*(4), pp.521-534.

Li, J., Song, C., Cao, L., Zhu, F., Meng, X. and Wu, J., 2011. Impacts of landscape structure on surface urban heat islands: a case study of Shanghai, China. *Remote Sensing of Environment*, *115*(12), pp.3249-3263.

Lourens, A.S., Beukes, J.P., Van Zyl, P.G., Fourie, G.D., Burger, J.W., Pienaar, J.J., Read, C.E. and Jordaan, J.H., 2011. Spatial and temporal assessment of gaseous pollutants in the Highveld of South Africa. *South African Journal of Science*, *107*(1-2), pp.1-8.

Monama T. E, 2016. Evaluating the urban heat island over the city of Tshwane Metropolitan Municipality using remote sensing techniques. 2016. Available at: http://hdl.handle.net/10210/124987

Msunduzi SDF, 2009. Msunduzi Spatial Development Framework: Consolidated Review. Available from: www.msunduzi.gov.za/site/search/downloadencode/nMyaaKWMqp2zp4Sx

Musakwa, W. and Van Niekerk, A., 2013. Implications of land use change for the sustainability of urban areas: A case study of Stellenbosch, South Africa. *Cities*, *32*, pp.143-156.

Ngie, A., Abutaleb, K., Ahmed, F., Darwish, A. and Ahmed, M., 2014. Assessment of urban heat island using satellite remotely sensed imagery: a review. *South African Geographical Journal*, *96*(2), pp.198-214.

Oke, T.R., 1973. City size and the urban heat island. *Atmospheric Environment (1967)*, *7*(8), pp.769-779.

Pal, S. and Akoma, O.C., 2009. Water scarcity in wetland area within Kandi Block of West Bengal: a hydro-ecological assessment. *Ethiopian journal of Environmental studies and Management*, *2*(3).

Pal, S. and Ziaul, S., 2017. Detection of land use and land cover change and land surface temperature in English Bazar urban centre. *The Egyptian Journal of Remote Sensing and Space Science*, *20*(1), pp.125-145.

Preston-Whyte, R.A., 1970. A spatial model of an urban heat island. *Journal of Applied Meteorology*, *9*(4), pp.571-573.

Qin, Z., Karnieli, A. and Berliner, P., 2001. A mono-window algorithm for retrieving land surface temperature from Landsat TM data and its application to the Israel-Egypt border region. *International Journal of Remote Sensing*, *22*(18), pp.3719-3746.

Rao, P. K. (1972). Remote sensing of urban “heat islands” from an environmental satellite. Bulletin of the American Meteorological Society, 53, 647−648.

Remer, L.A., Mattoo, S., Levy, R.C. and Munchak, L.A., 2013. MODIS 3km aerosol product: algorithm and global perspective.

Rosenthal, J.K., Sclar, E.D., Kinney, P.L., Knowlton, K., Crauderueff, R. and Brandt-Rauf, P.W., 2007. Links between the built environment, climate and population health: interdisciplinary environmental change research in New York City. *ANNALS-ACADEMY OF MEDICINE SINGAPORE*, *36*(10), p.834.

Rozenstein, O., Qin, Z., Derimian, Y. and Karnieli, A., 2014. Derivation of land surface temperature for Landsat-8 TIRS using a split window algorithm. *Sensors*, *14*(4), pp.5768-5780.

Sarrat, C., Lemonsu, A., Masson, V. and Guedalia, D., 2006. Impact of urban heat island on regional atmospheric pollution. *Atmospheric Environment*, *40*(10), pp.1743-1758.

Shah, B. and Ghauri, B., 2015. Mapping Urban Heat Island Effect in Comparison with the Land Use, Land Cover of Lahore District. *Pakistan Journal of Meteorology Vol*, *11*(22).

Shastri, H. and Ghosh, S., 2019. Urbanisation and Surface Urban Heat Island Intensity (SUHII). In *Climate Change Signals and Response* (pp. 73-90). Springer, Singapore.

Sithole, K. and Odindi, J.O., 2015. Determination of urban thermal characteristics on an urban/rural land cover gradient using remotely sensed data. *South African Journal of Geomatics*, *4*(4), pp.384-396.

Skokovic.D, Sobrino.J.A, Jimenez-Munoz.J.C, Soria.G, Julien.Y, Mattar.C and Jordi Cristobal, "Calibration and Validation of Land Surface Temperature for Landsat 8 – TIRS Sensor", Land product Validation and Evolution, ESA/ESRIN Frascati (Italy), pp 6-9, January 28-30, 2014.

Sobrino, J.A., Jiménez-Muñoz, J.C., Sòria, G., Romaguera, M., Guanter, L., Moreno, J., Plaza, A. and Martínez, P., 2008. Land surface emissivity retrieval from different VNIR and TIR sensors. *IEEE Transactions on Geoscience and Remote Sensing*, *46*(2), pp.316-327.

Song, C., 2004. Cross-sensor calibration between Ikonos and Landsat ETM+ for spectral mixture analysis. *IEEE Geoscience and remote sensing letters*, *1*(4), pp.272-276.

Statistics SA, Mid-Year population estimates, South Africa, 2009 (Statistical release P0302) in Lehohla P. (2009). South African Statistics, 2009. Statistic South Africa.

Stone Jr, B., 2005. Urban heat and air pollution: an emerging role for planners in the climate change debate. *Journal of the American Planning Association*, *71*(1), pp.13-25.

Streutker, D.R., 2002. A remote sensing study of the urban heat island of Houston, Texas. *International Journal of Remote Sensing*, *23*(13), pp.2595-2608.

Tan, J., Zheng, Y., Tang, X., Guo, C., Li, L., Song, G., Zhen, X., Yuan, D., Kalkstein, A.J., Li, F. and Chen, H., 2010. The urban heat island and its impact on heat waves and human health in Shanghai. *International Journal of Biometeorology*, *54*(1), pp.75-84.

Tyson, P.D. and Preston-Whyte, R.A., 2000. The Climate and Weather of southern Africa. Oxford University Press Southern Africa, Cape Town.

United States Geological Survey, 2016. Landsat 8 (L8) Data Users Handbook. Department of Interior U.S. Geological Survery. Available from: https://landsat.usgs.gov/sites/default/files/documents/Landsat8DataUsersHandbook.pdf (accessed 14 June 2017).

Voogt, J.A. and Oke, T.R., 2003. Thermal remote sensing of urban climates. *Remote Sensing of Environment*, *86*(3), pp.370-384.

Voogt, J.A., 2004. Urban heat islands: hotter cities. Available from: http://www.actionbioscience.org/environment/voogt.html?newwindow=true (accessed 8 June 2017).

Wang, F., Qin, Z., Song, C., Tu, L., Karnieli, A. and Zhao, S., 2015. An improved mono-window algorithm for land surface temperature retrieval from Landsat 8 thermal infrared sensor data. *Remote Sensing*, *7*(4), p.4268.

Wang, J. and Christopher, S.A., 2003. Intercomparison between satellite-derived aerosol optical thickness and PM2. 5 mass: Implications for air quality studies. *Geophysical Research Letters*, *30*(21).

Weng, Q., 2009. Thermal infrared remote sensing for urban climate and environmental studies: Methods, applications, and trends. *ISPRS Journal of Photogrammetry and Remote Sensing*, *64*(4), pp.335-344.

Weng, Q., Liu, H. and Lu, D., 2007. Assessing the effects of land use and land cover patterns on thermal conditions using landscape metrics in city of Indianapolis, United States. *Urban Ecosystems*, *10*(2), pp.203-219.

Weng, Q., Lu, D. and Schubring, J., 2004. Estimation of land surface temperature–vegetation abundance relationship for urban heat island studies. *Remote Sensing of Environment*, *89*(4), pp.467-483.

Wong, E., Akbari, H., Bell, R. and Cole, D., 2011. Reducing urban heat islands: compendium of strategies. *Environmental Protection Agency, retrieved May*, *12*, p.2011.

Wong, N.H. and Yu, C., 2005. Study of green areas and urban heat island in a tropical city. *Habitat international*, *29*(3), pp.547-558.

Xiao, R.B., Ouyang, Z.Y., Zheng, H., Li, W.F., Schienke, E.W. and Wang, X.K., 2007. Spatial pattern of impervious surfaces and their impacts on land surface temperature in Beijing, China. *Journal of Environmental Sciences*, *19*(2), pp.250-256.

Yuan, F. and Bauer, M.E., 2007. Comparison of impervious surface area and normalized difference vegetation index as indicators of surface urban heat island effects in Landsat imagery. *Remote Sensing of Environment*, *106*(3), pp.375-386.

Zha, Y., Gao, J. and Ni, S., 2003. Use of normalized difference built-up index in automatically mapping urban areas from TM imagery. *International Journal of Remote Sensing*, *24*(3), pp.583-594.

Zunckel, M., Venjonoka, K., Pienaar, J.J., Brunke, E.G., Pretorius, O., Koosialee, A., Raghunandan, A. and Van Tienhoven, A.M., 2004. Surface ozone over southern Africa: synthesis of monitoring results during the Cross-border Air Pollution Impact Assessment project. *Atmospheric Environment*, 38(36), pp.6139-6147.